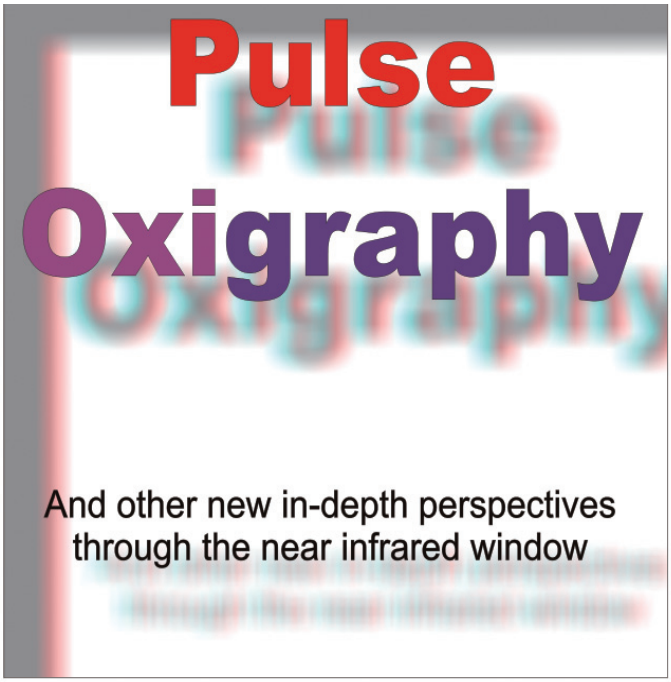
Pulse
Oxigraphy
And other new in-depth perspectives
through the near infrared window

F. P. Wieringa

PULSE OXIGRAPHY

And other new in-depth perspectives
through the near infrared window

The research presented in this thesis is the result of scientific co-operation between Erasmus MC and TNO Quality of Life.

ISBN: 978-90-5986-233-3

Pulse Oxigraphy

And other new perspectives through the near infrared window

Pulsoxygrafie

En andere nieuwe perspectieven door het nabij-infraroodvenster

Proefschrift

ter verkrijging van de graad van doctor aan de
Erasmus Universiteit Rotterdam
op gezag van de
rector magnificus

Prof.dr. S.W.J. Lamberts

en volgens besluit van het College voor Promoties.

De openbare verdediging zal plaatsvinden op
woensdag 9 mei 2007 om 11:45 uur

door

Fokko Pieter Wieringa

geboren te Haarlem

Promotiecommissie

Promotoren:	Prof.dr.ir. A.F.W. van der Steen
	Prof.dr. A.J.J.C. Bogers
Overige leden:	Prof.dr. D.J.G.M. Duncker
	Prof.dr. H.A.M. Neumann
	Prof.dr. I.T. Young

To my wife and children who missed me too much during the last years

“Have you seen the light ?!” (reverend Cleophis James – played by the late James Brown - in “the Blues Brothers”)

Table of contents

	Preface: What makes mankind a successful species ?	**11**
	Development of tools: Technology	12
	Technology in skilled hands	13
	Role of technology in medicine	14
	How to incubate new technology in medicine	15
	References	16
1	**An introduction to pulse oximetry**	**19**
1.1	The importance of visual diagnostic skills for the detection of cyanosis	19
1.2	Detection of cyanosis by opto-electronics: pulse oximetry	20
	1.2.1 Historical developments	20
	1.2.2 Basic principle of pulse oximetry	20
	1.2.3 Influences from blood composition	23
	1.2.4 Pulse oximetry cannot fully replace human observation	24
1.3	Pulse oximetry works fine as it is, why develop an imaging modality ?	25
1.4	Outline and aim of this thesis	25
1.5	References	27
2	**A possible concept for SpO_2 camera technology**	**29**
2.1	Explanatory introduction to this chapter	29
2.3	Imaging apparatus for determining concentration ratios	30
	2.3.1 Abstract	30
	2.3.2 Patent description	30
	2.3.3 Claims	36
3	**Contactless multiple wavelength photoplethysmographic imaging: A first step towards "SpO_2 camera" technology**	**39**
3.1	Abstract	39
3.2	Introduction	41
3.3	Methods	42
	3.3.1 Instrumental setup	42
	3.3.2 Experimental protocol 1	43
	3.3.3 Experimental protocol 2	43
	3.3.4 Image aquisition	44
	3.3.5 Image processing (experiments 1 & 2)	44
	3.3.6 ROI-pixel processing (experiment 1)	46
	3.3.7 ROI-pixel processing (experiment 2)	46

3.4 Results 46
3.4.1 Results of experiment 1 47
3.4.2 Results of experiment 2 47
3.5 Discussion 49
3.6 Conclusions 50
3.7 Acknowledgements 51
3.8 References 52

4 Concept for SpO_2 phantom technology 55
4.1 Explanatory introduction to this chapter 55
4.2 Phantom device 55
4.2.1 Abstract 55
4.2.2 Patent description 56
4.2.3 Claims 63

5 In vitro pulse oxigraphy: Demonstration of feasibility 65
5.1 Abstract 65
5.2 Introduction 67
5.3 Methods 69
5.3.1 Instrumental setup 69
5.3.2 Experimental protocol and data collection 71
5.3.3 Data processing 74
5.4 Results 76
5.4.1 Results - Heart rate 76
5.4.2 Results - Oxygenation 76
5.5 Discussion 79
5.6 Conclusions 80
5.7 Acknowledgements 81
5.8 References 82

6 Pulse oxigraphy demonstrated on a phantom with arterial and venous regions 83
6.1 Abstract 83
6.2 Introduction 84
6.3 Methods 84
6.4 Results 87
6.5 Discussion 88
6.6 Conclusions 88
6.7 Acknowledgements 89

7 Concept for visualization of buried vascular structures 91
7.1 Explanatory introduction to this chapter 91
7.1.1 General considerations 91
7.1.2 Selective enhancement of contrast from below the surface 92
7.1.3 Stereoscopy offers optimal use of depth clues 92
7.1.4 Shaping shadows to a helpful format 92
7.1.5 Improving depth range by exploiting backscatter 92
7.1.6 Combination with earlier patent possible 92
7.1.7 Illuminating the needle tip via the lumen 93
7.2 Patent description 93
7.2.1 Abstract 93
7.2.2 Imaging of buried structures 93
7.2.3 Claims 109
7.3 References 112

8 Remote non-invasive stereoscopic imaging of blood vessels: First in-vivo results of a new multispectral contrast enhancement technology 113
8.1 Abstract 113
8.2 Introduction 115
8.3 Methods 116
8.3.1 Instrumental setup 116
8.3.2 Data aquisition 118
8.3.3 Data processing 119
8.3.4 Data presentation 122
8.4 Results 123
8.4.1 Results for blood withdrawal 123
8.4.2 Results for dark skin 124
8.4.3 Results for vein detection through iodide 124
8.4.4 Results for varicose vein and nevi pigmentosum inspection 125
8.5 Discussion 126
8.6 Conclusions 127
8.7 Acknowledgements 128
8.8 References 129

9 Contrast enhancement of coronary arteries in cardiac surgery: A new multispectral stereoscopic camera technique **131**
9.1 Abstract 131
9.2 Introduction 133
9.3 Methods 134
9.3.1 Instrumental setup 134
9.3.2 Data aquisition 135
9.3.3 Data processing 136
9.3.4 Data presentation 136
9.4 Results 136
9.4.1 Results obtained with pigs' hearts 136
9.4.2 Results for human hearts 138
9.5 Discussion 139
9.6 Conclusions 140
9.7 Acknowledgements 140
9.8 References 141

10 General discussion and summary **143**
10.1 Pulse oxigraphy 143
10.2 Vascular enhancement 144
10.3 Conclusions 144
10.4 Future perspectives 145
10.5 References 146

11 Algemene discussie en samenvatting **147**
11.1 Pulsoxygrafie 147
11.2 Verbeterde visualisatie van bloedvaten 148
11.3 Conclusies 149
11.4 Toekomstperspectieven 149
11.5 Referenties 151

Dankwoord **153**

Curriculum Vitae **159**

Job history **163**

Publications **165**

Preface

What makes mankind a successful species ?

Archeological findings show that already in the earliest known societies, toys and games were popular, which indicates that even under harsh conditions human intelligence and creativity is not entirely spent on "serious" matters. Obviously, we like to play around and one might say that homo sapiens also is a homo ludens [1]. This playful attitude, combined with a well developed visual system and excellent manual dexterity, may well form an important contribution to the success of human species, since an invention may be seen as playing around with a problem until it is solved.
The history of mankind shows an abundance of ingenious tools, creatively developed to serve for a dazzling variety of applications. For the context of this (rather non-archeological) thesis it suffices to divide tools into a few crude categories. We may e.g. distinguish tools that:

- protect us from our environment and help us to master it (e.g. shelter, clothing, dams, bridges, boats, portable water containers, protective eye-wear);
- amplify our senses (e.g. a stick to gauge water depth or to probe a narrow hole, a stone dropped to estimate a depth range) or that even form completely new "senses" (like a compass);
- increase our handling capabilities and force (e.g. hammers, cantilevers, ropes, cranes, transport devices, weapons);
- speed-up and/or expand the sharing of knowledge (tam-tam, pictograms, scripture, telegraph, telephone, paintings, photos, movies).

Fire clearly can help us to master our environment and also forms a powerful weapon, but it is a too important issue to simply mention as an example of a tool. Since we cannot handle fire directly we need tools for any application of it. A development starting at "stealing" fire from nature, that via keeping this fire "alive" evolved to the ability to almost anywhere at any time deliberately kindle a fire with carefully designed dedicated tools, must have required all previously discussed human strongpoints. It is even more impressive that with the help of fire, we can create new tools like baked pottery and metal objects.
Historical artifacts, clearly manufactured by large organized groups (sometimes probably thousands), not only confirm the resourcefulness of mankind but also prove that the participating individuals must have had a high level of communication. An example is the pre-historic neolithical firestone mine in Rijckholt, south Limburg which already is impressive by itself, but the fact that tools made from the material of this mine were distributed across many hundreds of kilometers also illustrates the

power of trade and communication [2]. Records of expeditions that met isolated tribes still living at the stone-age level, consequently show that curiosity and eagerness to learn are universal characteristics of mankind [3]. It is also remarkable that within each human community, skills exists that help to increase chances of recovery from illness and injuries like knowledge about the properties of plants (e.g. digitalis, coca-leaves and asthma-weed) or the application of tools (e.g. splints and bandages) and that such knowledge is greatly valued [4]. Every tribe has its well respected (but mostly also feared) medicine (wo)man [5]. The level of care being taken of wounded, sick or disabled individuals may be regarded as one of the indicators of civilization level (although exceptions exist).

Development of tools: Technology

Many stone-age devices are very well engineered and clearly demonstrate that an impressive level of craftsmanship and patience was needed to make them. High-quality materials were transported over long distances and material properties were exploited very cleverly.

History shows that new, improved materials boost changes (Stone age, bronze age, iron age, silicon age). The same applies for new sources of energy (fire, watermills, windmills, steam engines, electricity, combustion engines, nuclear energy, solar cells). No matter what mix of new technology is presented, humans will exploit it and rapidly adapt to it. Papuas in New Guinea, for example, that never saw a car before they joined a Dutch expedition through the Sibil valley in 1959, were extremely curious to learn more about these metal monsters and quickly turned out to be excellent drivers and extremely resourceful car mechanics within less than a year [6].

History also shows that tools successfully amplifying human senses can drastically change our world model and boost scientific progress (telescope, microscope) or economies (telegraph, telephone). This is quite logical, since our sensory organs primary determine how much information we can gather from our environment in order to build a world model inside our mind. As humans we use technology to shape our world, but our world model is also shaped by technology.

The discovery of sensors that go beyond the boundaries of our human senses had an even greater impact. The compass is an excellent example of how such an artificial "sixth sense" boosted the development of mankind, by enabling us to navigate in unknown areas. For thousands of years this remained the only man-made magnetical device. Thanks to pioneers like Romagnosi, Oersted, Maxwell, Herz and many others, we learned to explore the electromagnetic (EM) spectrum [7-9]. This exploration of the EM-spectrum (of which we only can sense a very narrow region directly) in turn brought us wireless telecommunication, which has an ever increasing value for modern societies [10].

For any extension beyond human senses, the degree of intuitive understanding rises when we go from scalar information (1-dimensional) to "flat" imaging (2D-information) to 3D-information. Imaging techniques furthermore generally evolve from grey-

scale to color representation. Images at one hand can represent a lot of information at a glance, and on the other hand can give us an intuitive understanding of "invisible" phenomena (provided that the applied representation style matches well enough with our natural perception of the world). This explains the enormous impact on medicine of X-ray technology, gamma-cameras, ultrasound scanners, PET-scanners and MRI. It is not without a cause that in many languages *"ah, I see"* actually means *"ah, I understand"*.

Information without an understanding is quite useless, communication and perception thus are important. Language forms a primary means of human communication, but pictures form the oldest known communication records. Pictures combined with scripture provide an effective means to record information and transport it over large distances in space and/or in time. Printing technology considerably speeded up the spreading of knowledge, leading to a boost in scientific developments. The invention of photography and cinematography further increased this effect. Today many scientific journals offer their contents plus supporting software models, movies or animations on the internet, which may be regarded just as important as the discovery of book printing. Never before in history so many people had so much opportunities to communicate and explore such an abundance of information.

Technology in skilled hands

"Seeing is believing", but a matching combination of sight and touch is even stronger (remember "doubting Thomas") [11]. Human touch and especially proprioception are very strong sensory inputs, but the latter mostly remains unnoticed by our conscious mind; we learn to use these senses merely by playing around [12]. If, however, there is a mismatch between sight and proprioception this can cause great discomfort, confusion and disorientation.

For many professions we speak of "skilled hands" but actually we refer to a combination of professional knowledge, comprehensive understanding, trained observations and excellent eye-to-hand co-ordination.

Many professions require "skilled hands" and some additionally require accurate reactions within very narrow margins of space and time. For such professions technology typically can play an important role. As an example, we here discuss some striking similarities between a search-and-rescue helicopter crew and a surgical team.

In both teams there is a need for similar skills like well trained eyes, quick recognition of what's going on (and what's about to happen). Both need a "flowdiagram" of alternative remedies direct at hand (mind map) and they both also need excellent eye-to-hand co-ordination. Visual stereopsis is clearly important for depth perception, but also the importance of proprioception and force feedback should not be underestimated.

When comparing a crew involved in open heart surgery with a crew on a helicopter search-and-rescue mission we see a lot of similarities:

Just like a helicopter on a search-and-rescue mission, an operating theatre is a com-

plex environment with a crew of highly skilled specialists that closely work together using complex tools and sensory instruments to guide them in a stressful and time-critical situation.
Just like the helicopter pilot offers a stable platform while the hoist operator and the diver actually rescue the victim in the water, it is the anaesthesists job to monitor and stabilize the patient with help of the perfusionist while the surgeon and his team localize the problem and complete their task to fix it. Well-designed technology, put into skilled hands, can shift the frontier of possibilities.
It is, however, crucial that the ergonomy of technology is optimized continuously [13]. Apart from listening to user input, this also means that incidents and near-incidents should be carefully studied to find out what caused them. Poor design of the human-machine interface is e.g. the root cause of many errors [14].
If an incident occurs, the reason of failure can provide precious information for improvements. Such learning pays itself back [15]. Complex non-medical industries (e.g. aerospace and nuclear industry) have evolved incident reporting systems that focus on near misses and provide incentives for voluntary reporting [16]. Reporting of near misses offers numerous benefits over adverse events: greater frequency allowing quantitative analysis; fewer barriers to data collection; limited liability; and recovery patterns that can be captured, studied, and used for improvement. Education and engagement of all stakeholders of health care and negotiation of their conflicting goals will be necessary to change the balance of barrier incentives in favour of implementing reporting systems [17].
Thanks to the vigorous efforts of several medical doctors that sometimes initially stood alone and put their jobs at risk, these insights and according methods (e.g. anaesthesia recording systems) are being adopted in medicine [18-20]. The role of such pioneers should be acknowledged.

Role of technology in medicine

Feeling the pulse and temperature, checking the respiration and close observation of the patients' color and pupil reflex are ancient skills which still are firmly integrated in basic medical education.
Apart from these skills in using natural senses, instruments played an important role in medical progress [21]. Repeatable time measurement devices improved the objectivity of pulse counting and the reporting of disease progress [22]. With the invention of thermometry an objective indication of fever became at hand [23-28]. Microscopes facilitated the discovery of micro-organisms and helped to unravel the mysteries of life [29-31].
The stethoscope dramatically improved and facilitated diagnosis of cardiopulmonary diseases [32]. X-ray technology gave a giant boost in traumatology and after more than 100 years still offers new insights into the human body [33]. The electrocardiograph dramatically increased cardiological insights [34]. Computer-based automated

recognition of arythmia and other computer-based monitoring applications have proven their clinical value [35].
Nuclear imaging (gamma camera & positron emission tomography), echography, X-ray computer tomography and magnetic resonance imaging momentarily form the crown of imaging technologies and offer a wealth of possibilities to non-invasively explore the human body [36-38].
Numerous other examples of innovations can be brought forward, but even a book solely dedicated to the development of medical technology would probably not be sufficient to cover everything. For the purpose of this preface it is sufficient to state that, although a large percentage of new medical technologies quickly will be forgotten again, the devices that do prove to be extremely useful make all efforts worth while.

How to incubate new technology in medicine

Instruments can help doctors and their staff to do their job, although in many cases early embodiments of such instruments are difficult to operate for the user and require several technological generations to become more ergonomical. Logically the input of medical staff is a crucial component to improve ergonomy. Ideally, developers and users should form a closed communication loop.
Medical history has learned us that extended diagnostic tools (and especially imaging modalities) can lead to better understanding which in turn can lead to better possibilities for treatments [37]. Such innovative processes are not automatic and the word *"can"* is explicitly used twice in the previous sentence. Understanding and treatment are, however, surely catalyzed by close co-operation between medical and technological professionals. In such teams technicians on one hand should communicate to clinicians what they see as promising new technological possibilities, and on the other hand should use the *"Spice Girls method"* by continuously asking clinicians *"so tell me what you want what you really, really want"* [39].
The Thorax Centre of Erasmus MC was explicitly founded to facilitate research with such close co-operation. Ever since its' founding, the Thorax Centre has fostered it's supporting technical staff and facilities for in-house development of custom fine-mechanical constructions, high-end electronics and complex experimental software. Without such excellent technical support combined with the enthusiasm of medical specialists, none of the experiments described in this thesis would have been possible.
The most important contribution to the Dutch scientific community of the Noble prize winner Dr. Kamerlingh Onnes may well have been the foundation of the Leiden Instrument-maker School (LIS) which delivers the kind of top technicians that are needed to support empirical science [40].
I hope that time will prove that this thesis has supported the Thorax Centre philosophy and will contribute to its' persistence.

References

[1] Huizinga J, *Homo ludens. Proeve eener bepaling van het spelelement der cultuur*. 1938, Haarlem.

[2] NGV, *De prehistorische vuursteenmijnen van Ryckholt-St.Geertruid.* 1998, Beek.

[3] Heider KG, *Grand valley Dani: Peaceful warriors*. 3 ed. 1997: University of South Carolina. 193.

[4] Wefers Bettink H and Van Itallie L, *Pharmacopoea Nederlandica*. 4th ed. 1871, Amsterdam: J. H. de Bussy.

[5] Anderson RA, *Magic, science and health: The aims and achievements of medical anthropology*. 1996: Mills College. 454.

[6] Ltnt at sea ter Beest HW, *Personal communication*. 1984: Kollum.

[7] Maxwell JC, *A treatise on electricity and magnetism*. Clarendon press. series. 1873, London: MacMillan and Co.

[8] Herz H, *Untersuchungen über die Ausbreitung der elektrischen Kraft*. 1894: Johann Ambrosius Barth.

[9] Romagnosi GD, *Articolo sul galvanismo, in Gazeta di Rovereto*. 1802.

[10] Belrose JS. *Fessenden and Marconi: Their differing technologies and transatlantic experiments during the first decade of this century. in International Conference on 100 Years of Radio*. 1995. London.

[11] Johannes 20:24-29 *De verschijning aan Thomas*, in *De Bijbel*, Nederlands Bijbelgenootschap.

[12] Hadders-Algra M. *Homo ludens: Spelenderwijs in ontwikkeling*. in *Inauguration speech as professor of developmental neurology*. 2003. Groningen.

[13] Karsh BT and Holden RJ, *New technology implementation in health care*, in *Handbook of human factors and ergonomics in health care and patient safety,* P. Carayon, Editor. 2007, Lawrence Erlbaum associates: Mahwah, New Yersey, USA. p. 393-410.

[14] Fairbanks RJ and Caplan S, *Poor interface design and lack of usability testing facilitate medical error, in Using human factors engineering to improve patient safety*, J.W. Gosbee, Editor. 2005, Joint commision resources: Oakbrook Terrace, Michigan, USA. p. 105-112.

[15] Sequeira R, Weinbaum F, Satterfield J, Chassin J and Mock L, *Credentialing physicians for new technology: the physician's learning curve must not harm the patient*. Am Surg, 1994. 60(11): p. 821-823.

[16] Webster CS, *The nuclear power industry as an alternative analogy for safety in anaesthesia and a novel approach for the conceptualisation of safety goals*. Anaesthesia, 2005. 60(11): p. 1115-1122.

[17] Barach P and Small SD, *Reporting and preventing medical mishaps: lessons from non-medical near miss reporting systems*. BMJ, 2000. 320(7237): p. 759-763.
[18] Gravenstein JS, *Safety in anesthesia*. Anaesthesist, 2002. 51: p. 754–759.
[19] Smalhout B. *De dood op tafel*. in *Inauguration speech of professor in anaesthesia*. 1972. Utrecht.
[20] Hofer TP and Hayward RA, *Are bad outcomes from questionable clinical decisions preventable medical errors? A case of cascade iatrogenesis*. Ann Intern Med, 2002. 137 ((5 Part 1)): p. 327-333.
[21] Jackson R and La Niece S, *A set of roman medical instruments from Italy. Britannia*, 1986. 17: p. 119-167.
[22] Reiser SJ, *The technologies of time measurement: Implications at the bedside and the bench*. Annals of internal medicine, 2000. 132(1): p. 31-36.
[23] Martine G, *Essays and Observations on the Construction and Gradation of Thermometers, and on the Heating and Cooling of Bodies*. 1st edition ed. 1740, Edinburgh.
[24] Dominguez EA, Bar-Sela A and Musher DM, *Adoption of thermometry into clinical practice in the United States*. Rev Infect Dis, 1987. 9(6): p. 1193-201.
[25] Janssens PG, *Fever. A guideline in the development of medical thinking*. Verh K Acad Geneeskd Belg, 1991. 53(4): p. 305-61; discussion 361-4.
[26] MacKenzie MA, van Heteren GM and van der Meer JW, *Clinical thermometry. I. Historical developments*. Ned Tijdschr Geneeskd, 1997. 141(19): p. 954-6.
[27] Mackowiak PA and Worden G, Carl *Reinhold August Wunderlich and the evolution of clinical thermometry.* Clin Infect Dis, 1994. 18(3): p. 458-67.
[28] Wunderlich CRA, *Das Verhalten der Eigenwärme in Krankheiten.* 1868, Leipzig: Wigand.
[29] Belonoschkin B and Fenandez-Moran H, *From Leeuwenhoek (1632-1723) to electron microscopy; on discovery of human spermatozoa 275 years ago*. Dtsch Med Wochenschr. 1953 Jul 17;78(29-30):1038-9, 1953. 78(29-30): p. 1038-1039.
[30] Casida LE, *Leeuwenkoek's observation of bacteria*. Science, 1976. 192(4246): p. 1348-1349.
[31] Gest H, *The discovery of microorganisms by Robert Hooke and Antoni Van Leeuwenhoek, fellows of the Royal Society*. Notes Rec R Soc Lond, 2004. 58(2): p. 187-201.
[32] Hagopian EJ, Mann C, Galibert LA and Steichen FM, *The history of thoracic surgical instruments and instrumentation*. Chest Surg Clin N Am, 2000. 10(1): p. 9-43.
[33] Selvik G, *Roentgen stereophotogrammetric analysis*. Acta Radiol, 1990. 31(2): p. 113-126.

[34] Einthoven W, *Galvanometrische registratie van het menschelijk electrocardiogram, in Herinneringsbundel Professor S.S. Rosenstein*. 1902, Edouard IJdo: Leiden.
[35] Prakash O, Meij S, Zeelenberg C and van der Borden B, *Computer-based patient monitoring*. Critical Care Medicine, 1982. 10(12): p. 811-822.
[36] Bailey DL and Adamson KL, *Nuclear medicine: from photons to physiology*. Curr Pharm Des, 2003. 9(11): p. 903-916.
[37] Seibert JA, *One hundred years of medical diagnostic imaging technology.* Health Physics, 1995. 69(5): p. 695-720.
[38] Van Tiggelen R and Pouders E, *Ultrasound and computed tomography: Spin-offs of the world wars*. JBR-BTR, 2003. 86(4): p. 235-241.
[39] Stannard R, Rowe M, Chisholm M, Halliwell G, Brown M, Beckham V and Bunton E, *Wannabe,* R. Stannard and M. Rowe, Editors. 1996, Virgin Records.
[40] Pommerel I, *Een eeuw precies*, ed. K. Bougondiën. 2001, Leiden: Fonteyn & Andersen. 79.

Chapter 1

An introduction to pulse oximetry

This chapter is partly based upon the following publication:
"Pulsoxymetrie: Een techniek met toekomst maar ook randvoorwaarden"
by F.P. Wieringa and A.F.W. van der Steen
published in Klinische Fysica 2001/4

1.1 The importance of visual diagnostic skills for the detection of cyanosis

The visual diagnosis of cyanosis (skin color shift towards blue) probably is the earliest method for detecting decreased blood oxygenation (hypoxia) [1]. A skilled clinician recognizes a cyanotic patients' condition literally at a glance and can act accordingly. Such *"a vue"* diagnostic skills are extremely useful because cyanosis may indicate a life threatening condition that requires immediate attention. Throughout medical history close observation of patient color has been used to diagnose a variety of cardiopulmonary disorders. Some relatively recent examples are listed below:
In the period 1952-1953 Virginia Apgar introduced her famous score system for newborns, which included visually checking for signs of cyanosis [2].
In 1973 Paul re-emphasized the importance of skin color for the assessment of cyanosis in the newborn and the possibility to diagnose various heart/lung related conditions by comparing the color of various body parts. He also described variations in the spreading of redness when giving artificial respiration to apneic infants [3].
The differential diagnosis of various peripheral vascular diseases (Raynaud's phenomenon, acrocyanosis, livedo reticularis, pernio syndrome, erythermalgia, collagen diseases) performed by close observation of skin color appearance at well defined ambient temperatures, was described by Ross in 1965 [4].
In 1975 Winslow *et al*. published an excellent overview of the visual skills needed to carefully observe patients with cardiopulmonary disease, in which the importance of early visual detection of cyanosis was stressed [5].
The expression "to be seen by a doctor" emphasizes the importance of visual examination techniques like those described above. There is, however, a disadvantage in cases that need prolonged observation. Visual surveillance in combination with palpation of the pulse frequency is not a very efficient approach for long-term patient monitoring and is also rather unspecific in detecting the onset to cyanotic conditions.

This probably explains why, parallel to the refinement and publication of visual medical skills, another, more objective and quantitative, approach was developed.

1.2 Detection of cyanosis by opto-electronics: pulse oximetry

1.2.1 Historical development

From the 1930s on, light-sensitive electronic components like Selenium photocells began to become available and surprisingly fast were applied in attempts to somehow monitor the cardio-pulmonary condition of patients and pilots (for increased safety during high flights). From the 1930s to the 1970s various devices for non-invasive photoplethysmography and blood oxygenation measurement evolved [6, 7]. The Cylops, a device based on visible light reflectometry on the forehead, was the first commercial device with a more or less acceptable accuracy [8, 9]. Technology, however, remained cumbersome. Selenium photocells were reasonably small and robust but not very sensitive. Vacuum photomultiplier tubes were much more sensitive, but rather bulky and very delicate. In 1950, however, Nishizawa invented the PIN-diode, which by the 1970's had evolved to a small, stable, cheap and robust solid-state light detector with a wide dynamic range. Additionally, in 1974 Aoyagi published the brilliant insight that the pulsatile nature of arteries can be exploited as a discriminator between absorbance caused by arterial blood versus other tissue absorbance components and proved that arterial oxygen saturation could indeed be derived from two simultaneously aquired photoplethysmograms at 630 and 900nm [10]. This marked the birth of reliable bedside pulse oximetry, which spread rapidly, since it offered a simple non-invasive technique to simultaneously monitor heart rate, plethysmographic pulse waveform and arterial oxygen saturation (SpO_2). Since then, pulse oximetry has become indispensable in modern clinical practice and is applied in numerous ways [11, 12].

1.2.2 Basic principle of pulse oximetry

The benefits of pulse oximetry are evident. It is a non-invasive and hardly discomforting technique that facilitates continuous monitoring of the (approximate) arterial oxygen saturation and simultaneously reveals the pulse frequency. The underlying principle namely lies in determining the ratio between the amplitudes of two photoplethysmographic pulse wave registrations obtained at different wavelengths.

The oscillating intra-arterial pressure (pulse wave) periodically stretches the vessel walls. Because blood is a pronounced chromophore within the tissue the pulse wave accordingly modulates the absorbance of light passing through a given tissue volume (see figure 1). Although the static component of tissue light absorption is much larger than the small plethysmographic modulation, it is readily possible to selectively amplify these arterial pulsations and display them as a curve.

To reliably register such small dynamic changes within a large offset-span, stable detectors with a very large dynamic range are required, even in semi-static conditions.

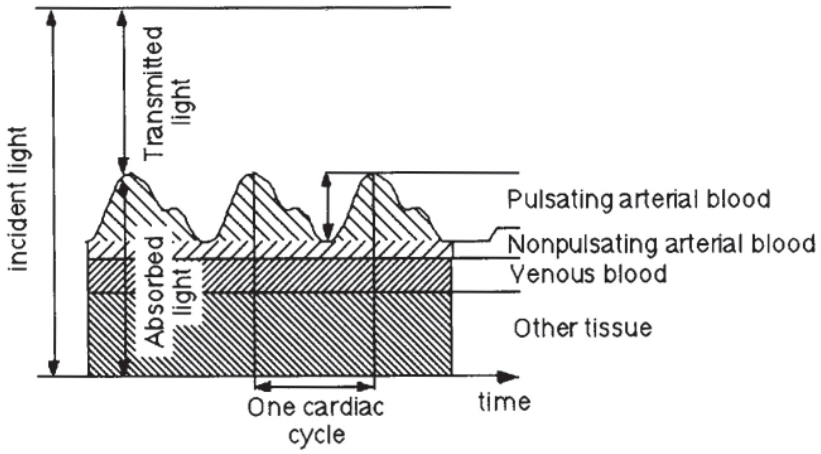

Fig. 1: Main absorption components for tissue [13]. The relative amplitudes are not drawn to scale, the "other tissue" component usually strongly dominates.

A pulse oximeter generally applies two photoplethysmographical registration channels that measure light absorbance variations at two different wavelengths, usually 660 nm and 940 nm. At a wavelength of 660 nm (red, visually well detectable light) the absorbance of non-oxygen-bound hemoglobin (Hb) is significantly stronger than the absorbance of oxygen-bound-hemoglobin (HbO_2). This is reversed at a wavelength of 940 nm but with a smaller difference in absorbance (see figure 2).

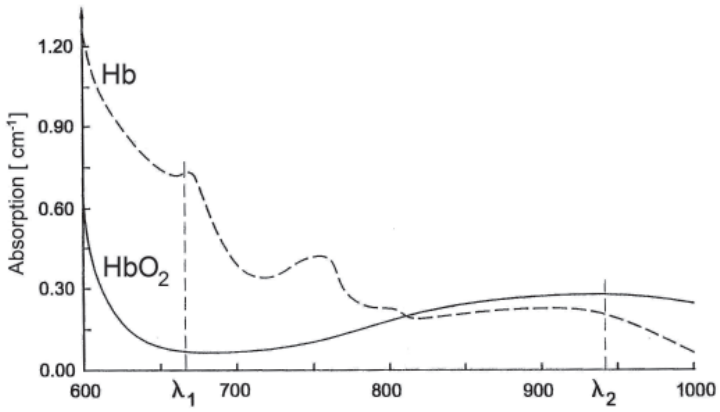

Fig. 2: Spectral absorption curves of reduced hemoglobin (Hb) and oxygenated hemoglobin (HbO_2) [14]

If the magnitude of the variation between peaks and valleys in the plethysmographic traces can be accurately detected for both wavelengths, then static tissue absorption can be ruled out and the functional oxygen saturation can be determined (see fig. 3).

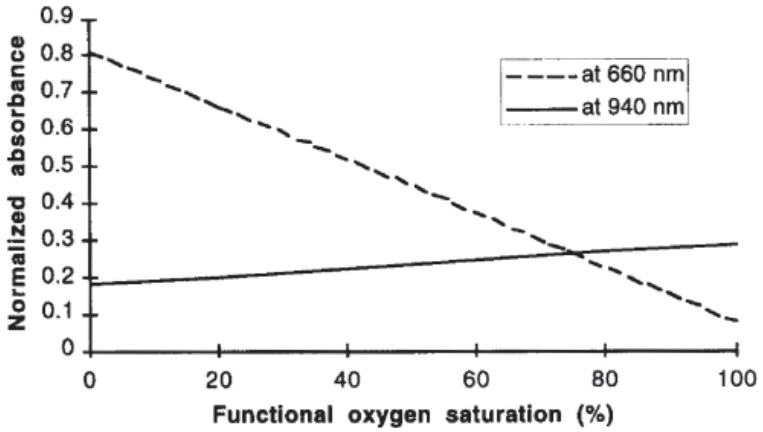

Fig. 3: Normalized absorptions at 660 nm and 940 nm as a function of blood oxygen saturation [13]

Clinical pulse oximeters commonly apply the so-called "ratio-of-ratios" method to derive arterial blood oxygen saturation. The principle of this method is to determine the difference between peaks and valleys for each of both plethysmographic traces and calculate the ratio between them. This ratio in turn is a measure for the arterial blood oxygenation.
Figure 4 shows the original "ratio-of-ratios" concept, as presented by Aoyagi in 1974 at the 13th congress of the Japanese society for medical electronics and biological engineering in Osaka [10].

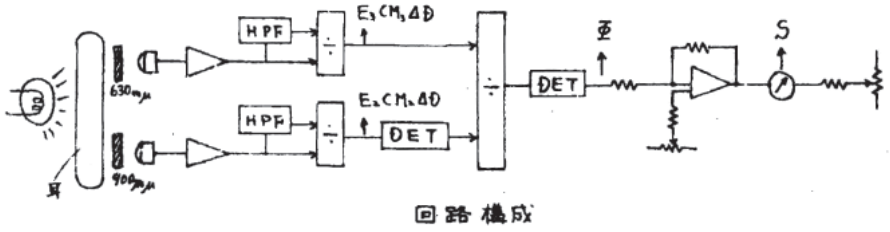

Fig. 4: Aoyagi's original device, a pulse oximeter based on the ratio of ratios at 630 and 900 nm [10].

Although over the decades this approach proved to work excellent in clinical practice, the underlying tissue optics still are not fully understood [15, 16].

Nevertheless, within the clinic (but also in ambulances, home-care and sport training) pulse oximetry is widely used for diagnosis and especially for monitoring. However useful pulse oximeters are, it should be kept in mind that they have a few limitations. Practical problems can arise due to:

- Problems that can occur within any technology like defect wiring, power failures, etc.
- Factors that are specifically inherent for the measurement principle like movement artifacts, poor perfusion of the measurement site, ambient light sources, pollution of the optical path, restrictions pertaining to electromagnetic compatibility (EMC), influences from blood composition, etc.
- Human factors like erroneous settings, neglecting of alarms, etc. but especially the assumption that monitoring devices can fully replace human observation.

1.2.3 Influences from blood composition

The application of two wavelengths inherently means that blood components with deviating spectral absorbance can disturb the measurements. The best known example is carboxyhemoglobin (HbCO). Victims of carbon monoxide (CO) poisoning have a blushing color tone and connected pulse-oximeters produce higher SpO_2-values than the actual blood oxygenation justifies. Experimental comparisons between pulse oximeter derived SpO_2-values and chemical full-blood gas analysis in patients having carbon monoxide poisoning confirmed erroneously high SpO_2-readings [17-20]. This inherent limitation for two-wavelength instruments at 660 and 940 nm is caused by the absorption curve of HbCO. There are, however, special CO-oximeters that are designed for the detection of carbon-monoxide poisoning [21].

The presence of methemoglobin also can cause shifting SpO_2-values.

Finally the absorption curves for fetal Hb and HbO_2 differ from those of adults. Many pulse oximeters are featured with a hardware- or software setting to select between fetal or adult patients. Awareness of this and an accordingly correct setting is particularly important if equipment circulates among various hospital departments.

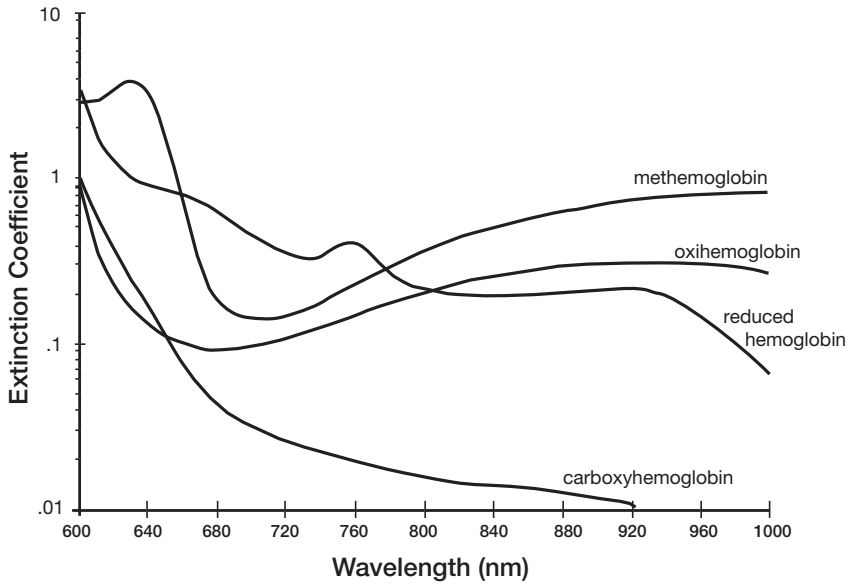

Fig. 5: Absorbtion spectra of different types of Hemoglobin [13].

The blood volume percentage occupied by cells (hematocrit) also influences the optical properties of blood and thereby of pulse oximeter values. This is caused by the fact that SpO_2-calculations are based upon Beer-Lamberts' law, which however has limitations in strongly scattering ("turbid") media like human tissue. The amount of scattering is (amongst others) depending from hematocrit (Twersky-effect).
Chromophores injected into the bloodstream (e.g. methylene blue) can also influence SpO_2-registrations. This knowledge can be usefully applied. Special pulse oximeters are commercially available that can derive cardiac output and blood volume from a single indocyanin green (ICG) injection [22].

1.2.4 Pulse oximetry cannot fully replace human observation

Technology should never be taken for granted and blindly applied. For staff it is always important to have insight in the backgrounds and constraints of any applied technology. Such knowledge is crucial for decisions when to believe an instrument and when to believe your own eyes .
Logically, in specialisms where the color of tissue offers crucial diagnostic information, proper lighting requirements should be met in order to keep an eye on the patient. The clinical view on the patient should never be neglected just because a patient is connected to a monitoring device.

1.3 Pulse oximetry works fine as it is, why develop an imaging modality?

The research described in this thesis was initiated and driven by the desire to realize an imaging modality for blood oxygenation. The reasoning behind this desire is as follows:
The near infrared offers a relatively large optical penetration depth into the human body, which is cleverly used by pulse oximetry. Still a pulse oximeter, however useful and sophisticated, only facilitates measurements on one contact spot, which does not necessarily have to represent the status throughout the whole body. Pulse oximetry is arguably a clinically relevant physiologic monitoring technique, and it is often called the fifth vital sign [23]. For such an important parameter even the faintest idea that might lead to further exploration of the near infrared window, is worth to take a closer look at. This thesis shows some technological possibilities that offer interesting new perspectives by extending the clinicians' vision beyond the boundaries of the human eye. Exploiting the imaging possibilities offered by the near infrared window may help clinicians to improve their view on the patient. Medical history has learned us that extended diagnostic tools (and especially imaging modalities) can lead to better understanding which in turn can lead to better possibilities for treatments.

1.4 Outline and aim of this thesis

The research described in this thesis was initiated by an idea for a camera-concept that should be capable of imaging tissue oxygenation. Chapter 2 contains the pertaining patent WO01/15597 which has been granted. Since the original formal style of the original patent text is rather incomprehensible for those not skilled in the art of patent law, a short patent description has been added as an explanatory introduction.
Unfortunately, the approach to straightforward build a camera device with full functionality as described within the patent would require an enormous investment and a combination of methods and materials at the edge of technology. Therefore it made sense, by performing relatively simple experiments, to investigate whether some important basic requirements needed for a successful device, indeed could be met.
The main question was whether the biological photoplethysmographic signals at 3 different wavelengths, which were needed to calculate oxygen saturation could be derived from the tissue in the first place. Therefore we performed the experiment described in chapter 3 and succeeded in demonstrating that such signals indeed could be recorded (although improvements clearly were desirable). With our simple camera setup, we could only sequentially measure each wavelength, whereas the core idea of the patent was to acquire all 3 traces simultaneously. Building hardware to achieve such parallel acquisition would require a large budget and a long lead time. Before undertaking such large efforts there should be some proof of principle that the invest-

ments would be justified. Therefore we designed a work-around which would allow us to use our existing camera with sequential acquisition of the 3 wavelengths. This involved a tissue phantom for which each heartbeat would be exactly the same, so that 3 registrations could be regarded as a virtual parallel acquisition. The idea behind such a tissue phantom is described in our patent application EP1726256A1 [24] which forms chapter 4 (again an explanatory description is added). Practical experiments carried out with a first prototype tissue phantom setup are described in chapter 5. In chapter 6 we use a modified tissue phantom to demonstrate that regions with high and low oxygen saturation indeed can be distinguished by our camera and represented in a false color image.

During the experiments as described in chapter 3, an idea for a spin-off technology arose. This idea came down to a method of non-invasive remote enhancement of the visibility of superficial blood vessels. This idea resulted in submission of a patent, published as EP1566142A1 [25] which forms chapter 7 (of course also here a short explanatory patent description has been added).

The next two chapters describe experiments within a clinical setting using a prototype of this blood vessel enhancer. Chapter 8 focusses on imaging through the intact skin, whereas chapter 9 describes results obtained by imaging exposed porcine and human hearts during open heart surgery.

1.5 References

[1] Gilbert DL, *The first documented report of mountain sickness: the China or Headache Mountain story*. Respir Physiol, 1983. 52(3): p. 315-26.

[2] Apgar V, *A proposal for a new method of evaluation of the newborn infant.* Current researches in anesthesia & analgesia, 1953. 32(4): p. 260-7.

[3] Paul Y, *Examination of the newborn*. Indian J Pediatr, 1973. 40(301): p. 69-78 contd.

[4] Ross JV, *Color changes in the extremities as they relate to peripheral vascular disease*. Angiology, 1965. 16(9): p. 514-20.

[5] Winslow EH, *Visual inspection of the patient with cardiopulmonary disease*. Heart Lung, 1975. 4(3): p. 421-9.

[6] Farmer J, *Blood oxygen measurement,* in *Design of pulse oximeters*, J.B. Webster, Editor. 1997, Institute of Physics Publishing, Dirac House, Temple Back, Bristol BS1 6BE, UK: Bristol. p. 21-39.

[7] Schotz S, Bloom SS, Helmsworth FW, Dodge HC and Birkmire L, *The ear oximeter as a circulatory monitor. II. The infrared pulse, a moment-to-moment guide to cardiac output*. British Journal of Aneasthesia, 1959. 31(5): p. 190-198.

[8] van Eck CR, *Oxymetry with the haemo-reflector and the cyclops*. Anasthesie et Analgesie, 1951. 8(4): p. 691-695.

[9] Tammeling GJ, Zijlstra WG and Mook GA, *Fundamentals & limitations of the Cyclops reflection method for continuous measurement of arterial oxygen saturation*. Thoraxchirurgie, 1957. 5(2): p. 119-138.

[10] Aoyagi T, Kishi M, Yamaguchi K and Watanabe S. *Improvement of an ear-piece oximeter.* in *13th annual meeting of the Japanese Society for Medical Electronics and Biological engineering*. 1974. Osaka.

[11] Severinghaus JW, Astrup P and Murray JF, *Blood gas analysis and critical care medicine*. Am J Respir Crit Care Med, 1998. 157(4 Pt 2): p. S114-22.

[12] Severinghaus JW and Honda Y, *History of blood gas analysis. VII. Pulse oximetry.* Journal of Clinical Monitoring, 1987.

[13] Wieben O, *Light absorbance in pulse oximetry,* in *Design of pulsoximeters*, J.G. Webster, Editor. 1997, Institute of Physics Publishing, Dirac House, Temple Back, Bristol BS1 6BE, UK: Bristol. p. 40-55.

[14] Wieringa FP, *Imaging apparatus for displaying concentration ratios*, WO 01/15597 A1, 2001.

[15] Miyasaka K, *Do we really know how pulse oximetry works?* Journal of Anesthesia, 2003. 17: p. 216–217.

[16] Aoyagi T, *Pulse oximetry: its invention, theory, and future*. Journal of Anesthesia, 2003(17): p. 259–266.

Chapter 2

A possible concept for SpO_2 camera technology

This chapter is based upon the following acknowledged patent:
"Imaging apparatus for displaying concentration ratios"
invented by F.P. Wieringa
published in 2001
by the World Intellectual Property Organization with reference WO 01/15597 A1

2.1 Explanatory introduction to this chapter

The content of this chapter is based upon patent document WO 01/15597 A1 *"Imaging apparatus for displaying concentration ratios"*, describing a method for non contact arterial oxygen saturation imaging, based upon simultaneous detection of a 2-dimensional-matrix of spatially resolved optical plethysmographic signals at 3 different wavelengths. In plain text this means that it is claimed to be possible to produce an image of blood oxygenation distribution in tissue by using a remote camera that simultaneously acquires images at 3 different wavelengths.
We know that a pulse oximeter is very well capable to measure arterial oxygen saturation by acquiring photoplethysmographic signals at 2 different wavelengths, but needs application of a sensor onto the tissue at a particular body site. Compared to a pulse oximeter, the camera virtues are: *no requirement for bodily contact and imaging of oxygenation distribution*.
The third wavelength is crucial to achieve these camera virtues. Just like with a pulse oximeter, the oxygen-related information is derived from two of the applied wavelengths (e.g. 660 and 940 nm). The third wavelength, however, does not contain any oxygen information at all, since it is deliberately set to a value (preferably 810 nm) where the absorption curves of Hb and HbO_2 intersect and cross each other. This offers an "oxygen-independent" reference image, containing all artefacts like shadows and reflections that are also contained in the other two images (which, however, both additionally contain the desired oxygen information).
Using appropriate software, the oxygen information can thus be distilled from the combined images while distortion from shadows , reflections, motion artefact, etc. can be largely suppressed.
The patent furthermore comprises an option to display normal color images in the visible range. Since the previously mentioned 660 nm already lies in the red range only a green and blue channel have to be added in order to also obtain RGB-images.

2.3 Imaging apparatus for determining concentration ratios

2.3.1 Abstract

Imaging apparatus for representing an image of concentration ratios between a first and a second substance in a region of interest of an object, with different measuring values being represented with different colors and/or gray shades.
The apparatus comprises a light source capable of irradiating the object with light, which light comprises at least three wavelengths λ_1, λ_2 and λ_3, λ_3 being an isobestic wavelength, λ_1 being a wavelength at which the first substance has a lower absorption than the second substance, and λ_2 being a wavelength at which the first substance has a higher absorption than the second substance. The apparatus further comprises detection means comprising a matrix of pixel detectors, for representing a virtually instantaneous image of the region of interest.

2.3.2 Patent description

This invention relates to an imaging apparatus for representing an image of concentration ratios between a first and a second substance in a region of interest of an object, with different measuring values being represented with different colors and/or gray shades, comprising a light source capable of irradiating the object with light, which light comprises at least three wavelengths λ_1, λ_2 and λ_3, λ_3 being an isobestic wavelength, λ_1 being a wavelength at which the first substance has a lower absorption than the second substance, and λ_2 being a wavelength at which the first substance has a higher absorption than the second substance; detection means for at least detecting the intensity of modified light emitted from the object at the respective wavelengths λ_1, λ_2 and λ_3, resulting in detection signals S_1, S_2 and S_3; a processing unit for calculating an optical image of the pattern of concentration ratios, from the respective signals S_1, S_2 and S_3; and display means for representing the calculated optical image.
Such an apparatus as described in the preamble is known from U.S. patent specification US-5,318,022. In this patent specification, it is described how with a narrow light beam consisting of three wavelengths a human eye is scanned, making use of the different absorption behavior of blood at different wavelengths. This is caused by the different absorption characteristics of oxyhemoglobin (HbO_2) and deoxyhemoglobin (Hb). The wavelengths are selected such that light of a first wavelength λ_1 sustains a relatively low absorption in oxygen-rich blood, while light of a second wavelength λ_2 is absorbed relatively strongly in oxygen-rich blood, both in relation to an absorption in oxygen-poor blood. The so-called isobestic wavelength λ_3 is the wavelength at which no difference in absorption occurs with respect to oxygen-poor blood. This wavelength λ_3 lies between the first and second wavelengths λ_1 and λ_2 and serves as reference.
Of interest, in practice, is the concentration ratio of those two substances, represented formulaically by $\frac{HbO_2}{Hb + HbO_2} \times 100\%$

It is clear that the apparatus according to the known technique is not suitable for making optical images with a high resolution, both in the time domain and in the place domain. An intrinsic limit on this resolution is imposed in that the images are built up by sequentially scanning a grid-shaped pattern with a narrow beam, from which an image is derived through synchronization. Clearly, such an apparatus can only yield images of limited grade. In particular, the apparatus is not suitable for producing a virtually instantaneous image of a region of interest of an object, which can be analyzed with sufficient resolution in time.

The object of the invention is to enable a reliable detection of the oxygen content in blood, which can be performed virtually continuously in time. To that end, the invention provides an imaging apparatus as described in the preamble, wherein the detection means comprise a matrix of pixel detectors for representing a virtually instantaneous image of the region of interest. This renders sequential scanning of a grid pattern superfluous, so that the feasible image frequency increases by a factor equal to the square of the desired number of pixels/inch. Thus, virtually instantaneous measuring results over a whole region of interest can be obtained.

In a preferred embodiment, the light signals S_1, S_2 and S_3 have a characteristic modulation. What is thus achieved is that the apparatus can be made insensitive to non-modulated signals, such as ambient light. Also, if the sensors in the apparatus have a sensitivity to different wavelength bands, the contributions of the different wavelengths to the output signal of the apparatus can be determined by demodulation of the signal. Modulating the light signal, finally, affords the possibility of raising the light intensity to a maximum without this leading to distortion. The applications hereof will be further elucidated in the description of the drawings.

In a further preferred embodiment, the imaging apparatus is suitable for determining measurements consecutive in time. The apparatus may further comprise means for analyzing the measuring values. Relevant parameters can be determined and analyzed, such as the time-average value and deviation, minimum and maximum, as well as, given an assumed cyclic change of the concentration ratio, the spectral features of the waveform.

In an application of the invention as a detector for determining the ratio of hemoglobin and oxyhemoglobin in blood, with the first and second substance being hemoglobin and oxyhemoglobin, respectively, the signal sources are so arranged that the first wavelength λ_1 is in the wavelength range of 600 to 700 nm, with a preference for 660 nm, the second wavelength λ_2 is in the wavelength range of 900 to 1000 nm, with a preference for 940 nm, and the third wavelength λ_3 is in the wavelength range of 790 to 830 nm, with a preference for 810 nm.

Preferably, the apparatus further comprises means for analyzing the measured values numerically. Such means can be image analysis means. They may also be means that represent the value of the reference signal S_3, thus yielding an image of the light absorption that is independent of the oxygen level. This reflects the actual vascular volume, which enables plethysmographic measurements to be performed. The means

can comprise the analysis means mentioned earlier, as well as the possibility of determining region averages and the time development of such parameters. The means may further comprise indicating means for defining such a region of interest, such as a light pen, tracker ball or mouse indication. Also, the analysis means may comprise the possibility of comparing the measuring values with reference values, or with the values measured in corresponding parts in the left-side or right-side parts of the body.

In a preferred embodiment, the apparatus comprises detectors which, in addition to the wavelengths λ_1, λ_2 and λ_3 , can also scan visible light, so that the apparatus is also suitable for forming an image of visible light. The measuring signals S_1, S_2 and S_3 can then be distinguished from the visible light by modulation technique. The combination of an image of visible light with the image of the oxygen concentration levels and/or the vascular system (called SpO_2 image for short) provides advantages in the application of the invention in probe examination, the probe then being provided with the apparatus according to the invention. By reading out the images of visible light, steering can be roughly controlled, while through the measuring signals in situ an accurate picture of the vascular system and/or the oxygen concentrations therein can be obtained. The image of visible light and the pattern of concentrations or concentration changes can be projected in a single overlapping image, which improves orientation in the body in manipulating the probe.

The invention further relates to an image observing apparatus, such as a camera or endoscope with an imaging apparatus as described above.

In the following, the invention will be further elucidated with reference to the drawings, wherein

Figure 1 is a graphic representation of the spectral absorption capacity of deoxyhemoglobin (Hb) and oxyhemoglobin (HbO_2);

Figure 2 is a diagram of an imaging apparatus according to the invention; and

Figure 3 is a representation of the spectral sensitivity of the light sensors arranged in the apparatus.

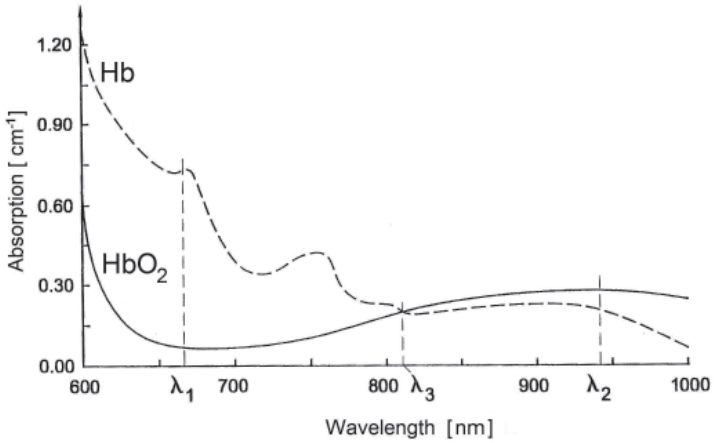

Figure 1

Referring to Figure 1, the broken line reflects the spectral absorption capacity of deoxyhemoglobin (Hb), while the full line reflects the spectral absorption capacity of oxyhemoglobin (HbO_2) in $10^{-6}cm^2$/equivalent. In the figure, it can be seen that the absorption capacity of Hb as well as of HbO_2 is virtually constant at 660 to 670 nm. This range relates to the first wavelength λ_1 mentioned in the preamble, at which the absorption coefficient of HbO_2 is much lower than that of Hb. This accounts for the brightly red color of oxygen-rich blood. At 810 nm the absorption capacity of Hb and HbO_2 is equally large (isobestic point). This wavelength relates to the third wavelength λ_3 mentioned in the preamble. Above this wavelength, HbO_2 absorbs more strongly, in particular in the range around 940 nm, which wavelength corresponds to the second wavelength λ_2 mentioned in the preamble. Through a comparative measurement at a wavelength above 810 nm with a measurement at about 660 nm, the ratio of Hb and HbO_2 can be determined.

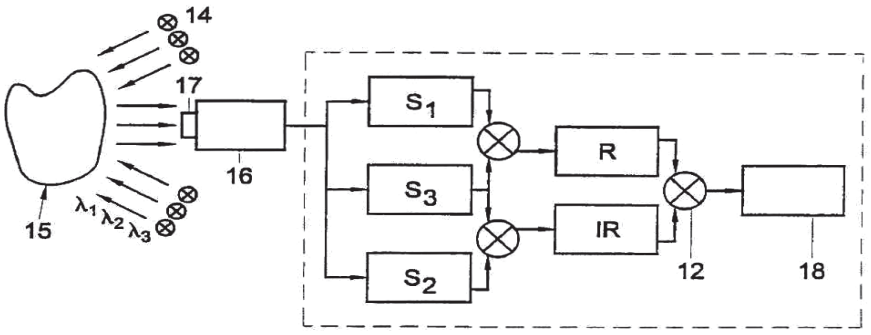

Figure 2

Figure 2 schematically represents a setup for a reflection measurement on an object 15, which consists of biological tissue. The object is illuminated by light source 14 with wavelengths λ_1, λ_2 and λ_3. The light source is arranged in a ring around a probe 16, so that a body part to be examined, which is disposed opposite the light passage 17, is uniformly exposed to light. The light that is reflected by the tissue is transmitted via glass fiber, optical fibers and/or lens systems to a camera, which has a sensitivity range in the above-mentioned wavelength ranges around λ_1, λ_2 and λ_3. The invention can be applied, for instance, by modifying commercially available CCD cameras or CMOS cameras by adapting the sensitivity range of the sensors by employing the filters as has been described hereinabove. In a preferred embodiment that utilizes a so-called 3 CCD camera, simultaneous measurements at the relevant wavelengths can be performed. It is also possible, however, to modify a simple black-and-white CCD camera, in which case, however, a (three times) lower sampling frequency needs to be used.

The signals S_1, S_2 and S_3 coming from the camera are combined into a normalized red image R, by subtraction of the signals S_1 and S_3, and into a normalized infrared image IR, by subtraction of the signals S_2 and S_3. The signals are subsequently applied to processing unit 12, which calculates the concentration ratio by comparing the signals S_1 and S_2 with respect to the signal S_3 by determining the ratio of the difference signal that is obtained by subtraction of the signals S_1 and S_3 and the difference signal that is obtained by subtraction of the signals S_2 and S_3.

The output values are graphically represented by means of a sliding color scale in a screen 18, where low output values, corresponding to a relatively low oxygen concentration, are indicated by a blue color, and high output values, corresponding to a relatively high oxygen concentration, are indicated by a red color. Further, the apparatus, given a sufficiently high sampling frequency, affords the possibility of representing the time-derived image, with high oxygen concentration fluctuations reflecting regions with an evidently high oxygen uptake. As such, the apparatus according to the invention provides the possibility of tracing tumors (in which an increased oxygen consumption occurs). The technique is further suitable for the in vivo analysis of

oxygen concentration in a tissue, thus yielding possibilities for vascular diagnostics. Tissue can be inspected for blood saturation, thrombosis and burns. In a surgical application, the technique offers possibilities of visualizing infarcts.

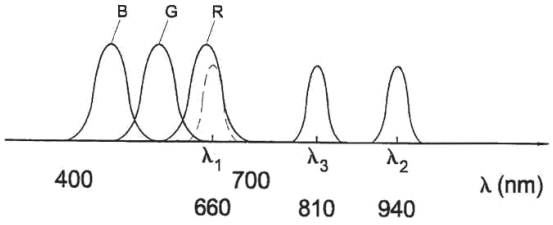

Figure 3

Fig. 3 represents the wavelength ranges in which the CCD camera is sensitive. A common color CCD camera has a triple band sensitivity, one in the red (R) range, one in the green (G) range and one in the blue (B) range. With these color sensitivities, as is well known, light from the entire visible spectrum can be discerned. The camera is stabilized for white light, so that a normal visible image can be projected. In addition, with the camera, for the purpose of determining the oxygen concentration, a calibration can be performed, whereby the camera is aimed at one or more surfaces having an absorption spectrum of a known value. In the SpO_2 mode, the visible light is cut off by an optical low pass filter, and the sensor is sensitive to the wavelength range of λ_1, λ_2 and λ_3, respectively. This is the case when the red light sensor (R) is also sensitive to the λ_1 (660 nm), the green light sensor (G) has a sensitivity to λ_2 (940 nm), and the blue light sensor (B) has a sensitivity to λ_3 (810 nm). Other combinations are also possible, but these combinations offer the best results in practice. The camera can be alternately brought into the normal and SpO_2 mode by emitting alternately visible light and (infra)red light or by arranging an ancillary filter, so that the camera is rendered sensitive to a different wavelength range. A different manner of simultaneous sampling can be employed, for instance by modulating the measuring signal, and emitting the visible light with a constant intensity. By frequency decomposition of the signal, the visible light can be separated by the measuring light.

The alternation between the visible image and the SpO_2 image can be set by the user, so that, given a sufficiently high sampling, both images are available simultaneously. These images can be projected in one screen or on two separate screens.

In a separate mode, through a different processing of the measuring signal S_3, the carbon monoxide content in blood can be determined. The signal is then not used as a reference signal. The signal is related to the oxygen concentration in blood as determined in the classic manner (i.e. determined once per pulse). Since HbCO (i.e., carbon monoxide bound to hemoglobin) has a deviant absorption at 810 nm, the content of HbC0 can subsequently be determined. The apparatus can be arranged such that work is done in alternating mode.

With the apparatus, for all registered time-dependent parameters, given a sufficiently high sampling frequency during a cardiac cycle the course can be analyzed, e.g. by means of Fourier analysis. The apparatus provides the possibility of analyzing the measured values numerically, and to determine time-average values and deviation, minima and maxima, etc., as well as the time development of such parameters. This is understood to mean, though not exclusively so: the provision of brighter or more contrastive images, inter alia by (noise) filtering. Also, the value of the reference signal S_3 can be separately represented, so that an image is formed of the light absorption that is independent of the oxygen level. This reflects the actual vascular volume, so that plethysmographic measurements can be performed. The apparatus affords the possibility of determining time-average values and deviation, minima and maxima, as well as region averages and time development of such parameters. The apparatus can further comprise indicating means for defining a region of interest, such as a light pen, tracker ball or mouse indication. Also, measuring values can be compared with reference values, or with the values measured in corresponding parts in left-side or right-side parts of the body.

Although the exemplary embodiments described relate to an endoscope, the technique can also be used in other invasive or non-invasive image observing equipment, such as an otoscope, colposcope or (surgery) microscope. Further, the invention can be employed in combination with other measuring devices, such as, for instance, an ECG apparatus or a monitoring monitor. As a consequence, it is possible, for instance, to relate the parameters registered by the apparatus according to the invention to an ECG curve. The invention is therefore not limited to the exemplary embodiments described with reference to the drawing, but comprises all kinds of variations thereof, naturally insofar as they fall within the scope of protection of the following claims.

2.3.3 Claims

1. An imaging apparatus for representing an image of concentration ratios between a first and a second substance in a region of interest of an object, with different measuring values being represented with different colors and/or gray shades, comprising:

- a light source capable of irradiating the object with light, which light comprises at least three wavelengths λ_1, λ_2 and λ_3, λ_3 being an isobestic wavelength, being a wavelength at which the first substance has a lower absorption than the second substance, and λ_2 being a wavelength at which the first substance has a higher absorption than the second substance;
  detection means for at least detecting the intensity of light emitted by the object at the respective wavelengths λ_1, λ_2 and λ_3, resulting in detection signals S_1, S_2 and S_3;
- a processing unit for calculating an optical image of the pattern of concentration ratios, from the respective signals S_1, S_2 and S_3;
- display means for displaying the calculated optical image, characterized in that the detection means comprise:

- a 3CCD camera, each CCD of said camera adapted for receiving one of said wavelengths λ_1, λ_2, λ_3, said CCD's generating signals S_1, S_2, S_3 respectively, to be processed in said processing unit, thereby representing a virtually instantaneous image of the region of interest.

2. An imaging apparatus according to claim 1, characterized in that the apparatus is arranged for forming an image of visible light and that the pattern of concentration ratios is projected in one overlapping image with the visible image.

3. An imaging apparatus according to at least one of claims 1-2, characterized in that the light signals of wavelengths λ_1, λ_2 en λ_3 have a characteristic modulation.

4. An imaging apparatus according to claim 3, characterized in that it is arranged, given an assumed cyclic change of the concentration ratio, such that it can analyze the spectral features in the frequency domain thereof.

5. An imaging apparatus according to any one of the preceding claims, characterized in that to determine the ratio of hemoglobin and oxyhemoglobin in blood, with said first and second substance being hemoglobin and oxyhemoglobin, respectively, the signal sources are so arranged that the first wavelength λ_1 is in the wavelength range of 600 to 700 nm, with a preference for 660 nm, the second wavelength λ_2 is in the wavelength range of 900 to 1000 nm, with a preference for 940 nm, and the third wavelength λ_3 is in the wavelength range of 790-830 nm, with a preference for 810 nm.

Chapter 3

Contactless multiple wavelength photoplethysmographic imaging: A first step towards "SpO_2 camera" technology

This chapter is based upon the following publication:
"Contactless multiple wavelength photoplethysmographic imaging: A first step towards "SpO2 camera" technology"
by F.P. Wieringa, F. Mastik and A.F.W. van der Steen
published in Annals of Biomedical Engineering Vol. 33, No. 8, August 2005 pp. 1034-1041

3.1 Abstract

We describe a route towards contactless imaging of arterial oxygen saturation (SpO_2) distribution within tissue, based upon detection of a 2-dimensional-matrix of spatially resolved optical plethysmographic signals at 3 different wavelengths.

As a first step towards SpO_2-imaging we built a monochrome CMOS-camera with apochromatic lens and 3λ-LED-ringlight (λ_1 = 660 nm, λ_2 = 810 nm, λ_3 = 940 nm; 100LEDs λ^{-1}). We aquired movies at 3 wavelengths while simultaneously recording ECG and respiration for 7 volunteers. We repeated this experiment for 1 volunteer at increased frame rate, additionally recording the pulse wave of a pulse oximeter. Movies were processed by dividing each image frame into discrete Regions Of Interest (ROIs), averaging 10 x 10 raw pixels each. For each ROI, pulsatile variation over time was assigned to a matrix of ROI-pixel time traces with individual Fourier spectra.

Photoplethysmograms correlated well with respiration reference traces at 3 wavelengths. Increased frame rates revealed weaker pulsations (main frequency components 0.95 Hz and 1.9 Hz) superimposed upon respiration-correlated photoplethysmograms, which were heartbeat-related at 3 wavelengths.
We aquired spatially resolved heartbeat-related photoplethysmograms at multiple wavelengths using a remote camera. This feasibility study shows potential for non-contact 2-D imaging reflection-mode pulse oximetry. Clinical devices, however, require further development.

Keywords
Pulse oximetry
Multispectral imaging
Contactless measurement of respiration and heart action

3.2 Introduction

The visual diagnosis of cyanosis (skin colour shift towards blue) probably is the earliest spectrally resolved optical method for detecting decreased blood oxygenation (hypoxia) [1]. Cyanosis combined with a weak, irregular or absent palpable pulse indicates a life threatening condition that requires immediate attention. However, prolonged manual and visual monitoring of critical patients is both inaccurate and impractical. This may explain early attemps to use primitive opto-electronic devices for haemodynamic patient monitoring. Various devices for photoplethysmography and blood oxygenation measurement evolved since the 1930s, but technology remained cumbersome until Aoyagi exploited the pulsatile nature of arteries as a discriminator between absorbance caused by arterial blood versus other tissue absorbance components [2]. This marked the birth of reliable bedside pulse oximetry, which spread rapidly, since it offered a simple non-invasive technique to simultaneously monitor heart rate, plethysmographic pulse waveform and arterial oxygen saturation (SpO_2) [3-7].

Within a few decades, pulse oximetry has changed many clinical routines just as drastically as the introduction of reliable thermometry did within three centuries [8-10]. Beside this clinical impact, there is another analogy between pulse oximeters and conventional thermometers: In both cases contact with the body is required to produce a numerical value that relates to one particular spot. As for temperature measurement however, developments continued and pyrometers (contactless single-spot thermometers) emerged, soon followed by thermal cameras which currently serve many useful applications.

Remote-sensing images offer added value for any parameter by appealing to human cognition and literally facilitate insights that would otherwise be difficult or even impossible to obtain [11]. On the basis of the practice-proven added value of our thermal imaging example, we therefore suggest the development of an SpO_2 camera as a next step in oxygen-saturation measurement.

Contact technologies offering SpO_2 imaging have already been developed in various forms, all requiring optical probes to be positioned on the tissue [12-14].

Contactless single-spot SpO_2 measurement without imaging functionality also has been demonstrated [15]. Apart from the non-contact feature, this single-spot technique is based upon the calculus applied most widely within contemporary clinical pulse oximeters, i.e. the “ratio of ratios” method [16-18]. This method derives arterial oxygenation from the ratio between photoplethysmographic peak-to-peak pulse wave amplitudes aquired at ≥ 2 different wavelengths.

While our approach to develop an SpO_2 camera is also based upon the ratio of ratios method, it involves simultaneous non-contact detection of a 2-dimensional matrix of spatially resolved optical plethysmographic signals at 3 different wavelengths [19]. Amongst other variables (such as geometry, shadows and reflections) the images captured at two of these wavelengths contain oxygenation-related information. The third wavelength, however, is used to aquire images that exclude oxygenation-rela-

ted information but which include the other variables referred to above. In this paper we report upon an experimental camera device (intended as a first step towards an SpO_2 camera) as well as upon recordings of image-derived photoplethysmographic signals aquired from the lower arms of 7 volunteers at 3 wavelengths. We correlated these signals to simultaneously recorded physiological signals (ECG, Respiration and Photoplethysmographic pulse wave) in order to estimate their physiological significance.

3.3 Methods

3.3.1 Instrumental setup

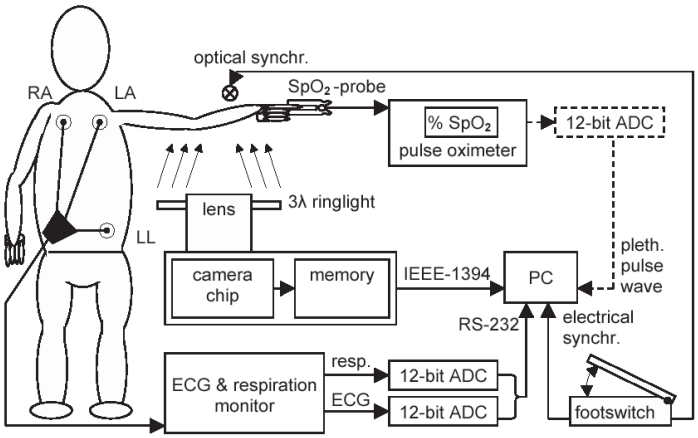

Figure 1: Experimental setup

The experimental setup is schematically drawn in figure 1. A pulse oximeter probe (Nellcor, N-200) was placed on the index finger of the left hand. Furthermore a monitor offering combined 3-lead ECG and respiration registration (Hewlett & Packard, 78354A) was connected to the subject. The analog ECG and respiration signal outputs of this monitor were fed into a 2-channel 12-bit A/D converter and then logged into a PC (18000 samples; sample rate 100 Hz).

An experimental monochrome CMOS-camera (Fillfactory Belgium, modified) with a global shutter and a detector resolution of 1024 x 1280 pixels was focussed at the skin of the subjects' left inner arm (elbow to wrist region) using a custom built apochromatic lens. The distance between camera lens front and skin was approximately 72 cm.

Around this lens a custom built 3-wavelength LED-ringlight was mounted (λ_1 = 660 nm, λ_2 = 810 nm, λ_3 = 940 nm; 100LEDs λ^{-1}). Camera settings and LED-currents were adjusted to compensate for spectral sensitivity variations by white balancing on a Spectralon® target.

A small incandescent lamp (collimated to avoid straylight on tissue) was placed within a fixed position in a corner of the cameras' field of view. Lamp voltage (DC) was logged into the PC as an event marker, thus facilitating software synchronization between aquired images and recorded physiological signals.
All experiments were performed in a darkroom, using only one wavelength at a time. A black baffle prevented optical crosstalk by shielding camera and tissue from optical display emissions of other equipment.

3.3.2 Experimental protocol 1

Healthy human volunteers (caucasian; n = 7; 6 male; 1 female; age 28.1 ± 5.6 yr; age range 23 – 39 yr). The subjects were seated on an adjustable chair with their left arm resting on a cushioned support, which was covered with a black cloth. The spectral neutrality of this cloth had been verified from 400 to 1000nm. Subjects were asked to sit at ease and rest their left arm as still as possible during the examination. Using a pulse oximeter (probe on left index finger) the subjects' SpO_2 was monitored and manually annotated. The left inner arm of each subject was exposed to diffuse non-coherent monochromatic optical radiation and filmed with a digital CMOS-camera. For each subject 3 movies at different wavelengths were recorded. Each movie had a duration of 18 s and consisted of 120 frames (6.7 frames s^{-1}; 1280 x 1024 raw pixels per frame; $T_{exposure}$ = 85 ms). ECG and respiration were recorded for a period of 3 minutes (thus allowing verification of stable heartrate and respiration). Approximately halfway this period the camera was started. Just after camera start, a footswitch was engaged for approximately 10 seconds thus synchronously adding an electrical marker to the recorded physiological signals and an optical marker to the aquired images. During off-line processing physiological signals and images were synchronized using these markers.

3.3.3 Experimental protocol 2

In order to investigate the nature of pulsatile variatons, superimposed upon the camera derived respiratory signals that resulted from experiment 1, an additional experiment with 1 volunteer (male, age 28 yr) was performed. This volunteer had a low and stable heartrate, thus resulting in a high number of image frames per heartbeat, which facilitated Fourier analysis. The hardware setup for this additional experiment was extended with an extra 12 bit A/D converter to record the plethysmographic pulse wave output signal of the pulse oximeter. In order to increase framerate and movie duration, the stored image portion was reduced (640 x 480 raw pixels; $T_{exposure}$ = 50 ms per frame) and by placing the ringlight 10 cm closer to the skin, $T_{exposure}$ could be shortened to 50 ms. These measures facilitated recording of 780 frames over a 57 s time span (13.7 frames s^{-1}). The optical synchronization lamp was furthermore coupled to an optical fiber to allow placement within the narrowed field of view. All other factors were kept the same as during the previous experiment.

3.3.4 Image aquisition

For each subject subsequential discrete runs were taken using three different wavelengths (λ_1 = 660 nm, λ_2 = 810 nm and λ_3 = 940 nm) always starting with the shortest wavelength. Ringlight currents (350 mA @ λ1 ; 350 mA @ λ_2 ; 400 mA @ λ_3) and diaphragm settings (F2.8 @ λ_1 ; F4.0 @ λ_2 ; F2.0 @ λ_3) were chosen so that for each run the cameras' dynamic range was optimally used while avoiding pixel saturation. During camera standby mode, a preview window allowed aiming and focussing of the camera. After software triggering the camera stored a sequence of 10-bit digitally encoded images in an internal memory (using auto-incremental frame numbering). All image frames then were automatically downloaded via an IEEE1394 bus and saved on harddisk in an uncompressed 16-bit format. All physiological signals and the synchronization marker were stored together in a separate ASCII file.

3.3.5 Image processing (experiments 1 & 2)

Processing was performed with custom developed software (using Matlab®, Mathworks). Figure 2 represents this process. The upper half of figure 2 shows the aquired raw image frames combined in a 3D-matrix. Each raw image frame was divided into discrete Regions Of Interest (ROIs) measuring 10 x 10 pixels each.

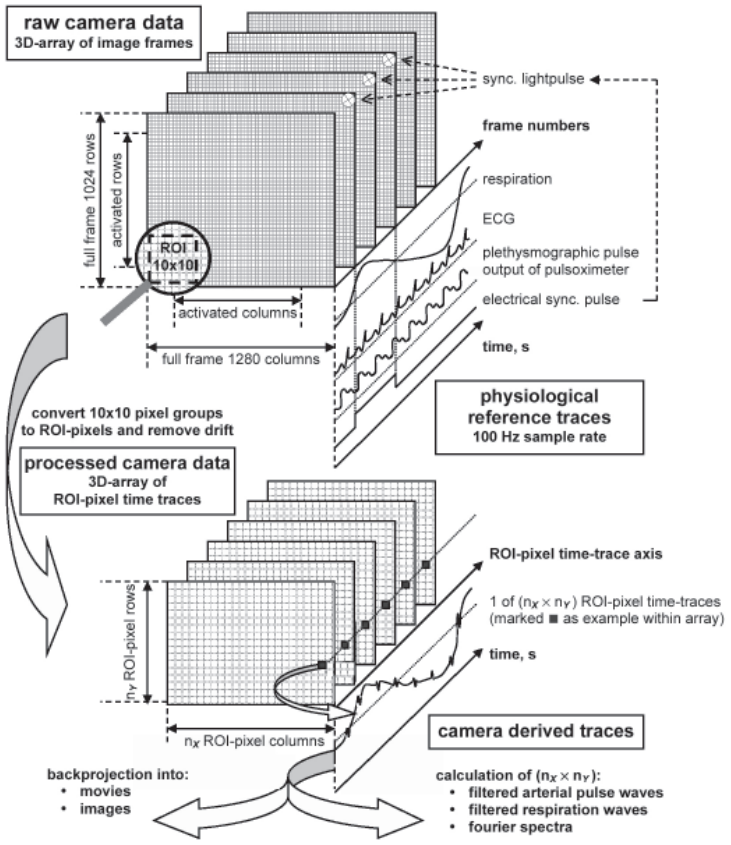

Figure 2: Schematic diagram of image processing.

All recorded images and signals are shown in the upper half of this figure. The raw image frames form a 3D-matrix. An enlarged frame portion shows an ROI containing 10 x 10 raw pixels. Recorded reference traces are projected along the time domain axis.

The lower half of the figure contains processed data in a 3D-array of ROI-pixels. A sketch of a typical time domain trace, derived from an ROI-pixel located on the tissue, is projected in a similar perspective as the recorded physiological reference traces.

Camera-derived traces like arterial pulse waves, respiration waves and Fourier spectra are shown in figure 4.

Raw pixel values within each ROI were averaged, and the value of each ROI-pixel, plotted versus frame number, was subjected to an individual least square third order polynominal fit to remove offset and/or drift in order to distinguish the true pulsatile component. This resulted in a new 3D-matrix of image frames consisting of ROI-pixels as drawn in the lower half of figure 2.

For the upper 3D-array containing raw camera data, time was only encoded within framenumbers. In order to calculate the true time as needed for the lower 3D-array, we synchronized raw camera data with the recorded physiological reference traces (which did have a time stamp). By checking all ROI-pixel versus framenumber traces,

the ROI-Pixel co-ordinates of the applied synchronization lamp were located automatically and the framenumbers for “lamp on” and “lamp off” were manually selected using a graphical interface (accuracy plus or minus one image frame). Subsequently the apropriate ASCII file containing the recorded reference data was read. Using a second graphical interface, the sample numbers for “lamp on” and “lamp off” were manually selected from the recorded electrical synchronization marker trace (drawn underneath the upper 3D-matrix in figure 2). Using these markers, both data sets were synchronized, thus providing accurate true-time stamps for all recorded image frames. The resulting 3D-array contained n_X x n_Y ROI-pixel time-traces (one example is drawn underneath the lower 3D-matrix in figure 2).

3.3.6 ROI-pixel processing (experiment 1)

For this experiment n_X x n_Y equalled 100 x 125 which resulted in 12500 ROI-pixels. For all ROI-pixel time-traces, the cross-correlation with the recorded respiration signal, as well as the phase relation compared to the recorded respiration signal, were determined. This method produces asymmetrically distributed results which are limited to an upper value of +1 and a lower value of –1. Hence, in order to obtain an average correlation across all ROI-pixel time-traces (i.e. per movie) the Fisher-Z transform function was applied to the correlation co-efficients before averaging. After averaging the inverse Fisher-Z transform function was applied. This revealed one mean absolute correlation value per recorded movie.

3.3.7 ROI-Pixel processing (experiment 2)

For this experiment n_X x n_Y equalled 48 x 64 which resulted in 3072 ROI-pixels. ROI-pixel time traces could be displayed for each part of the viewed area using a graphical interface. The availability of 50 heartcycles within the recorded movies also facilitated Fourier analysis of all individual ROI-Pixel time-traces.

In order to summarize these data, 3 false colour images were calculated per movie (see figure 5). These images show the spatial distribution of the relative spectral power values at the respiration frequency (0.16 Hz), the fundamental heart frequency (0.95 Hz) and the first harmonic of the heart frequency (1.9 Hz) respectively.

Possibly heartcycle-related signals were isolated for each ROI-pixel time-trace by filtering out the respiration component using an 8^{th} order 0.5 Hz high-pass phase-neutral Butterworth function. The resulting ROI-pixel time traces were displayed separately.

3.4 Results

3.4.1 Results of experiment 1

For all 7 volunteers the aquired images revealed the superficial subcutaneous vascular structure quite well at all 3 wavelengths. Figures 5j, 5k and 5L show examples of preview-mode images for all applied wavelengths. At 940 nm (figure 5L) more details of the vascular pattern were revealed and pigmented artefacts like hairs were much less pronounced than at shorter wavelengths (figure 5j and 5k). However, due to a relatively low spectral sensitivity of the camera at 940 nm, also more noise was present.
For all 7 volunteers pulsatile signals were found at all 3 wavelengths. These signals correlated well with the recorded respiration reference traces. Figure 3 shows the calculated absolute correlation values for all individual movies.

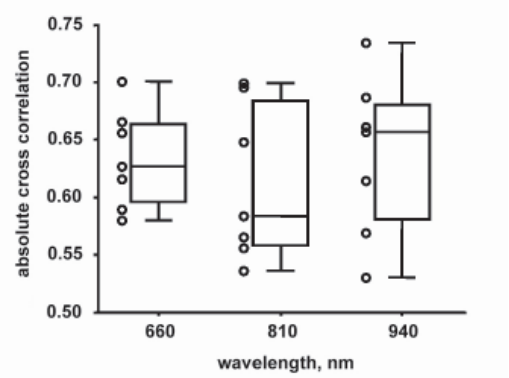

Figure 3: Calculated absolute correlation values for all individual movies
Box and whisker plot of the absolute correlation with the recorded respiration signal, describing the median 90% confidence interval and range of data for 7 volunteers filmed at 3 wavelengths.

Upon close examination of the various ROI-pixel time traces a weak pulsatile variation with higher frequency seemed to be superimposed upon the respiration-correlated signal component. Signal to noise ratios and framerate, however, were insufficient to verify whether this was noise or an arterial pulsation. Therefore an additional experiment was scheduled for one volunteer.

3.4.2 Results of experiment 2

For each wavelength a 20 s sample of the recorded physiological reference data and two camera-derived signals (with and without respiration filter applied) are shown in the left column of figure 4. The full length of all recorded movies was 57 s. The Fourier spectra, shown within the right column of figure 4, were calculated from all 50 heartbeats occuring during aquisition of a movie.

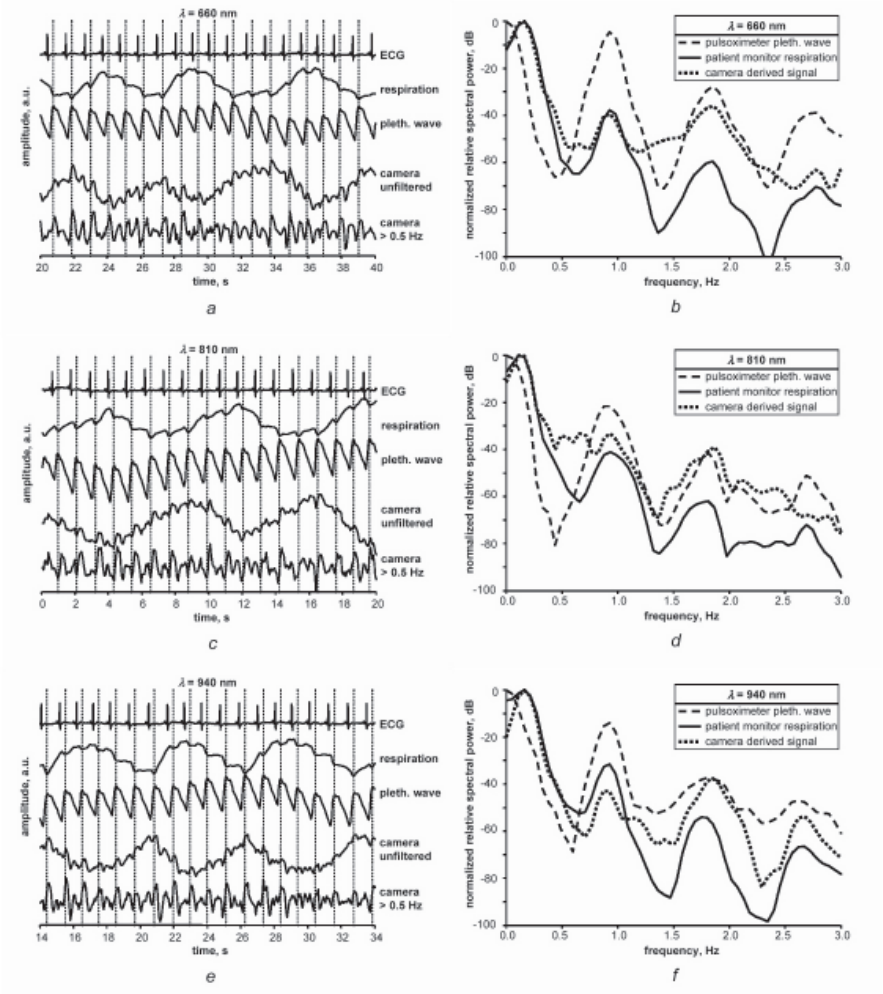

Figure 4: Time domain traces and Fourier spectra of obtained data and reference data

The figures 4a, 4c and 4e show examples of recorded physiological reference traces (ECG, respiration and pulse oximeter plethysmographic output wave) compared to camera-derived signals (unfiltered and 0.5 Hz highpass filtered) at three wavelengths. ECG-derived trigger lines are provided to identify cardiac cycles. The pertaining Fourier spectra displayed in figures 4b, 4d and 4f show distinct frequency peaks at 0.16 Hz (respiration), 0.95 Hz (fundamental heart frequency) and 1.9 Hz (first harmonic of heart frequency).

These Fourier spectra show that the camera-derived signals match well with the respiration reference signal peak at 0.16 Hz, but also with the fundamental heartbeat frequency at 0.95 Hz and its' first harmonic at 1.9 Hz. Note that the pulse oximeter plethysmographic wave has a large offset at 0 Hz but no distinct respiration-matched peak.

The geometrical distribution of relative spectral power at these 3 frequencies (0.16 Hz, 0.95 Hz and 1.9 Hz) is plotted for all 3 wavelengths (660 nm, 810 nm and 940 nm) within figure 5. For orientation purposes, also raw image frames (no processing) are shown.

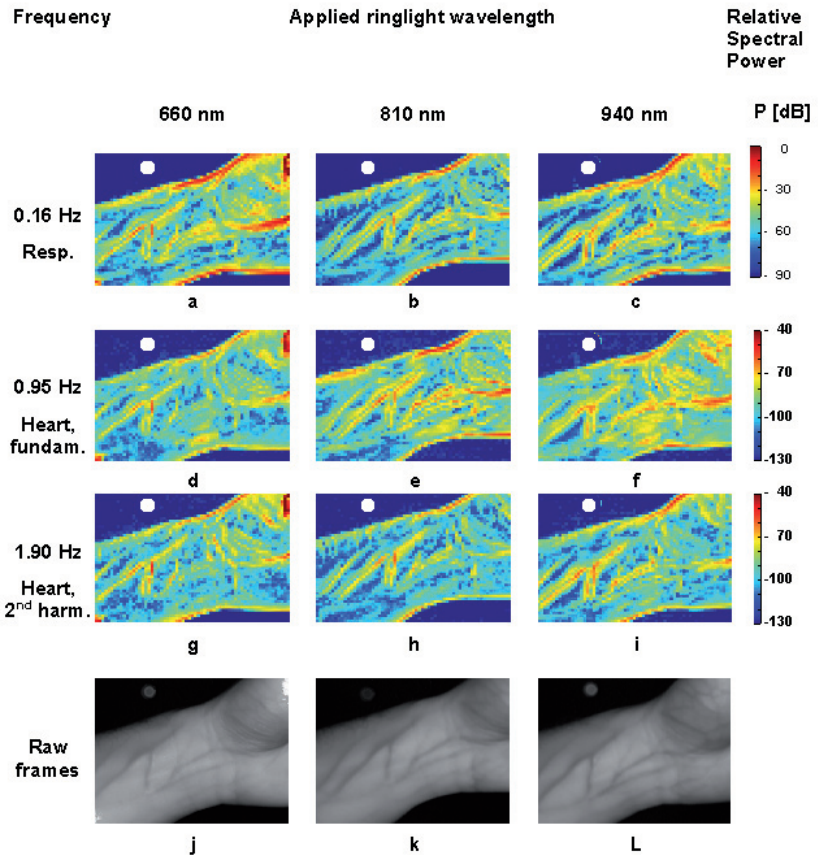

Figure 5: Colour encoded spatial distribution of relative spectral power at 3 different frequencies for 3 different applied ringlight wavelengths.

The synchronization fiber area has been excluded from Fourier analysis and is marked white.

3.5 Discussion

Optical plethysmographic signals have been aquired in 7 volunteers using a non-contact reflection mode imaging technique at 3 wavelengths. These camera-derived plethysmographic signals all contained a distinct respiration-correlated pulsatile com-

ponent. Superimposed upon this respiration correlated component, smaller amplitude variations at a higher frequency were observed.
With an additional experiment (1 test subject at 3 wavelengths) it could be demonstrated that these superimposed variations indeed were heartcycle-related. This is in accordance with earlier observations by Graaff [20], Dassel [21] and Franceschini [22] who however all used contact probes to aquire their photoplethysmographic signals.
We have aimed to acquire all movies of each volunteer at the same framerate for all 3 wavelengths. Since our cameras' quantum efficiency dropped off within the near-infrared, the maximum framerate was thus limited by the maximum output of the ringlight and the minimal required $T_{exposure}$ (plus image frame storage time) with a fully opened diaphragm at a wavelength of 940 nm.
Allthough we have tried to avoid pixel saturation, this has occurred in one case. In two corners of figure 6j (top right and bottom left) some saturated pixels can be discerned. The corresponding areas in the figures 6a, 6d and 6g therefore contain artefacts.
Along the tissue edges, relatively high spectral power values are plotted. This is due to the large contrast being present on tissue boundaries. Any movement of such a boundary region thus results in a very strong ROI-pixel pulsation if either the whole arm moves or if the arm pulsates volumetrically. By plotting the vertical geometrical positions of upper and lower tissue boundaries along the time axis we checked whether they moved simultaneously in one direction (movement of whole arm) or counterphased (volumetric arm pulsation). For all movies of experiment 2, volumetric pulsation dominated.
Our experiments were done at the edge of technical specifications. Especially at a wavelength of 940 nm we experienced a poor signal to noise ratio. Our ROI-pixel Fourier spectra show a span of 100 dB. This, however, was only possible because under dark room conditions the full dynamic range of our camera was reserved for the tissue and because dynamic range could be enlarged by averaging across a large number of raw pixels per ROI. No movement artefact suppression was attempted since the ringlights' limited tissue irradiance restricted framerate (via exposure time). Tissue glare furthermore lowered the pixel saturation treshold, which resulted in limited contrast of subcutaneous structures. The influence of factors like subcutaneous fat, skin thickness, skin pigmentation and blood pressure have not yet been investigated. These problems have to be adressed in further research.

3.6 Conclusions

We demonstrated the feasability of aquiring heartbeat-related spatially resolved plethysmographic signals at multiple wavelengths using a remote camera. This has potential for non-contact 2-D imaging reflection-mode pulse oximetry (SpO_2-camera technology). Clinically useful devices can however only be realized if effective solutions are found for: poor signal to noise ratio, lack of dynamic range, motion artifacts,

ambient light interference, and tissue glare. Additionally the roles of factors like subcutaneous fat, skin thickness, skin pigmentation and blood pressure deserve further attention.

3.7 Acknowledgements

This study was sponsored by TNO Quality of Life in Leiden, the Netherlands.
Custom mechanical constructions were made by Mr. L. Bekkering and support on electronics was given by Mr. J. Honkoop (Biomedical Engineering Thorax Centre, Erasmus MC).

3.8 References

[1] Gilbert DL, *The first documented report of mountain sickness: the China or Headache Mountain story.* Respir Physiol, 1983. 52(3): p. 315-26.

[2] Aoyagi T, Kishi M, Yamaguchi K and Watanabe S. *Improvement of an ear-piece oximeter*. in *13th annual meeting of the Japanese Society for Medical Electronics and Biological engineering*. 1974. Osaka.

[3] New W and Corenman JE, *Pulse oximeter*, US414176, 1982.

[4] Yoshiya I, Shimada Y and Tanaka K, *Spectrophotometric monitoring of arterial oxygen saturation in the fingertip*. Med Biol Eng Comput, 1980. 18(1): p. 27-32.

[5] Aoyagi T, Kobayashi N and Sasaki T, *Apparatus for determining the concentration of a light-absorbing material in blood*, US4832484, 1989.

[6] Severinghaus JW and Honda Y, *History of blood gas analysis. VII. Pulse oximetry*. Journal of Clinical Monitoring, 1987.

[7] Severinghaus JW, Astrup P and Murray JF, *Blood gas analysis and critical care medicine*. Am J Respir Crit Care Med, 1998. 157(4 Pt 2): p. S114-22.

[8] Wunderlich CRA, *Das Verhalten der Eigenwärme in Krankheiten*. 1868, Leipzig: Wigand.

[9] Eberhart RC and Shitzer A, Volume 1 - *Chapter 1: Introduction, in Heat transfer in medicine and biology: analysis and applications*, A. Shitzer and R.C. Eberhart, Editors. 1985, Plenum Press: London. p. 2-4.

[10] Martine G, *Essays and Observations on the Construction and Gradation of Thermometers, and on the Heating and Cooling of Bodies*. 1st edition ed. 1740, Edinburgh.

[11] Woods DD, Patterson ES and Roth EM, *Can we ever escape from data overload? A cognitive systems diagnosis*. Cognition Technology & Work, 2002(4): p. 22-36.

[12] Boas DA, Franceschini MA, Dunn AK and Strangman G, *Noninvasive imaging of cerebral activation with diffuse optical tomography,* in *In vivo optical imaging of brain function*, R.D. Frostig, Editor. 2002, CRC press. p. 193-221.

[13] Franceschini MA, Gratton E and Fantini S, *Noninvasive optical method of measuring tissue and arterial saturation: an application to absolute pulse oximetry of the brain*. Optics Letters, 1999. 24(12): p. 829-831.

[14] Siegel A, Marota JJA and Boas DA, *Design and evaluation of a continuous-wave diffuse optical tomography system*. Optics Express, 1999. 4(8): p. 278-298.

[15] Smith PR and Hayes MJ, *Artefact reduction in photoplethysmography*, WO 99/32030, 1999.

[16] Palreddy S, *Signal Processing Algorithms,* in *Design of pulse oximeters*, J.G. Webster, Editor. 1997, Institute of Physics Publishing, Dirac House, Temple Back, Bristol BS1 6BE, UK: Bristol. p. 124-158.
[17] ISO/TC121/SC3-IECSC62D/JWG4, IEC/CD 60601-2-54 *Medical electrical equipment - Part 2-54: Particular requirements for the basic safety and essential performance of pulse oximeters for medical use*. 2002, ISO/IEC.
[18] ISO/TC121/SC3, ISO/DIS 9919 *Medical electrical equipment - Particular requirements for the basic safety and essential performance of pulse oximeters for medical use*. 2003, ISO.
[19] Wieringa FP, *Imaging apparatus for displaying concentration ratios*, WO 01/15597 A1, 2001.
[20] Graaff R, *Tissue optics applied to reflectance pulse oximetry*, in *Thesis*. 1993, RUG: Groningen. p. 235.
[21] Dassel C, *Experimental studies on reflectance pulse oximetry: Specific aspects of intrapartum fetal monitoring,* in *Thesis*. 1997, RUG: Groningen. p. 157.
[22] Franceschini MA, et al., *Near-infrared spiroximetry: noninvasive measurements of venous saturation in piglets and human subjects*. Journal of Applied Physiology, 2002. 92(January 2002): p. 372-384.

Chapter 4

Concept for SpO_2 phantom technology

This chapter is based upon the following pending patent:
"Phantom device"
invented by F.P. Wieringa, D. Bakker and R.G.M. van Melick
published in 2006 by the European Patent Office with reference EP 1 726 256 A1

4.1 Explanatory introduction to this chapter

The content of this chapter is patent document EP1726256A1 *"Phantom device"*, describing a method to obtain a tissue-mimicking device with well-defined regions which produce pre-determined oxygen saturation values, when measured with a pulse oximeter or an SpO_2-camera.
The core of the phantom is an electrically controllable liquid crystal device (LCD) for which the optical scattering characteristics can be varied in proportion to the electric control signal.
Using materials with suitable absorptive, reflective and scattering properties, it is possible to construct a device with an artificial skin layer (with e.g. areas having different levels of pigmentation and/or molds), an artificial subcutaneous fat layer, and underlying tissue with artificial arterial and venous vasculature.
Simultaneous with the optical scattering characteristics of the LCD, also the ultrasonic scattering properties vary in proportion to the electric control signal. The patent also describes an embodiment that exploits this controllable ultrasound scattering behaviour by using an array of LCD-elements to mimick the Doppler effect of blood flow.

4.2 Phantom device

4.2.1 Abstract

A phantom device for mimicking anatomical structures, comprising: at least one electronic device layer comprising segmented areas of liquid crystals for forming a graphic layout of an anatomical structure; the segments comprising dyes of various absorbing characteristics for mimicking anatomical structures such as blood vessels; the areas further comprising electrically controllable optical diffuser and/or absorber elements for varying the absorption in the segments so as to mimic dynamical properties of said anatomical structure.

4.2.2 Patent description

The invention relates to a phantom device for mimicking anatomical structures.
Imaging techniques like photography and filming using visible, infrared or ultraviolet optical radiation are generally known in the art and commonly used to image, measure and characterize the surfaces of tissue. Optical imaging techniques have also been described to detect and display anatomical structures buried beneath the surface of biological tissue.
Principles for optical imaging techniques to detect and display the value of physiological parameters (such as heart beat rate, respiratory rate, pulse oximetry, etc) have also been described. Some of these principles offer a combination of anatomical imaging and physiological parameter imaging as for example disclosed in WO10/15597. Said publication discloses an imaging apparatus for imaging buried structures using various infrared wavelengths. The absorption ratios are used to derive the oxygenation of blood and other physiological parameters of interest.
One of the problems associated with said imaging apparatus and other prior art imaging techniques, is that calibration is difficult. For true calibration controlled oxygen studies on volunteers are performed which is costly and laborious. While phantom devices in the art are known to test certain functionality of imaging devices, they are generally static in nature and not reliable to reproduce clinically viable solutions for testing the imaging devices. One known device is described in US patent No. 6400973. An electronic device is disclosed mimicking an arterial blood pulse using a polymer dispersion liquid crystal device. However, this device is not designed for testing the imaging performance of an imaging apparatus.
The invention has as one of it's objections to provide a phantom device for mimicking anatomical structures, wherein the imaging performance of an imaging apparatus can be tested and calibrated using predetermined dynamical behavior.
To this end, the invention provides a phantom device according to the features of claim 1. In particular, according to the invention, the phantom device, comprises at least one electronic device layer comprising segmented areas of liquid crystals for forming a graphic layout of an anatomical structure; the segments comprising dyes of various absorbing characteristics for mimicking anatomical structures such as blood vessels; the areas further comprising electrically controllable optical diffuser and/or absorber elements for varying the absorption in the segments so as to mimic dynamical properties of said anatomical structure.
It is noted that the use of pigments in a polymer dispersion liquid crystal device is known from for example EP0434366. However, in this application, the dichromatic pigment is used for homogeneously increasing contrast of a display device.
While the various dyes in the segmented areas mimic multiple DC components corresponding to different stages of for instance oxygenation in blood vessels, the dynamic variation of the absorption may be realized by the scattering crystals, which cause the light to diffuse and vary the translucence of the device.
In one embodiment, the phantom device further comprises a tissue layer covering said

at least one electronic device, for mimicking tissue covering said anatomical structure. In particular, preferably, multiple electronic device layers are embedded in tissue layers to mimic the 3D properties of an organic object such as an arm or the like. In its simplest form, the phantom device provides a series of predetermined static and dynamical test parameters which can be measured by an imaging device. Preferably, however, the phantom device comprises an output unit for outputting signals representative for a predetermined dynamical behavior of said phantom device, for calibrating an imaging device for imaging buried structures.

The invention will be further illustrated with reference to the accompanying drawings. In the figures:
Figure 1 shows a first embodiment of a phantom device according to the invention;
Figure 2 shows a cross section of the phantom device according to Figure 1;
Figure 4 shows a second embodiment of a phantom device according to the invention; and
Figure 5 shows a cross section of the phantom device according to Figure 4 along line A-A;
Figure 6 shows another embodiment of the phantom according to the invention;
Figure 7 shows a system of a phantom device according to the invention and an imaging device to be calibrated; and
Figure 8 shows another imaging device to be calibrated by a phantom device according to the invention.
In the figures, the same or corresponding features will be referenced using the same reference numerals.

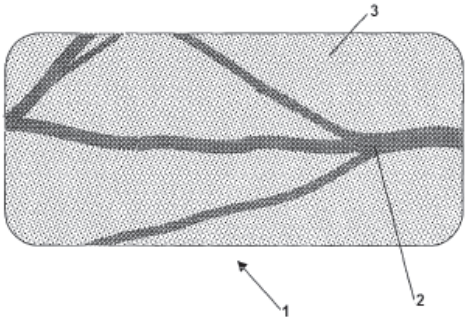

Figure 1

In Figure 1 a phantom device 1 is illustrated having a dyed structure 2 embedded on a substrate 3 to represent realistically a structure of blood vessels in an object such as a human arm. Such as follows from the cross sectional view illustrated in Figure 2, the dyed structure is preferably covered with a material 4 rendering similar absorption, reflection, scattering and transmission properties similar to normal biological tissue.

In this structure, different regions having different optical properties may be present, for example, to represent a fat layer, bones etc.
The dyed structure 2 is provided on a substrate, preferably, a polymer substrate 3 which houses segmented areas that are doted with dyes of various absorbing characteristics for mimicking anatomical structures such as blood vessels to be imaged by a imaging device 5. Furthermore, in the areas electrically controllable optical diffuser and/or absorber elements are provided for varying the absorption in the segments so as to mimic dynamical properties of said anatomical structure. In one embodiment, the dyed areas are provided with boundaries that are formed by conductive zones for forming an electrodes. In this way, the diffuser/absorber elements can be electrically controlled to vary the diffusing/scattering properties of the elements. By varying these properties, as a result, the path length of optical radiation used for imaging purposes is varied, resulting in a variation in scattering and/or absorption or other optical characteristics of the dyed area. In this way, dynamic characteristics of blood vessels can be imitated to mimic the pulsating properties of the vessels. Using various sorts of dyes, absorption characteristics can be exactly predetermined, so that a variety of degrees of oxygenation of blood the vessels can mimicked. In particular, venous and arterial blood vessels can be mimicked, wherein, as is illustrated in Figure 2 the arterial blood vessels may be formed by the deepest electronic device 6 and the venous blood vessels may be formed by the more superficially arranged electronic device 3. Between the devices 3, 6 a tissue layer 7 is provided.
In the electronic devices 1, 6, vessel patterns 2 can be formed by traces filled with a suitable dye mixture. In case of liquid dyes these may be mixed with a liquid crystal fluid. The scattering and absorption properties of the LCDs assigned to different areas can be electrically modulated in a reproducible manner.

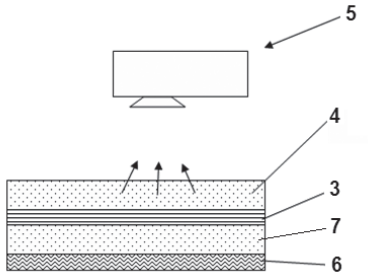

Figure 2

In the embodiment shown in Figure 2 two devices each having differing vessel patterns are stacked. The top layer is a diffuse layer having optical properties of a tissue surface, for example, skin, bladder wall, stomach wall, etc. In or upon the top layer, natural chromophores (e.g. melanine) or artificial dyes may be incorporated to imitate e.g. skin color.

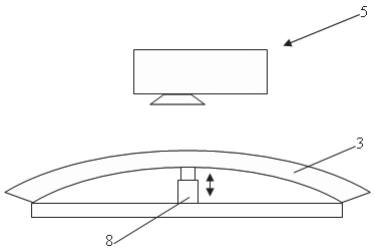

Figure 3

Figure 3 schematically shows a preferred embodiment where the device 1 is deformable and comprises an actuator 8 for deforming said device 1 into predetermined forms. Such an embodiment allows to create dynamic convex or concave distortion of the tissue phantom 1. Defined dynamic behavior of curved surfaces is very important to test the dynamic behavior of the equipment to be tested/calibrated (e.g. alternating reflections on such surfaces can lead to temporal detector saturation).
Further mechanical actuators may be provided that allow well defined movements up to 3 dimensions in space (X, Y and Z axis) as well as over time (controlled speed of movements). For imaging equipment such dynamic features are important to standardize checks and adjustment procedures for artifacts like blurring due to limited frame rate, the accuracy of movement compensation mechanisms, etc.

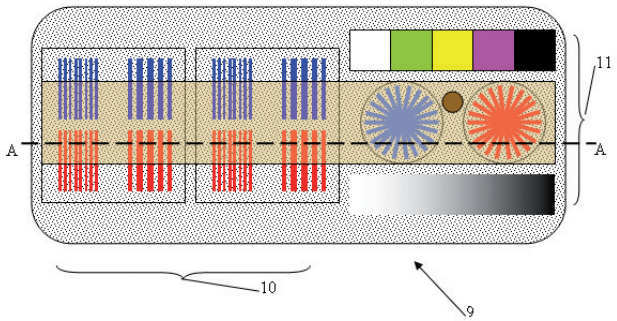

Figure 4

Figure 4 shows an alternative embodiment of a phantom device 9 according to the invention. In this device, the segmented areas comprise test patterns 10, 11 for testing a resolving power of a imaging device for imaging buried structures. The test patterns 10 as will be apparent from the cross sectional view of Figure 5 may be provided on different depths of the phantom device 9. In another (not shown) embodiment, a pattern may be provided, so that the tissue layer is increasing in thickness. With such a test pattern, a maximum penetration depth can be determined for the imaging apparatus.

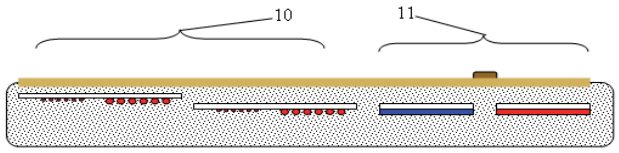

Figure 5

As illustrated, several test patterns (e.g. parallel line pairs 10 and/or fanned beams 11 at various pitches and with various spectral behavior) are embedded in a tissue-like optical material. Electrically controllable LCD-devices can be combined with these test patterns in order to add physiological signals (e.g. respiration and heartbeat). Also a spectrally neutral gray scale and a reference color pattern (incl. IR) may be incorporated. The test patterns 10, 11 may have well known 3-dimensional shapes and patterns (e.g. slits, trenches, cylinders, etc.). The external and internal surfaces of the device 9 can have an irregular shape that closely matches a part of the body.
The phantom can be used as a reference or training tool in combination with devices that enable the imaging of buried structures like blood vessels. On the phantom a region of a soft material, suitable for puncturing (e.g. with a needle) may be used in combination with an underlying target (e.g. a vessel pattern). This would allow users to practice their surgical, injection or blood withdrawal skills. It would also be a well defined and repeatable method to compare the functional parameters of different devices for imaging beneath the tissue surface.

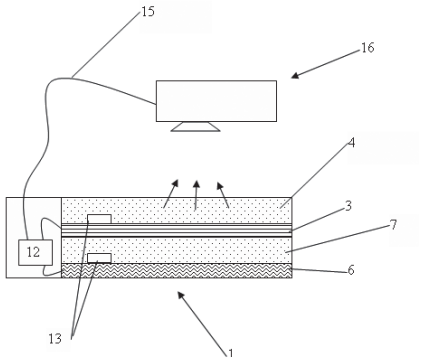

Figure 6

Figure 6 shows that the phantom 1 can be equipped with a central processing unit 12, one or more optical detectors 13, connections offering physiological reference signals 14 and a means of communication 15 with the device 16 to be calibrated or tested. Some devices that optically extract physiological parameters from tissue are designed to make use of an accepted clinical parameter by methods generally known in the art.

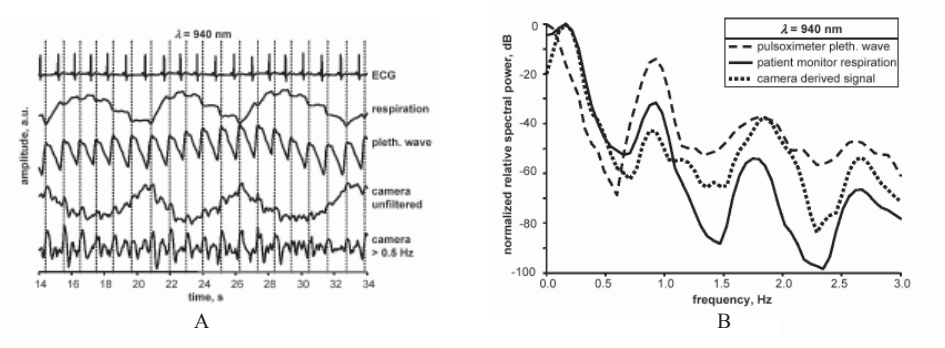

Figure 7

Typically this would be physiological registrations as illustrated in Figure 7 of Electro Cardio Grams (ECG), a photoplethysmographic trace as derived from a traditional pulse oximeter, a respiration signal from a ventilator or patient monitor, dynamic blood pressure, and the like. In particular, Figure 7A shows an example of reflectance mode photoplethysmographic signals derived from a camera (lower two traces). The upper three traces are reference signals obtained using clinical devices (HP-patient monitor and Nellcor pulse oximeter). Figure 7B shows Fourier spectra of two reference traces (respiration and pulse oximeter plethysmographic output) compared to a camera-derived signal.

The device already needs to generate signals like these in order to modulate the LCD-devices, which also allows to make these signals externally available using standard connections as accepted by the field. By not only presenting these signals but also their setting values (e.g. using a digital communication protocol) an automatic calibration can be performed.

Even if automatic adjustment is not desired, the phantom can provide comparison between a stored waveform or image and the actually obtained waveform or image. Automatic recognition of devices that are compatible (and of those that are non-compatible) with the phantom can be achieved by the aforementioned communication bus and/or by comparing signals received by optical detectors in the phantom with reference parameters (i.e. if via a communication bus the device would present itself as a model X but send out a different characteristic wavelength or modulation, then compatibility is not warranted and e.g. an error message could be displayed.

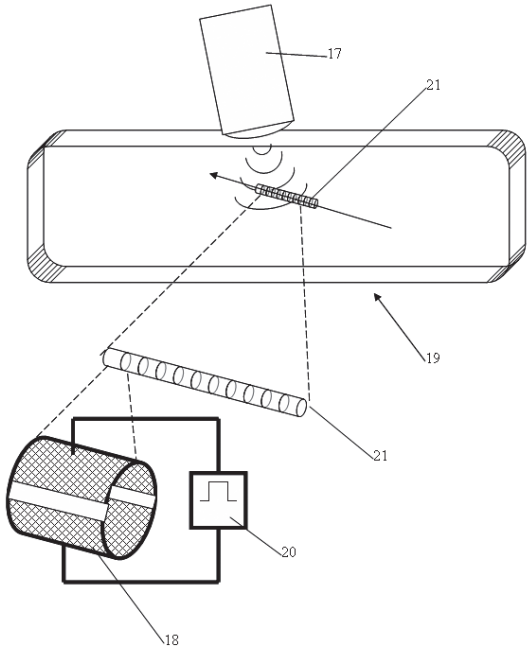

Figure 8

Figure 8 shows another imaging device to be calibrated. In particular, the imaging device is an ultrasound imaging device 17 since it has been found that the electronically orientable crystals 18 of the liquid crystal device 19 are also effective in varying the acoustic properties of the phantom device. Indeed it can be shown that in the phantom device, when electrically controlled by a controller 20, the scattering behaviour of liquid crystal materials also varies for ultrasonic waves and it is thus possible to construct a 3-dimensional array of individually controllable ultrasound scattering volume elements.

In traditional ultrasound phantoms a dynamic scattering behaviour can be achieved using a liquid or gel filled phantom with interchangeable mechanical parts, liquids or gels. Such devices are not very stable and difficult to transport.

In contrast, the liquid crystal devices such as PDLCs are very stable and behave like solid state components. Their reproduceability is excellent and individually controllable segments can be integrated into complex detailed 3-dimensional structures ("holographic structure simulators").

3D-structures 21 (as seen in Figure 8, mimicking a 3D blood vessel or also as shaped as described previously in this patent application in the section about optical behaviour) with variable known scattering properties can be used as a calibration tool for general echoscopic imaging devices.

Due to the contiuous variability of scattering behaviour from non-scattering liquid to

scattering liquid, the contrast level for discerning contrast between various structures can be determined. This contrast level is an indicator of echoscopic imaging quality.
The PDLC technique is also highly applicable for the calibration of harmonic ultrasound imaging devices (which use non-linear scattering behaviour to form an image). A typical application would e.g. be a bladderscan calibration phantom with stepwise variable scattering levels of the liquid volume within the simulated bladder.
PDLC technology can also be used to calibrate doppler ultrasound devices. By sequentially varying the scatter behaviour of a large amount of PDLC elements placed in a line, the propagation of a pulsating bloodflow can be imitated. Since the pitch of segments and timing of segment excitation can be controlled very accurately, a well determined time/speed profile can be generated for the simulated pulsating flow.
Existing calibration devices for doppler systems pump a suspension of micro-particles (e.g. latex spheres) through a liquid or gel phantom. These devices are cumbersome because the particles tend to clutter and portability is very restricted.

4.2.3 Claims

1. A phantom device for mimicking anatomical structures, comprising:
   at least one electronic device layer comprising segmented areas for forming a graphic layout of an anatomical structure; the segments comprising dyes of various absorbing characteristics for mimicking anatomical structures such as blood vessels; the areas further comprising orientable diffuser and/or absorber elements for varying the optical and/or ultrasonic absorption in the segments so as to mimic dynamical properties of said anatomical structure.
2. A phantom device according to claim 1, further comprising a tissue layer covering said at least one electronic device, for mimicking tissue covering said anatomical structure.
3. A phantom device according to claim 1 or 2, comprising multiple electronic device layers embedded in tissue layers.
4. A phantom device according to claim 2, wherein said tissue layer is increasing in thickness.
5. A phantom device according to any of the preceding claims, wherein said segmented areas comprise test patterns for testing a resolving power of an imaging device for imaging buried structures.
6. A phantom device according to any of the preceding claims, wherein said device is deformable and comprises an actuator for deforming said device into predetermined forms.
7. A phantom device according to any of the preceding claims, wherein said electronic device layer is a polymer dispersion liquid crystal device.

8. A phantom device according to any of the preceding claims, further comprising an output unit for outputting signals representative for a predetermined dynamical behavior of said phantom device, for calibrating an imaging device for imaging buried structures.
9. A system comprising an imaging device for imaging buried structures and a phantom device according to claim 8, said imaging device comprising an input for receiving said output signals and a unit for adjusting the calibration of said imaging device based on said output signals.
10. A system according to claim 9 wherein said imaging device is an infrared camera.
11. A system according to claim 9, wherein said imaging device is an ultrasound imaging device.
12. A system according to claim 11, wherein the ultrasound imaging device is of the harmonic ultrasound imaging device or a doppler ultrasound device.
13. A method of calibrating an ultrasound imaging device, the method comprising: using at least one electronic device layer comprising orientable diffuser and/or absorber elements for varying the ultrasonic absorption in the segments so as to mimic dynamical properties of an anatomical structure.
14. A method according to claim 13, further comprising sequentially varying an absorbing characteristic of adjacent liquid crystal elements that are formed in a 2D or 3D region mimicking a blood vessel, for mimicking a blood flow in the region.

Chapter 5

In vitro pulse oxigraphy: Demonstration of feasibility

This chapter is based on the following publication:
"In vitro pulse oxigraphy: Demonstration of feasibility"
by F.P. Wieringa, F. Mastik, R.H. Boks, A. Visscher, A.J.J.C. Bogers and A.F.W. van der Steen
as submitted to Annals of Biomedical Engineering

5.1 Abstract

We tested the feasibility of non-contact oxygen saturation imaging, based upon camera-derived 2-dimensional-matrices of spatially resolved photoplethysmograms at 3 wavelengths (λ_1=660nm, λ_2=810nm, λ_3=940nm).
By varying $O_2/CO_2/N_2$ mixtures a heart-lung machine preconditioned 3 blood pools, aiming for oxygen saturation setpoints of: 98, 96, 94, 92, 90, 88, 85, 80 and 75% (pH 7.35 ± 0.05). Applying in-line monitoring this blood circulated through a transparent reservoir, with an electrically modulated LCD-scatterer and a Delrin™ diffuser in front. For each setpoint, a monochrome CMOS-camera with apochromatic lens and 3λ-LED-ringlight (100LEDs λ^{-1}) sequentially recorded 3λ-movie-sets of the phantom at 60, 80 , 100 and 120 beats min^{-1}, followed by reflectance mode pulse oximetry. Each acquisition at 120 beats min^{-1} was followed by laboratory blood gas analysis.
Compared to laboratory results, the pulse oximetry phantom-response-slope was much steeper than for normal tissue. Third-order least-squares spline approximations revealed monotone transfer functions $f_{PULSE-LAB}$ (between pulse oximetry and laboratory results, n=29) and $f_{CAM-LAB}$ (between camera and laboratory results, n=29).
Using independent paired data sets, we subjected pulse oximetry values to $f_{PULSE-LAB}$ on one hand and corresponding camera-derived ratio of ratios to $f_{CAM-LAB}$ on the other hand. Thus theoretical laboratory values were calculated via two different paths. Comparison revealed excellent correlation (n=87, R^2=0.997).
We demonstrated quantitative non-contact 2-dimensional imaging pulse oximetry on a phantom. Devices suitable for in vivo clinical application, however, will require extensive development.
We propose the term "pulse oxigraphy" for the imaging modality and "SpO_2-camera" for the device.

Keywords
Pulse oxigraphy
Pulse oximetry
Multispectral imaging
SpO_2 camera

5.2 Introduction

Bedside pulse oximetry offers a simple non-invasive technique to simultaneously monitor heart rate, photoplethysmographic pulse waveform and arterial oxygen saturation (SpO_2) and is part of many clinical routines [1-5].

Commonly used clinical pulse oximeters produce a numerical value that is derived from photoplethysmographic signals at 2 different wavelengths. The obtained oxygen saturation value relates to only one particular contact site at the body. This can be interpretated as a contact image consisting of only one pixel. As a next step in oxygen-saturation measurement, we have suggested the development of an SpO_2 camera, involving the non contact detection of a 2-dimensional matrix of spatially resolved optical plethysmographic signals at 3 different wavelengths (660, 810 and 940 nm). The core of this method is to exploit the isobestic behaviour of Hb versus HbO_2 at 810 nm as a reference to correct for image artifacts like shadows, reflections and pigmentation [6].

In a previous article we demonstrated that the photoplethysmographic signals, needed to achieve this goal, indeed can contactlessly be derived from the human body, but the obtained signal-to-noise conditions were yet insufficient to calculate meaningfull SpO_2 values [7]. Additionally, the previously in-vivo recorded photoplethysmograms were sequentially recorded (one wavelength at a time), so that due to differences in the sequentially recorded heartbeats no valid SpO_2 values could be derived.

Furthermore, for a proper investigation of the technique, a wide range of SpO_2 values should be investigated and there is no practical and ethically acceptable method to expose volunteers to very low arterial oxygen saturation levels for a prolonged period [8]. We therefore decided to develop a tissue-mimicking SpO_2 phantom, offering sufficient signal-to-noise-ratio, having beat-to-beat repeatable heartcycles and being capable of reaching not only high but also low oxygen saturation values for a prolonged period.

The 660 and 940 nm camera-derived photoplethysmograms were processed using the well known two-wavelength ratio-of-ratios method, similar to traditional pulse oximetry [4, 9-12]. The application of the 810 nm channel as a reference to correct for image artifacts like shadows, reflections and pigmentation did not make sense, since our in-vitro experiment was designed to exclude such artifacts. Instead we investigated the ratio-of-ratios for 660 and 810 nm as well as for 810 and 940 nm as a comparison.

In this paper we describe the developed phantom and applied procedures. Off-line laboratory blood gas analysis was used as a “gold standard” for comparison with the results of our experimental SpO_2 camera device as well as with the readings of a normal reflectance mode clinical pulse oximeter when both were sequentially applied to the tissue phantom.

The experiment was designed in a “triangular” setup (see also figure 1) using the in-vitro phantom as a stable (but not necessarily exactly tissue-mimicking) transfer standard to apply the lab-derived blood oxygenation level as an input stimulus to the pulse oximeter (being a proven method) and the camera (being an experimental

method). Since camera and pulse oximeter both are based upon optical reflectance measurements within comparable wavelenght ranges, both are likely to react similarly upon imperfections in the tissue-mimicking properties of the phantom.

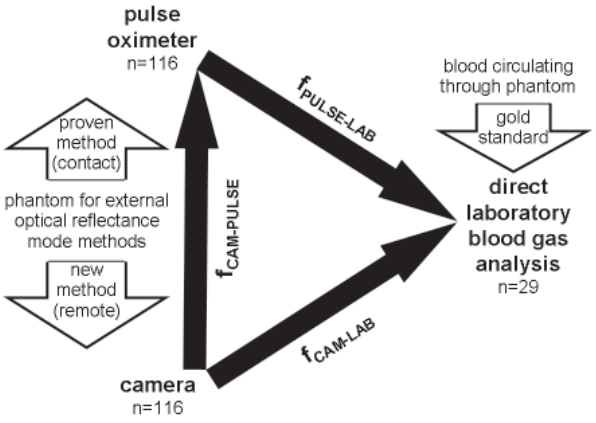

Figure 1: Triangular setup of the experiment

5.3 Methods

5.3.1 Instrumental setup

The instrumental setup is schematically drawn in figure 2. The main components were: an in-vitro phantom, an experimental SpO_2-camera and a pulse oximeter in combination with off-line blood gas analysis.

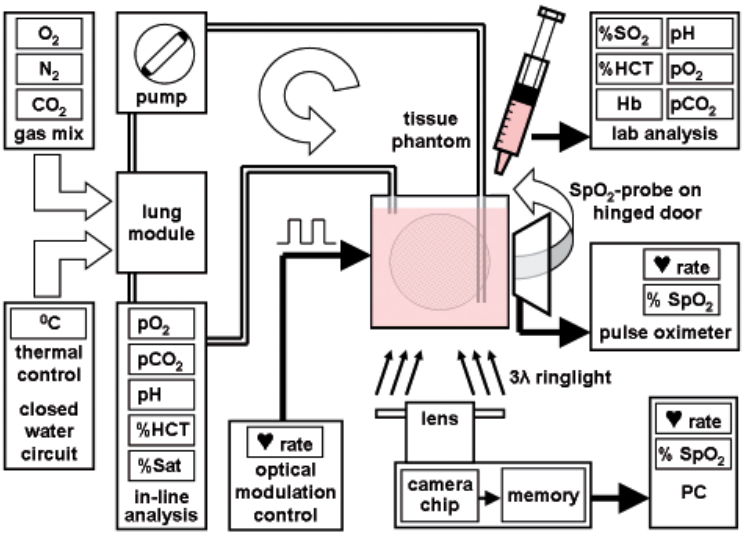

Figure 2: Experimental setup

In-vitro phantom

The in-vitro phantom basically consisted of a heart-lung machine and an optical setup within a light-tight enclosure. The following components were used:

- A gas mixing circuit to obtain freely adjustable mixtures of O_2, N_2 and CO_2.
- A blood gas conditioning system (lung module) consisting of a Jostra Quadrox^D diffusion membrane (Maquet Cardiopulmonary, Hirrlingen, Germany), a Jostra venous hardshell 4200ml cardiotomy reservoir (Maquet Cardiopulmonary, Hirrlingen, Germany) and a multiflow rollerpump (Stöckert Shiley, Münich, Germany). The gas conditioning system was equipped with a CDI-500 in-line blood gas monitor (Terumo, Leuven, Belgium) and a labSAT/HCT in-line oxygen saturation & hematocrite monitor (Cobe Cardiovascular, Arvada, Colorado USA). Calibration was obtained by application of an i-stat1 external calibrator (Abbot, Illinois USA). The in-line continuous blood gas analysis of the heart-lung machine was only used as a stability indicator.

- A heater-cooler control unit (Stöckert, Münich, Germany) with a closed water circuit to keep the diffusion membrane and cardiotomy reservoir at a constant temperature of 36.8 ^{0}C.
- A 0.5 mm thick translucent layer, consisting of Delrin™ (polyoxymethylene with 20% glassfiber filling) which forms a reasonable optical approximation of human skin at wavelengths > 600 nm [13]. Adjacent to the Delrin™ layer, a Spectralon™ target (Labsphere, North Sutton, USA) with > 99% reflectance from 400-1500 nm, a carbon black target with < 1% reflectance from 400-1000 nm and a printed gray-scale were attached for image quality control purposes.
- An electrically controllable spectrally neutral LCD-shutter device (Anteryon, Eindhoven, the Netherlands), capable of switching between clear transparant and diffuse optical state. This LCD-shutter (including power supply and control unit) served as an optical modulator to simulate arterial plethysmographic pulsation (see also figure 3a and 3b). The LCD-shutter was fixed at the backside of the translucent Delrin™ layer. LCD-shutter on/off was controlled by a 50% duty-cycle 0-5V block wave from a 33250A digital waveform generator (Agilent Technologies, Santa Clara, California USA).
- A small blood reservoir, consisting of a CLS3055 polystyrene cell culture flask (Corning, Schiphol-Rijk, the Netherlands) positioned at the backside of the LCD-shutter. Via two luer lock connectors this flask was fitted to the artificial blood circulation.

The above described blood reservoir, translucent Delrin layer and LCD-shutter as well as the camera and pulse oximeter probe at the hinged door, were placed together in a light tight enclosure with a side acces light tight hatch door. Figure 3c shows this optical setup, photographed throug the opened hatch door.

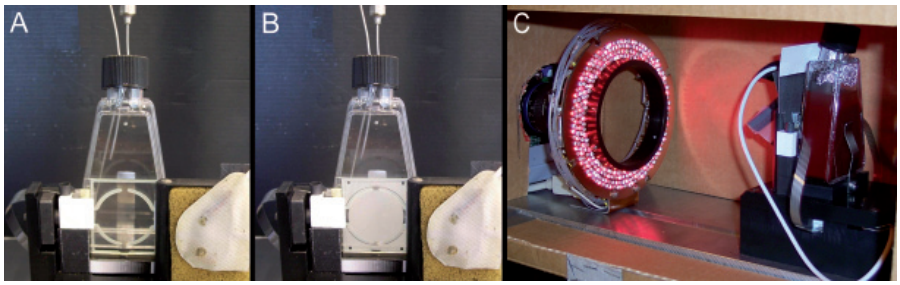

Figure 3: LCD-shutter (off & on) and overall optical setup

In figure 3A and 3B, the Delrin™ diffuser has been removed to clearly illustrate the scattering LCD-shutter principle. Figure 3A shows the transparent state of the LCD-shutter when not active. Figure 3B shows the white diffuse appearance of the scattering LCD-shutter when activated. Figure 3C shows an overall impression of the optical setup (shielding enclosure opened for photograph) with the Delrin™ diffuser in place and the hinged door open.

Experimental SpO_2-camera

A monochrome CMOS-camera (Fillfactory, Mechelen, Belgium), equipped with a MeVis-C apochromatic lens (Linos, Zoetermeer, the Netherlands) and a custom self-built 3λ-LED-ringlight (λ_1 = 660 nm, λ_2 = 810 nm, λ_3 = 940 nm; 100LEDs λ^{-1}), was applied to sequentially record sets of movies at 3 different wavelengths from the in-vitro phantom.

Pulse oximeter

Maintaining the same phantom settings, also an N-200 clinical bedside pulse oximeter equipped with an R15 reflectance mode SpO_2-probe (Nellcor, Hayward, Califonia USA) was applied to the in-vitro phantom. The SpO_2-probe was mounted to a small hinged door, equipped with a magnet snapper. Closing this hinged door applied the SpO_2-probe to the front surface of the in-vitro phantom in a reproducable and stable manner. During camera acquisitions the hinged door was kept open and covered with a spectrally neutral black cloth (reflectance < 2% from 600-1000 nm).

Offline blood gas analysis

Offline blood gas analysis took place in a laboratory located within 40m walking distance using an ABL 725 automated laboratory blood gas analyzer (Radiometer, Copenhagen, Denmark).

All blood pools were obtained from Sanquin Blood Bank Rotterdam. In accordance with the delivery conditions, informed consent was obtained from all donors.

5.3.2 Experimental protocol and data collection

The distance between camera lens front and the front surface of the Delrin™ layer was fixed at 22cm. The camera was focussed and camera settings plus LED-currents were adjusted to compensate for spectral sensitivity variations by white balancing on the Spectralon™ target. These settings (ringlight currents 110mA @ λ_1 ; 70mA @ λ_2 ; 400mA @ λ_3 and lens diaphragm setting F4.0) were applied throughout all further experiments. Camera frame rate was calibrated by filming a stopwatch (160 frames in 11.35 s = 14.1 frames s^{-1}).

Heart rate detection validity of the applied pulse oximeter and the experimental camera were checked first by varying the phantom heart rate from 40 to 140 beats $minute^{-1}$ (bpm) using incremental steps of 20 bpm. Subsequently the oxygen-related experiments were carried out. Experiments at 29 oxygen saturation settings, each applying 4 different heart rates (60, 80, 100 and 120 bpm) were performed using 3 different blood pools. Thus in total 116 sets of experimental data, each consisting of all annotated parameters and an associated 3λ-movie-set, were collected. During adjustment of the tissue phantom, the following oxygen saturation values were used as aimed setpoints: 98, 96, 94, 92, 90, 88, 85, 80 and 75%. However, due to the long required stabilization times between setpoints, the stability of readings had priority over exactly reaching the desired setpoint value.

All blood pools (800 ml per pool) were collected ≤ 24 h prior to experiments and stored at room temperature (21 ± 3 ^{0}C). During all experiments blood flow was maintained constant at 4 liter min^{-1}. First, the heart-lung machine circulation was allowed to stabilize for at least 30 minutes. Then, following standard perfusion procedures, the base excess level was brought within the normal range by adding an appropriate (small) amount of $NaHCO_3$.

By adjusting the gas mixture input of the diffusion membrane, the blood gas conditioning system was set to a stable oxygen saturation reading on the inline CDI 500 monitor. The CO_2 gas flow was adjusted so that the lab-derived pH value was kept at 7.35 as close as reasonally achievable but at least ± 0.05. The in-line continuous blood gas analysis of the heart-lung machine was only used as a stability indicator (otherwise, due to the long settling times between setpoints, the experiment would not have been feasible from a logistic point of view). Once the in-line analysis readings were stable, the measured in-line values (pO_2, pCO_2, pH and hematocrite) were annotated. With the hinged door closed, the pulse oximeter readings for heart rate and SaO_2 were also annotated. Finally, the hinged door was opened and the camera aquired 3 movies of 160 frames each (14.1 frames s^{-1}; 800 x 600 10-bit deep pixels per frame; T_{EXP} = 45ms) using three different wavelengths (λ_1 = 660 nm, λ_2 = 810 nm and λ_3 = 940 nm) always starting with the shortest wavelength. After software triggering, the camera stored a sequence of 10-bit digitally encoded images in an internal memory (using auto-incremental frame numbering). All image frames then were automatically downloaded via an IEEE 1394 connection and saved on harddisk in an uncompressed 16-bit format. Pulse oximetry and 3λ-camera recordings were repeated using 4 different heart rate settings (60, 80, 100 and 120 bpm).

The stability criterium for starting acquisition of a series at 4 heart rates was: No change for neither in-line values (pO_2, pCO_2 and pH) nor pulse oximeter readings during at least 2 minutes. Once a series of camera recordings was started, the data was collected for all 4 heart rates (starting at 60 bpm) , no matter whether changes in readings were observed. Pulse oximetry was performed just before each 3λ-camera recording. For each setpoint the blood sample for laboratory analysis was drawn immediately after the last 3λ-movie-set (at 120 bpm) and rushed to the laboratory for analysis (interval between sampling and analysis < 5 min).

During all recordings, the optical set-up was shielded from ambient light by an enclosure with a light-tight side hatchdoor. After PC-storage of the fourth (120 bpm) 3λ-movie-set, the reflectance mode pulse oximeter probe was re-applied onto the Delrin™ phantom surface layer and the settings of the blood gas conditioning system were adjusted to obtain the next experimental value, etc.

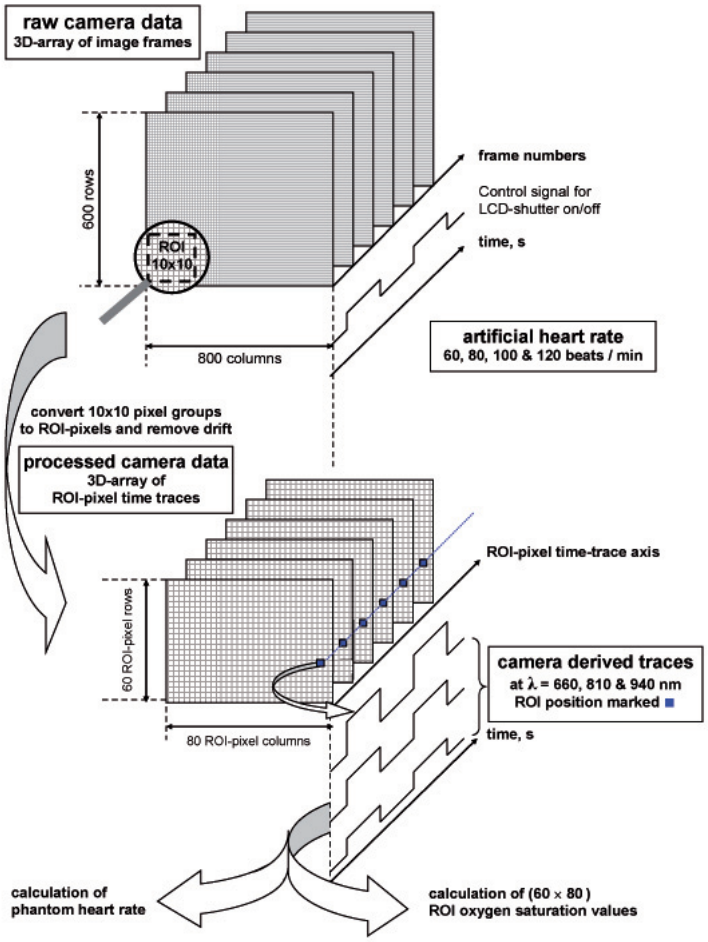

Figure 4: Data acquisition and processing

The recorded images and LCD control signal (phantom heart rate) are shown in the upper half of this figure, projected along the time domain axis. The raw image frames form a 3D-matrix. An enlarged frame portion shows an ROI containing 10 x 10 raw pixels.

The lower half of the figure contains processed data in a 3D-array of ROI-pixels. Sketches of typical time domain traces, derived from an ROI-pixel located on the tissue at 3 wavelengths, are projected in a similar perspective as the LCD control signal. Note that the acquisition of 3 wavelengths occurs sequentially.

While the Delrin™ diffuser and the LCD-shutter are spectrally neutral, the spectral absorption of the blood is oxygenation dependent (except for the isobestic wavelength of 810 nm). To illustrate this effect the 3 ROI-pixel time traces are schematically drawn with different amplitudes for the three different wavelengths.

5.3.3 Data processing

Data processing – Heart rate

The annotated pulse oximeter readings for heart rate did not require processing, but could directly be compared with the phantom settings for heart rate and the laboratory values for oxygen saturation.

The 3λ-movie sets recorded by the camera needed processing with custom developed software (using Matlab®, Mathworks, Natick, Massachuchets USA) in order to reveal heart rate and oxygen related values. Figure 4 schematically represents this process. The upper half of figure 4 shows the aquired raw image frames seqentially placed at the time-axis, thus forming a 3D-matrix. Each raw image frame was divided into discrete Regions Of Interest (ROIs) measuring 10 x 10 pixels each.

The 100 raw pixel values within each ROI were averaged, and the resulting value of each ROI-pixel, plotted versus time, was subjected to a detrending algorithm that was calibrated using the Spectralon™ image area as a non-pulsatile reference to exclude offset and/or drift influences (e.g. from the light source) in order to distinguish the true pulsatile component. This resulted in a new 3D-matrix of image frames consisting of ROI-pixels. The variation of each ROI-pixel over time was determined, resulting in a matrix of ROI-pixel-time-traces, as drawn in the lower half of figure 4. These ROI-pixel-time traces were checked for the presence of a valid plethysmographic pulse (i.e. the presence of a heart rate) for all 3 wavelengths using an autocorrelation criterium ($\rho \geq 0.8$) and an additional amplitude treshold ($A \geq 0.6\%$ of ROI-mean DC value). ROIs meeting both these criteria were considered to contain a valid pulse wave. Heart rate then was calculated using the camera frame rate as a time base.

Note: Only ROI-pixels that fulfilled both above mentioned criteria could be used for oxigram calculations. The geometrical distrubution of these "valid" ROI-pixels is thus included in the oxigrams shown in the figures 7B and 7C.

Data processing – Oxygenation

Pulse oximeter values for oxygen saturation were directly read from the display and did not require any processing. As for the camera, each 3λ-set of ROI-pixel-time-traces was also processed to calculate the blood oxygen saturation related ratio-of-ratios value. First of all, for each wavelength and all ROI-pixel-time-traces (S_λ) the difference between the mean high plateau and mean low plateau value of the block wave (AC component) was determined by $AC_\lambda = S_{\lambda,high} - S_{\lambda,low}$ resulting in distinct AC "peak-to-valley" values for λ = 660, 810 and 940 nm.

The DC component DC_λ was defined as the mean value of S_λ over the full length of the recording (160 frames).

These values were used to calculate the so-called ratio-of-ratios R for 660 nm and 940 nm:

$$R_{660/940} = \frac{\frac{AC_{660}}{DC_{660}}}{\frac{AC_{940}}{DC_{940}}}$$

Our experimental setup was designed to exclude image artifacts like shadows, reflections and pigmentation. Therefore the application of the 810 nm channel as a reference to exclude such artifacts was not tested. Instead we applied the ratio-of-ratios method to likewise derive:

$$R_{660/810} = \frac{\frac{AC_{660}}{DC_{660}}}{\frac{AC_{810}}{DC_{810}}} \quad \text{and} \quad R_{810/940} = \frac{\frac{AC_{810}}{DC_{810}}}{\frac{AC_{940}}{DC_{940}}}$$

The values obtained at all setpoints for the ratio-of ratios $\overline{R_{660/940}}$, $\overline{R_{660/810}}$ and $\overline{R_{810/940}}$ respectively, (averaged over a fixed centred area, see dotted area in figure 7A) were compared to the pulse oximeter SaO_2 readings and to the lab-derived SO_2 values.
By subjecting all individual ROIs for which a valid heart rate was determined to $f_{CAM-LAB}$ and assigning a false color scale to the results, oxygrams obtained at several oxygenation settings could be superimposed upon the oxygen independent 810 nm grey-scale image. Within the applied false color scale blue represents low oxygen saturation values and red represents high oxygen saturation values (see figure 7).

5.4 Results

5.4.1 Results – Heart rate

Table 1 contains a listing of all phantom heart rate settings, pulse oximeter heart rate readings and camera-derived heart rate (independently determined for all three wavelengths).

phantom setpoint heart rate [bpm]	**pulse oximeter measured heart rate [bpm]**	**camera-derived signals at wavelengths of:**					
		660 nm		810 nm		940 nm	
		heart rate [bpm]	stdv [bpm]	heart rate [bpm]	stdv [bpm]	heart rate [bpm]	stdv [bpm]
40.00	**40**	40.2	0.11	40.1	0.06	40.2	2.42
60.00	**60**	60.0	0.04	60.0	0.03	60.0	0.08
80.00	**80**	80.2	0.39	79.9	1.09	80.1	0.59
100.00	**100**	100.1	0.59	100.7	0.20	99.9	0.61
120.00	**120**	119.2	0.10	119.2	0.05	119.2	0.06
140.00	**140**	138.7	0.10	138.7	0.11	138.8	0.43

Table 1: Heart rate related results
Abbreviations: bpm = beats min^{-1}
stdv = standard deviation

5.4.2 Results – Oxygenation

Figure 5 contains all collected oxygenation-related data and illustrates the triangular setup of the experiment. The upper half of figure 5 shows (along the vertical axis) the values obtained at all setpoints for $\overline{R_{660/940}}$, $\overline{R_{660/810}}$ and $\overline{R_{810/940}}$ respectively, in relation to the corresponding pulse oximeter SaO_2 readings (along the horizontal axis).
A third-order least-squares spline approximation was fitted throug the 29 observations of $\overline{R_{660/940}}$, $\overline{R_{660/810}}$ and $\overline{R_{810/940}}$ for which a corresponding laboratory value was available. Then the *residues* of all observations (n=116) were determined in relation to this fit. The results (mean ± standard deviation) were: 0.000±0.028 for $\overline{R_{660/940}}$; 0.000±0.026 for $\overline{R_{660/810}}$ and 0.000±0.009 for $\overline{R_{810/940}}$.
The lower half of figure 5 illustrates the transfer function $f_{PULSE\text{-}LAB}$ of the phantom. Here also pulse oximeter SaO_2 readings are plotted along the horizontal axis, but the vertical axis represents the "gold standard" lab-derived SO_2-value. Note that this lower half of figure 5 only contains the 29 pulse oximeter SaO_2 readings for which a corresponding lab-derived SO_2-value was measured. In the upper half of figure 5 the corresponding datapoints are highlighted by filling-up their markers. A third-order least-squares spline approximation revealed a monotone transfer function between pulse oximetry and laboratory results (n=29, maximum -1.0 and +1.8% deviation from fit).

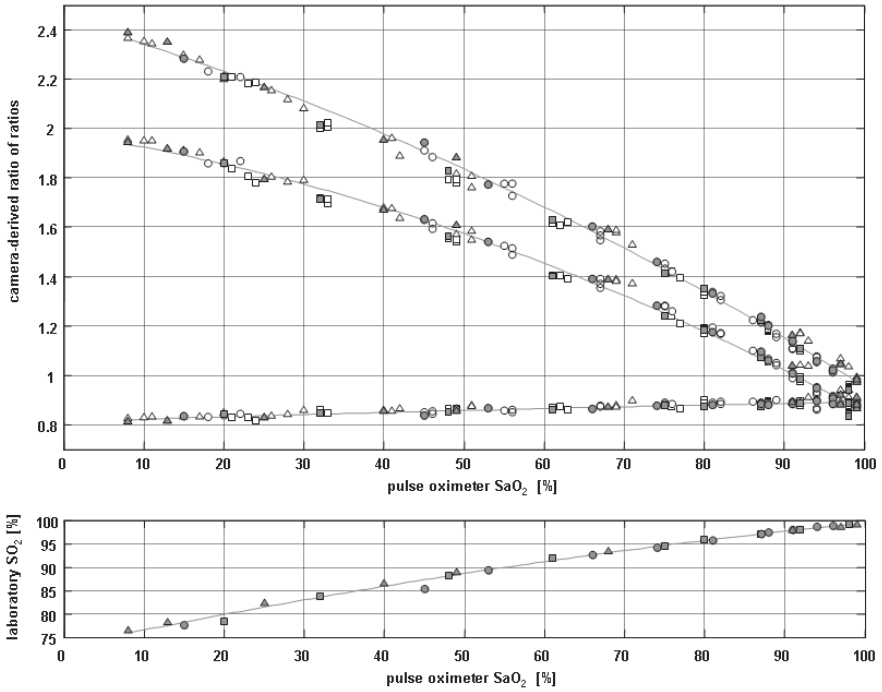

Figure 5: Oxygenation related results

The relationship between camera derived data and pulse oximetry is illustrated by the upper half of figure 5. The vertical axis represents the dimensionless values of $\overline{R_{660/940}}$ (upper trace), $\overline{R_{660/810}}$ (middle trace) and $\overline{R_{810/940}}$ (bottom trace) respectively. The horizontal axis represents the pulse oximeter SaO_2 readings. A third-order least-squares spline approximation is fitted throug the 29 observations of $\overline{R_{660/940}}$, $\overline{R_{660/810}}$ and $\overline{R_{810/940}}$ having a corresponding laboratory value.

The lower half of figure 5 directly illustrates the transfer function $f_{PULSE\text{-}LAB}$ of the phantom. Here also pulse oximeter SaO_2 readings are plotted along the horizontal axis, but the vertical axis represents the "gold standard" lab-derived SO_2-value. In both the upper and lower half of figure 5, the three different blood pools are indicated using circular, triangular and square markers, whereas filled-up markers indicate data points for which a laboratory value was measured. Note: For reasons of clarity, the horizontal axis differs from the $f_{PULSE\text{-}LAB}$ representation in figure 6C.

In order to facilitate an optimal visualization of mutual relationships between graphs, a representation of $f_{PULSE\text{-}LAB}$ (with a different aspect ratio than in figure 5) has also been included in figure 6.

Due to the triangular setup of the experiment (illustrated by figure 1), the transfer functions $f_{CAM\text{-}PULSE}$ and $f_{CAM\text{-}LAB}$ could also be derived from the gathered data. These transfer functions are shown in figure 6A and 6B (for completeness $f_{PULSE\text{-}LAB}$ is repeated in figure 6C).

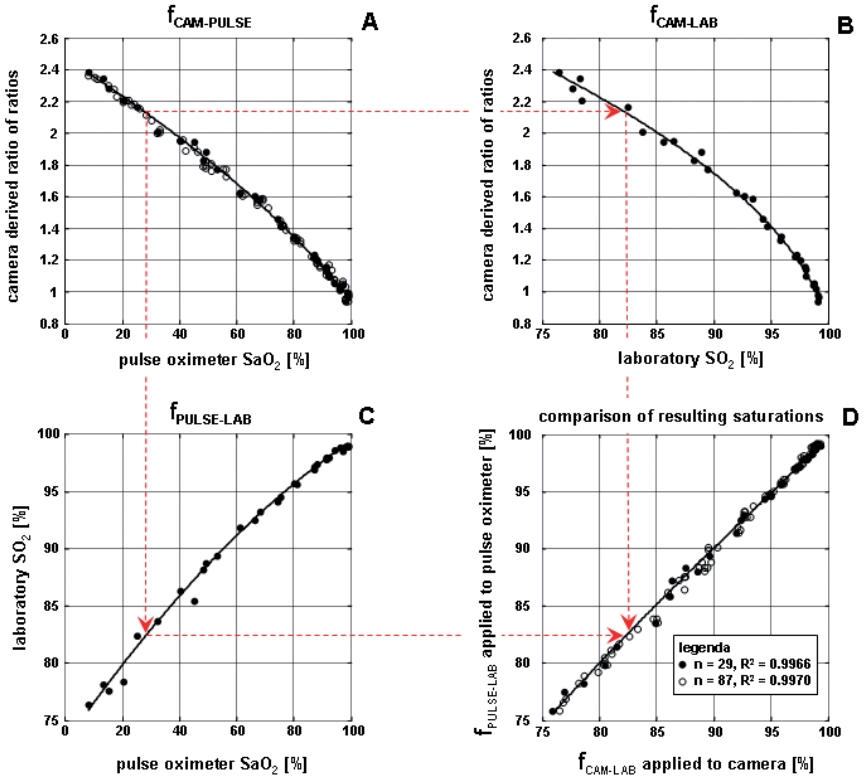

Figure 6: Derived transfer functions and a comparison of their results when applied

In figure 6A filled-up markers indicate data points for which a laboratory value was measured (n=29), whereas non-filled markers represent measured pulse oximeter data without associated laboratory measurements (n=87). The transfer functions $f_{CAM\text{-}LAB}$ (figure 6B) and $f_{PULSE\text{-}LAB}$ (figure 6C) were derived from spline fit approximations involving only those measured values for which corresponding laboratory measurements were available. Hence figure 6B and 6C only show filled markers.

By subjecting the remaining 87 "lab-less" pulse oximetry values to $f_{PULSE\text{-}LAB}$ on one hand and subjecting the "lab-less" camera-derived ratio of ratios to $f_{CAM\text{-}LAB}$ on the other hand, theoretical corresponding lab values could be calculated via two independent paths. Comparison of the resulting calculated oxygen saturations revealed an excellent linear correlation (figure 6D).

Note: In order to facilitate an optimal visualization of the relationship with $\overline{R_{660/940}}$, $\overline{R_{660/810}}$ and $\overline{R_{810/940}}$ an $f_{PULSE\text{-}LAB}$ representation with a different aspect ratio between X and Y axis was used in the lower half of figure 5.

By definition, the transfer functions $f_{PULSE\text{-}LAB}$ and $f_{CAM\text{-}LAB}$ could only be derived from the 29 observations for which associated laboratory values were available. Within the figures 6A, 6B and 6C, filled-up markers indicate these observations. Applying a pulse oximeter reading to $f_{PULSE\text{-}LAB}$ and applying a value of $\overline{R_{660/940}}$, to $f_{CAM\text{-}LAB}$ both result in an approximated laboratory value.

The remaining pairs of pulse oximeter readings and camera-derived values for $\overline{R_{660/940}}$ without associated laboratory values (non-filled markers in figure 6A) formed an

independent set of observations. Using these results as input values to $f_{PULSE-LAB}$ and $f_{CAM-LAB}$ enabled us to compare the accuracy of these both transfer functions as a cross-check. The result is displayed in figure 6D, where filled markers represent approximation results of data points from which the transfer functions $f_{PULSE-LAB}$ and $f_{CAM-LAB}$ were derived (n=29, R^2=0.9966). Non-filled markers represent the cross-check approximation results of remaining "lab-less" data points (n=87, R^2=0.9970).

Examples of experimental oxigrams are displayed in figure 7. Figure 7A shows a greyscale reference image obtained at 810 nm. Figure 7B shows an oxigram of the phantom perfused with highly oxygenated blood, whereas figure 7C shows the result for poorly oxygenated blood.

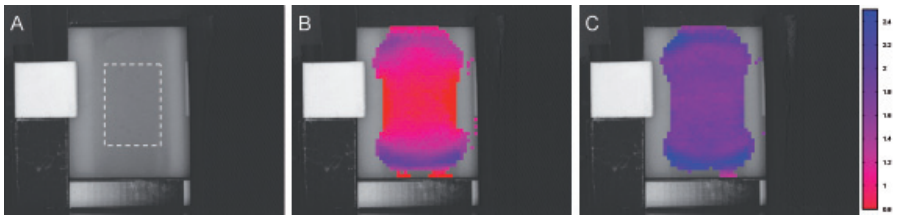

Figure 7: Reference image and oxigrams

Figure 7A shows a greyscale reference image acquired at a wavelength of 810 nm with the 0.5 mm thick Delrin™ diffuser in place (note the difference in comparison with figure 3A and 3B). The dotted central area indicates for which ROI-pixels the values of the averaged ratio-of-ratios $\overline{R_{660/940}}$, $\overline{R_{660/810}}$ and $\overline{R_{810/940}}$ (as plotted in figure 5) were determined. At 810 nm, the absorption curves of Hb and HbO_2 intersect (so-called isobestic point). Thus recordings at this wavelength are oxygenation-independent, and provide the possibility to apply them for compensation of shadow- and reflection-related image artifacts as well as to extract a photoplethysmographic amplitude reference for gain control purposes in ratio-of-ratios calculations. Figure 7B shows an oxigram corresponding to a lab-derived SO_2 value of 99% and a camera-derived $\overline{R_{660/940}}$ of 0.973. Figure 7C shows an oxigram corresponding to a lab-derived SO_2 value of 93% and a camera-derived $\overline{R_{660/940}}$ of 1.530. The color scale at the right indicates the full range of camera-derived $\overline{R_{660/940}}$ values.

5.5 Discussion

In the first minute after switch-on the lightsource showed some slow thermal drift, but once warmed up, it remained very stable. Yet, to exclude these (minor and slow) variations induced by thermal drift, the ROIs located within the Spectralon™ target area were used as a reference.

The applied in vitro phantom proved to be extremely stable with respect to heart rate detection by the pulse oximeter, despite the fact that a non-physiologic block wave was used to simulate the arterial pulse. Phantom stability was quite satisfactory in the range from 100 to 85% of blood oxygen saturation laboratory values. However, below laboratory saturation values 85% the pulse oximeter saturation readings slowly decreased during recording at 4 different heart rates.

Due to logistical reasons, lab-derived SO_2 values were only available for the 3λ-movie

sets aquired at 120 bpm. The in-vitro phantom proved to be a useful intermediate to transfer the lab-derived blood oxygenation level as an input stimulus to the pulse oximeter and the camera. It did, however not exactly mimick human tissue. For the applied reflectance mode pulse oximetry, the response slope of the phantom was much steeper than that of normal tissue, yet a monotone transfer function $f_{PULSE\text{-}LAB}$ between pulse oximetry and laboratory results could be derived from the 29 setpoints having a corresponding laboratory value.

Monotone and reproducible relations were also found between pulse oximeter readings and all three sets of camera-derived ratio-of-ratios ($\overline{R_{660/940}}$, $\overline{R_{660/810}}$, and $\overline{R_{810/940}}$) as shown in figure 5. By definition the applied third-order least-squares spline approximations result in mean residue values near zero for the 29 observations that were used as input values. It is, however, not trivial that a mean residue value near zero *also* results when considering all 116 observations. The mean values of zero and small standard deviations found for the residues of $\overline{R_{660/940}}$, $\overline{R_{660/810}}$ and $\overline{R_{810/940}}$ therefore indicate an excellent reproduceability of camera-derived results.

Application of independent input values to the transfer functions $f_{CAM\text{-}LAB}$ (see fig. 6B) and $f_{PULSE\text{-}LAB}$ (see fig. 6C) to cross-check whether the same results could be obtained by following different vectors from the "experiment-triangle" revealed an excellent linear correlation (see figure 6D).

In addition to the experiments described in this article, we demonstrated the ability to contactlessly detect photoplethysmographic pulse waves in living tissue in a previous publication (12).

5.6 Conclusions

In 2003 the importance of a phantom with a broad oxygen saturation range and the possible application of a forefront diffuser, as well as the possible usefulness of a third wavelength, already were stated by Aoyagi (1). We could derive a monotone and reproducable transfer function between pulse oximeter readings and camera-derived ratio-of-ratios as well as between pulse oximeter readings and laboratory values. Since both laboratory analysis and reflectance mode pulse oximetry are clinically well accepted, this triangular experiment, combined with previous research (12), indicates that non contact imaging pulse oximetry (11) in principle is feasible.

We propose the term "pulse oxigraphy" for the imaging technique and the term "SpO_2-camera" for the device.

5.7 Acknowledgements

This study was sponsored by TNO Quality of Life (personal thanks to Mr. C. Zeelenberg) and O_2view B.V. (personal thanks to Mr. R.G.M. van Melick and Mr. D. bakker), both sponsors based in Leiden, the Netherlands.
Custom mechanical constructions were made by Mr. L. Bekkering and Mr. G. Springeling, also support on electronics was given by Mr. J. Honkoop and Mr. W. van Alphen (Biomedical Engineering Thorax Centre, Erasmus MC).
We greatly appreciate the help of Mr. J. Sweep and Mr. A. Klippel (Biomedical Instrumentation Sophia Childrens Hospital, Erasmus MC) with building the gas mixing system. Furthermore, we explicitly would like to thank all members of the perfusionists-group and the full staff of the Thorax Centre Clinical Laboratory for their splendid support.

5.8 References

[1] New W and Corenman JE, *Pulse oximeter*, US414176, 1982.

[2] Yoshiya I, Shimada Y and Tanaka K, *Spectrophotometric monitoring of arterial oxygen saturation in the fingertip*. Med Biol Eng Comput, 1980. 18(1): p. 27-32.

[3] Aoyagi T, Kobayashi N and Sasaki T, *Apparatus for determining the concentration of a light-absorbing material in blood*, US4832484, 1989.

[4] Severinghaus JW and Honda Y, *History of blood gas analysis. VII. Pulse oximetry.* Journal of Clinical Monitoring, 1987.

[5] Severinghaus JW, Astrup P and Murray JF, *Blood gas analysis and critical care medicine*. Am J Respir Crit Care Med, 1998. 157(4 Pt 2): p. S114-22.

[6] Wieringa FP, *Imaging apparatus for displaying concentration ratios,* WO 01/15597 A1, 2001.

[7] Wieringa FP, Mastik F and Van der Steen AFW, *Contactless multiple wavelength photoplethysmographic imaging: A first step towards "SpO_2 camera" technology*. Annals of biomedical engineering, 2005. 33(8): p. 1034-1041.

[8] Miyasaka K, *Do we really know how pulse oximetry works?* Journal of Anesthesia, 2003. 17: p. 216–217.

[9] Aoyagi T, Kishi M, Yamaguchi K and Watanabe S. *Improvement of an ear-piece oximeter.* in *13th annual meeting of the Japanese Society for Medical Electronics and Biological engineering*. 1974. Osaka.

[10] Palreddy S, *Signal Processing Algorithms*, in *Design of pulse oximeters,* J.G. Webster, Editor. 1997, Institute of Physics Publishing, Dirac House, Temple Back, Bristol BS1 6BE, UK: Bristol. p. 124-158.

[11] Schubert H, *Messtechnik in der medizinischen Diagnostik - Pulsoximeter (SaO_2)*. Medizintechnik, 2003. 123(2): p. 68 - 70.

[12] Wieringa FP and Van der Steen AFW, *Pulsoxymetrie, een techniek met toekomst maar ook randvoorwaarden*. Klinische Fysica, 2001(4): p. 4-8.

[13] Okamoto Ugnella A and Öberg PÅ, *The optical properties of the cochlear bone.* Medical Engineering & Physics, 1997. 19(7): p. 630-636.

[14] Aoyagi T, *Pulse oximetry: its invention, theory, and future.* Journal of Anesthesia, 2003(17): p. 259–266.

Chapter 6

Pulse oxigraphy demonstrated on a phantom with arterial and venous regions

This chapter is based upon the manuscript:
"Pulse oxigraphy demonstrated on a phantom with arterial and venous regions"
by F.P. Wieringa, F. Mastik, R.H. Boks, A. Visscher, A.J.J.C. Bogers and A.F.W. van der Steen.
Submitted to: Euro Intervention

6.1 Abstract

We performed an experiment to demonstrate pulse oxigraphy as an imaging modality. In previous work (chapter 5 of this thesis) we proved the principal feasibility of pulse oxigraphy by recording 660, 810 and 940 nm movie-sets of a phantom circulating heart-lung machine preconditioned blood through a transparent reservoir, equipped with an electrically modulated LCD-scatterer and a Delrin™ diffuser. In this experiment we used the same camera and processing on a dual reservoir phantom, with added shielding (having dual rectangular slits) inserted between diffuser and LCD-shutter. We simultaneously injected 30ml arterial and venous blood, collected from heart-lung machine-perfused patients (n=2), into both reservoirs.
Using transfer function $f_{CAM\text{-}LAB}$ (obtained at pH = 7.35 ± 0.05) between camera-derived average ratio-of-ratios $\overline{R_{660/940}}$, and laboratory SO_2 results, we produced pulse oxigrams of the phantom.
Distinct arterial and venous regions were visualized. Camera-derived *arterial* oxygen saturations versus laboratory measurements were: 97.0% versus 99.5% (patient 1, pH=7.41) and 97.5% versus 99.5% (patient 2, pH=7.37). The *venous* region produced: 86.5% versus 74.4% (patient 1, pH=7.39) and 89.1% versus 86.2% (patient 2, pH=7.34).
Pulse oxigraphy using the ratio-of-ratios method can visualize differences in geometrical distribution of blood oxygen levels in-vitro. Improving the phantom's response characteristics is target of ongoing research.

6.2 Introduction

In a previous study (see chapter 5 of this thesis) we circulated heart-lung machine preconditioned blood through a transparent reservoir, equipped with an electrically modulated LCD-scatterer and a Delrin™ diffuser. Using this phantom, we recorded 116 movie-sets at three wavelengths being 660, 810 and 940 nm (further called 3λ-movie-sets) and we demonstrated that, using the ratio-of-ratios method, we could derive three oxygen dependent parameters from each 3λ-movie-set. These three camera-derived parameters were the average ratio-of-ratios $\overline{R_{660/940}}$, $\overline{R_{660/810}}$ and $\overline{R_{810/940}}$.
For 29 of the 116 above-mentioned 3λ-movie-sets, also laboratory blood gas analysis data were available.
A third-order least-squares spline approximation revealed a monotone transfer function $f_{CAM\text{-}LAB}$ between the 29 pairs of *camera-derived* average ratio-of-ratios $\overline{R_{660/940}}$ and *laboratory* results for SO_2.
In this paper we apply the transfer function $f_{CAM\text{-}LAB}$ to new 3λ-movie-sets acquired from a modified phantom, being capable to simultaneously provide two regions having different oxygen saturations. The aim of this study is to verify whether (and how) both phantom regions can be displayed using our experimental camera setup and in how far camera-derived oxygen saturations match with laboratory results.

6.3 Methods

The general setup of the experiment is shown in figure 1.

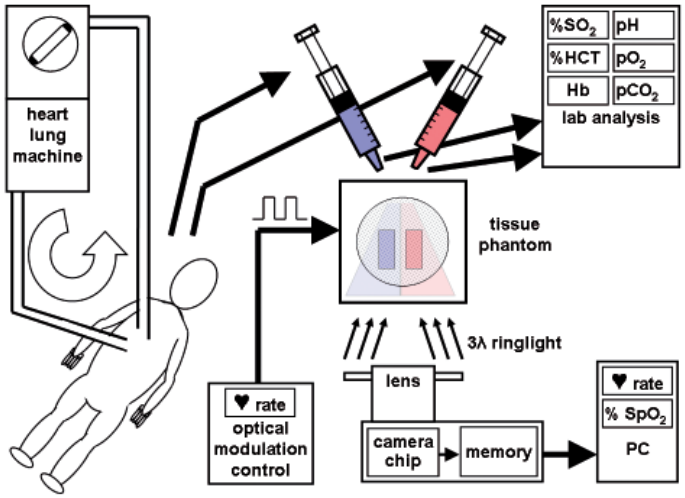

Figure 1 General setup of the experiment

We recorded new 3λ-movie-sets, partly using the same hardware as described in the previous chapter. The setup, however, had some differences, namely:
For each patient we applied a disposable modified blood reservoir, having a 2 mm thick grey PVC separation wall glued in the middle, which divided the transparent reservoir into a left and right chamber (see figure 2).

Figure 2 Dual chamber cuvette filled with arterial and venous blood (shown without Delrin™ diffuser and slitted shielding in front).

Two verticular slits (5 x 20 mm) were cut out in a small piece of paper (80g m^{-2}; front side white, back side printed with carbon black toner), which then was placed between the 0.5 mm thick Delrin™ diffuser and the LCD-shutter. The positions of the slits (diffusely visible in figure 4B) matched with the centres of the left and right reservoir chambers.
Instead of using a heart-lung machine to artificially oxygenate a stand-alone blood pool being circulated through the phantom, we used an arterial and a venous bloodsample (both 30ml) simultaneously withdrawn from stable patients (n=2) connected to a heart-lung machine during cardiac surgery. The operating room was located within < 2 minutes walking distance from the laboratory, where the camera setup was stationed next to an ABL720 blood gas analyzer (Radiometer, Copenhagen, Denmark). Immediately after withdrawal, both blood samples were rushed to the laboratory and injected respectively in the left and right chambers of the dual chamber reservoir, followed by recording of a 3λ-movie-set at 660, 810 and 940 nm at an LCD “heart rate” of 60 beats min^{-1}. While movie recordings took place, laboratory blood gas analysis

was performed. First the recorded 3λ-movie-sets were processed to obtain the individual oxygen dependent ratio-of-ratios $\overline{R_{660/940}}$, of all ROI-pixels regarded as valid by the processing software (as decribed in the previous chapter).
Then the transfer function $f_{CAM\text{-}LAB}$ (see figure 3) was applied to all valid ROI-pixels in order to compose a pulse oxigram. Note: only ROIs meeting a pulsation autocorrelation criterium ($\rho \geq 0.8$) and an additional amplitude treshold ($A \geq 0.6\%$ of ROI-mean DC value) were considered to contain a valid pulse wave.
Finally the median of the calculated SO_2 values assigned to all valid ROI-pixels was compared with laboratory results.

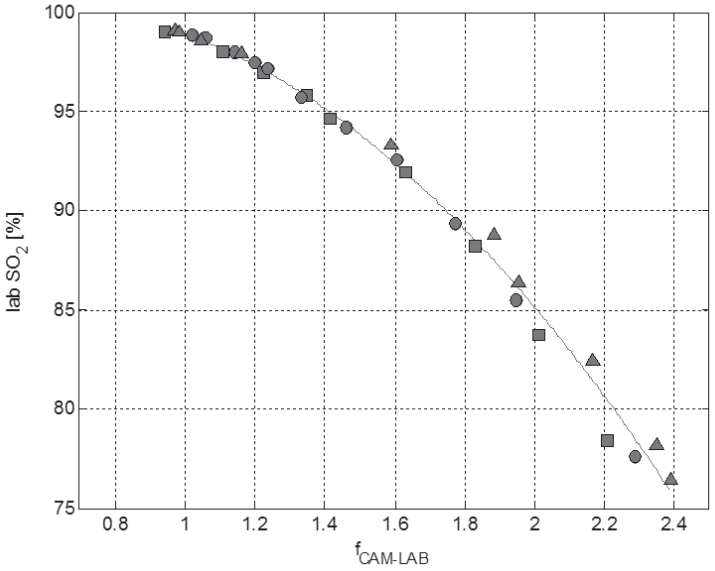

Figure 3 Transfer function
Transfer function $f_{CAM\text{-}LAB}$ between $\overline{R_{660/940}}$ and the laboratory values of SO_2 as derived from a previous study.

6.4 Results

Both camera-derived pulse oxigrams showed two distinct pulsatile regions with clearly different oxygen saturation values. Table 1 lists the numerical results of the median arterial and venous SO_2 values that were derived from the camera recordings by applying the transfer function ($f_{CAM\text{-}LAB}$) in relation to laboratory results for SO_2 and pH.

			Arterial	Venous
Patient 1	Camera	SO_2 [%]	97.0	86.5
	Laboratory	SO_2 [%]	99.5	74.0
		pH	7.41	7.39
Patient 2	Camera	SO_2 [%]	97.5	89.1
	Laboratory	SO_2 [%]	99.5	86.2
		pH	7.37	7.34

Table 1

Oxygen saturation values derived by calculation from camera recordings in comparison with laboratory measurements. The camera-derived venous saturation value for patient 1 falls at the edge of the range for which $f_{CAM\text{-}LAB}$ originally was derived.

Figures 4A and 4C show the obtained pulse oxigrams using a false color scale (red = high saturation, blue = low saturation) backprojected on an oxygen-independent grey scale image acquired at 810 nm, displayed for comparison in figure 4B.

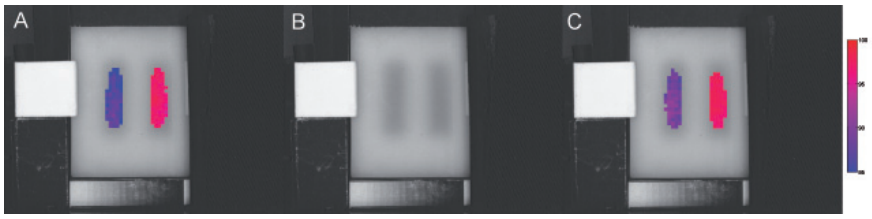

Figure 4 Pulse oxigrams

Figure 4A shows the pulse oxigram from the dual chamber phantom filled with arterial and venous blood of patient 1. Figure 4C shows the results when using arterial and venous blood originating from patient 2. Figure 4B in the middle shows the grey scale reference image of patient 2 obtained at 810 nm (this wavelength contains no oxygen information, therefore only 1 reference image is shown here)

6.5 Discussion

The processing algorithm was applied to the whole field of view. Both pulsatile regions were well discriminated against the stationary background.
Within the *arterial* phantom region, the deviations in oxygen saturation (camera-derived value minus laboratory value) were relatively small (-2.5% and -2.0%), the camera thus slightly *under*estimated saturation.
Within the *venous* phantom region, however, the camera *over*estimated saturation (+12.1% and +2.9%).
The reason for the relatively large deviation between the camera-derived and laboratory results for the venous region of patient 1 may be that here venous saturation was beyond the range for which transfer function $f_{CAM\text{-}LAB}$ had been derived.
However, the outcome is also likely to be influenced by geometrical differences in the dual chamber phantom compared to the single chamber phantom as used to derive $f_{CAM\text{-}LAB}$ (e.g. addition of the PVC separation wall, addition of the slitted shielding of paper and blackening a diffusing surface facing the blood).
From only 2 patients such reasoning remains speculative. In order to investigate the usefulness of pulse oxigraphy, further research (e.g. determination of $f_{CAM\text{-}LAB}$ for multiple values of pH and hematocrite) will anyhow be needed.
Our priority is to first improve the phantom's response curve to a much more physiological behaviour with regard to pulse waveform and to normalize pulse oximetry response in relation to laboratory values, before performing such extensive additional research.

6.6 Conclusions

We proved that pulse oxigraphy based upon the ratio-of-ratios method can visualize differences in geometrical distribution of blood oxygen levels in a simple in-vitro configuration. Improvement of the phantom's characteristics is target of ongoing research.

6.7 Acknowledgements

This study was sponsored by TNO Quality of Life (personal thanks to Mr. C. Zeelenberg) and O_2view B.V. (personal thanks to Mr. R.G.M. van Melick and to Mr. D. bakker), both sponsors based in Leiden, the Netherlands. Custom mechanical constructions were made by Mr. L. Bekkering and Mr. G. Springeling, also support on electronics was given by Mr. J. Honkoop and Mr. W. van Alphen (Biomedical Engineering Thorax Centre, Erasmus MC). We greatly appreciate the help of Mr. J. Sweep and Mr. A. Klippel (Biomedical Instrumentation Sophia Childrens Hospital, Erasmus MC) with building the gas mixing system. Furthermore, we explicitly would like to thank all members of the perfusionists-group and the full staff of the Thorax Centre Clinical Laboratory for their splendid support.

Chapter 7

Concept for visualization of buried vascular structures

This chapter is based on the following pending patent:
"Imaging of buried structures"
invented by F.P. Wieringa, D. Bakker, A.F.W. van der Steen, F. Mastik and R.G.M. van Melick
published in 2005 by the European Patent Office with reference EP 1 566 142 A1

7.1 Explanatory introduction to this chapter

7.1.1 General considerations

The content of this chapter is patent document EP1566142A1 *"Imaging of buried structures"*, describing a method to visualize vascular structures in biological tissue by combining information derived from tissue images in the visible (VIS) range and the near infrared (NIR) range [1].
VIS images mainly contain contrasts from the tissue surface because the penetration depth of visible light in tissue is quite limited. Within the NIR range, however, optical penetration depth increases. This effect is known as the *"near infrared window"*. Blood vessels at a reasonably shallow depth can be visualized in transillumination or reflectance mode by using a NIR light source and NIR camera, which has been known for long [2-4]. The contrast is not very high, because within the NIR range the absorption difference between blood and surrounding tissue is rather limited. It is thus obvious to use image enhancement techniques to improve the contrast. But…when enhancing the contrast in a simple NIR-image, there is no simple way to tell whether a contrast originates from the tissue surface or from below the surface. Thus all contrasts, including body hairs, molds, shadows cast by e.g. needles and skin folds are boosted, instead of only blood vessels from below the surface. That is a pity, because electronically enhanced vision might be very useful to facilitate e.g. insertion of a needle into a blood vessel.

7.1.2 Selective enhancement of contrast from below the surface

Our innovative technique, however acquires VIS and NIR images that are exactly pixel-to-pixel matched, using VIS and NIR light sources that send their combined beams in the same direction (thus causing matching shadows and reflections). Our

software then selectively enhances contrasts at those pixel locations where the NIR image shows a higher contrast than the VIS image. In other words: we selectively enhance the blood vessels and combine them with the normal VIS image, without disturbing important depth clues like shadows and reflections on the surface.

7.1.3 Stereoscopy offers optimal use of depth clues

By using a separate Left and Right camera/display combination, the method offers intuitive stereoscopic reflection mode images in normal full color as well the possibility to enhance vascular structures at shallow depth underneath the skin (or beneath e.g. a fat layer). It is clear that image guided surgery benefits from stereoscopic imaging.

7.1.4 Shaping shadows to a helpful format

By using a Left and Right light source, we create additional useful depth clues from shadows: When e.g. a needle approaches the tissue, it casts two shadows that form a V-pattern when the tissue surface is touched. This helps to more precisely estimate the distance to the tissue.

7.1.5 Improving depth range by exploiting backscatter

The patent describes an additional trick to increase the depth range. One problem is, that light emanating from deeper parts of the tissue is much weaker than the light directly from the surface. Separation of specular light reflections from the surface and light emerging from deeper parts of the object can improve the visualization of underlying structures like vasculature.

A “traditional” method to suppress surface reflections is the so-called “crossed polarizer” method [5, 6]. This approach requires much stronger light sources, because even if both polarizers would be ideal they each transmit maximum 50%. This loss of light may be overcome by the use of more powerful light sources in order to receive sufficient light from deeper within the tissue. However, when imaging structures in living tissue, there is a maximum allowable irradiance [7-16].

An innovation that we claim in patent document EP1566142A1 can be described with help of a chess board. For all even image frames, we project a pattern of laser dots on the center all black sections while viewing the white sections, and for all odd frame numbers we project a pattern of laser dots on the center of all white sections while viewing the black sections. In this way we insert the light into the tissue sideways from a region of interest. The backscattered light forms a diffuse “backlit” so that the bloodvessels are illuminated from behind. Using this method surface reflections do not occur, so they don’t have to be suppressed either!

7.1.6 Combination with earlier patent possible

The device has no restrictions for pulsatility analysis (e.g. hart beat frequency analysis and/or respiratory frequency analysis). The functionality of the patent previously described in chapter 2 thus in principle can be built into our blood vessel enhancer.

7.1.7 Illuminating the needle tip via the lumen

By cleverly shining with e.g. an infrared LED or laser diode through the needle lumen, the needle tip can be illuminated which helps to distinguish the moment of puncturing a vessel wall and to illuminate the vessel interior. We added the option to flash this tip illumination in order to help identify the tip in the tissue.

7.2 Patent description

7.2.1 Abstract

A method of obtaining an image of buried structures in an object, comprising: providing a camera for imaging visual and infrared-images; providing a bounded light source; partly irradiating said object by said bounded light source; imaging a non-irradiated area of said object by said camera to image said buried structure; and combining said buried structure image with a visual image of said object. Accordingly an image can be obtained while discarding specular reflections of the object. Additionally the invention offers a method of enhancing imaging of buried structures in an object, comprising: aligning said infrared light source with a visual light source; providing a first edge analysis of said infrared image; providing a second edge analysis of said visual image; comparing said first and second edge analysis; and discarding edges in said infrared image that are also detected in said second image.

7.2.2 Imaging of buried structures

The invention relates to a method of obtaining an image of buried structures in an object, in particular to imaging structures such as vascular structures in biological tissue by means of selective combining information derived from tissue images in the visible range and the infra-red range.

A method describing such is disclosed in the international application WO0115597 by the same inventor. It has been found, that obtaining a sufficiently clear image is difficult due to various problems. One problem is, that light emanating from buried, in particular deeper parts of the object is often much weaker than the light that is reflected directly by the surface of the object. In practice, this means that a separation of the specularly reflected light and light emerging from deeper parts of the object may be needed in order to identify underlying structures.

While separating these two types of light, for instance by a known method of using polarized light and using the fact that specularly reflected light keeps its polarization direction, so that it can be filtered out by means of a polarizing filter, a substantial amount of the light is lost that is originating from the lower parts of the object, thus resulting in a loss of image brightness and resolution. This invites to the use of powerful light sources in order to receive sufficient light from the lower parts in the process of separating the two parts. However, especially in the area of imaging structures in live objects, there is a maximum amount of light that may be irradiated on the object.

WO01/50955 shows a reflective arrangement where specular light is filtered by a polarizator. The image of an underlying structure is combined with a visual image to present a single image. However, it has been found that straightforward combination of these images offers problems, in particular, since certain artefacts occur that are inconvenient to reliably detect and locate an underlying structure.

US2001/0037811 shows a probe for determining a circumference of a finger. Additionally, the joint is transilluminated for inspecting arthritis inflammation from a scattering analysis. This arrangement cannot be used for visually imaging body parts with a freedom comparable to the human eye.

The invention has as an object to provide an imaging technique that does not suffer from the afore described problems and that is able to provide an enhanced image of the underlying structure. Moreover, the invention has as an object to provide an imaging enhancement technique to enable a person to combine visual information and information of buried objects in one image.

To achieve these and other goals, in one aspect, the invention offers a method according to the features of claim 1. In another aspect, the invention offers a method according to the features of claim 14.

In particular, by providing a camera for imaging visual and infrared-images; providing a bounded light source for partly irradiating said object by infrared light; partly irradiating said object by said bounded light source; imaging a non-irradiated area of said object by said camera to image said buried structure; and combining said buried structure image with a visual image of said object, infrared light incident on the image that is originating from a direct reflection is spatially filtered out of the image. The remaining partial image hence does not suffer from saturation effects due to direct illumination of specularly reflected light. In a preferred embodiment, a full image is provided by varying said partial irradiation in time so as to provide a full image by subsequent combining of said partial images.

In a further preferred embodiment, said partial image is obtained by scanning a light beam over said object. In addition or alternatively, said partial image is obtained by subsequently irradiating said object by predetermined patterns. One particularly preferred embodiment comprises obtaining said partial image by alternatingly irradiating said object by a predetermined complementary patterns. For instance, in an embodiment said patterns may be matrix-patterns, line patterns, dot patterns, concentric or circular patterns.

Further, preferably said object is irradiated only at predetermined positions that are spaced apart. By spacing the irradiation area and the light detection area, deeper parts of the buried structure may be enhanced.

By alternatively illuminating said object, a full image may be provided, and wherein all areas of the object are irradiated in a time-dependent manner.

The invention further offers particular benefits while using a CMOS-camera, since these camera's have a high degree of decorrelation of adjacent pixels. Thus, the effect of "blooming" is prevented, so that there is a high contrast between the directly reflec-

ted area (that is discarded) and the remaining area which receives diffuse light originating from deeper layers.
Furthermore, the invention is preferably used while aligning said infrared light source with a visual light source; providing a first edge analysis of said infrared image; providing a second edge analysis of said visual image; comparing said first and second edge analysis; and discarding edges in said infrared image that are also detected in said second image. This offers the benefit of obtaining a "normal" visual image (as seen by the human eye), that is enhanced by identifying the underlying structure (detected using infrared light) within the visual image while discarding false edges formed by shadowing or aliasing artifacts (e.g. shadows or reflections from a scalpel or needle). For instance, for surgical purposes, the method offers a convenient tool for deciding an optimal entry point in the object, for instance for cutting tissue or the like.
Preferably, said edge-detection is performed by a gradient analysis of said first image. The invention offers a convenient embodiment when said images are provided stereoscopically. Furthermore, said first image may be spectrally analysed, and wherein said spectral analysis is projected into said second image. Furthermore, said spectral analysis may comprise a pulsatility analysis and/or a hart beat frequency analysis and/or respiratory frequency analysis. Such analysis thus offers a convenient non-contact tool for measuring body parameters of interest. Under "pulsatility analysis" is understood at least a determination of pulsating parts in the object of interest.
The invention is further related to a method of enhancing imaging of buried structures in an object, comprising: as defined in claim 14. Furthermore, the invention is related to a system as defined in claim 16.

Further features and benefits will become apparent from the figures:

Figure 1 shows a schematic view of a scanning irradiating method of an object according to the invention;
Figure 2 shows a schematic view of foton-migration in live tissue due to diffusion;
Figure 3 shows an illumination method by illuminating an overlapping pattern on the object;
Figure 4 shows an illumination method by illuminating a circular patterns on the object;
Figure 5 shows an illumination method by illuminating a grid of patterns on the object;
Figure 6 shows a testing arrangement for testing the apparatus according to the invention using one visible wavelength and two infrared wavelengths;
Figure 7 shows a series of analysis steps for processing and routing of data acquired from the arrangement of Figure 6;
Figure 8 shows a spectral analysis of the pulsatile components in said image for light of three different wavelengths;
Figure 9 shows a simple vizor-like construction comprising the apparatus of the invention;
Figure 10 shows the vizor-like construction of Figure 9 in use;
Figure 11 shows the VIS and NIR images collected by the eyepiece of Figure 9;
Figure 12 illustrates the steps according to the method of the invention; and
Figure 13 shows a further embodiment of the inventive system including an infrared emitting puncture tool.

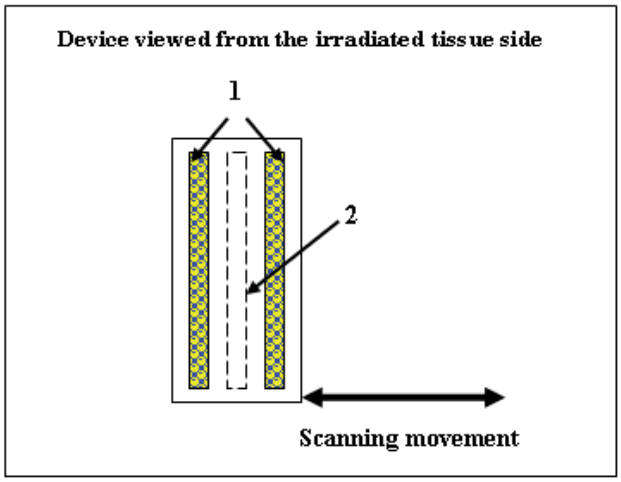

Figure 1

Figure 1 shows an alternative to the above described polarization filtering method. This method comprises dynamic complementary lighting/scanning of alternating patterned image sections. This method does not require the use of polarization filters. It is based on the fact that photons entering biological tissue will strongly scatter within the tissue which partly results in backscattering.

Furthermore the viewed area is divided into parallel linear areas , which we will call "line sections". These line sections can be divided into even and uneven line sections 1, 2 respectively.

Using a camera that has good anti-blooming specifications and allows the read-out of freely selectable rectangular pixel regions we then can acquire image information in a special sequence.

During a certain period the bounded light source will light all even line sections 1 and the camera will acquire image information from all uneven line sections 2. Here, the term bounded encompasses light that is bounded spatially, so that an illuminated object comprises, in a direction of view which is also a direction of illumination, non-illuminated areas which are not reached by the bounded light source. Such bounding can be typically reached by focusing, collimating or shielding the light source. Also various other light sources, such as laser lights (e.g. in combination with a holographic grating) and LEDs, can produce bounded lights. During the next period the uneven line sections 2 are lighted and the camera will acquire image information from the even line sections. This can either be done with a line camera that scans the entire tissue or with a normal camera that scans all even lines simultaneously and during the next period all uneven lines.

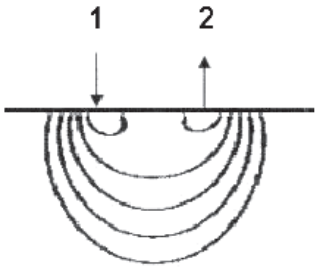

Figure 2

In Figure 2 is illustrated how light diffused within the tissue can be used to image deeper parts of the object. Light enters the object at one position 1 and leaves the object at another position 2. From the figure it becomes clear that light entering at further distanced positions can collect information from parts deeper within the object. By applying a variety of illumination patterns as will be further described with reference to Figure 3 - Figure 5, illumination from "within" the object can be achieved, thus imaging deeper parts of the object.

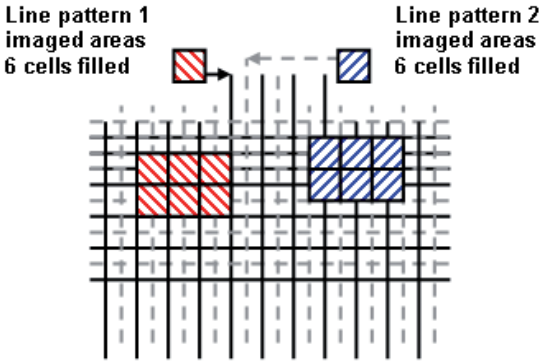

Figure 3

To this end, in Figure 3, instead of even and uneven parallel lines shown in Figure 1, alternate spatially shifted crossed line patterns can be used as lighting pattern whilst image acquisition occurs within the areas between the lines. It is also possible to first project an "even" dot pattern on the cross point of line pattern 1 and then project an "uneven dot pattern on the cross sections of line pattern 2.

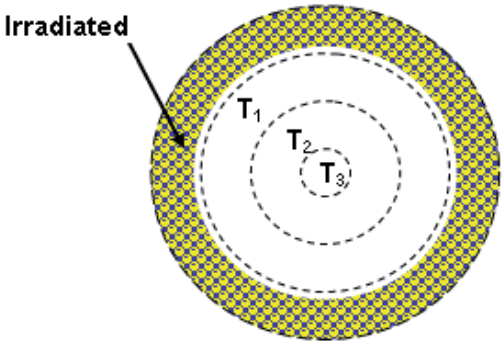

Figure 4

Also, in Figure 4 discrete concentric circular areas can be used. Satisfying results were obtained by a simple test of circular irradiation geometry disclosed in Figure 4. A 6mm thick slice of pink foam (3M ethafoam) was laid upon the shielding pipe. On top of this foam slice a plastic office clamp was placed, with its' white plastic paper retaining slice laying across it. Finally a second slice of pink foam was laid on top. Outside the camera's field of view, a ring light injected photons of 660 nm, 810 nm and 940 nm into the foam, perpendicular to the foam surface.

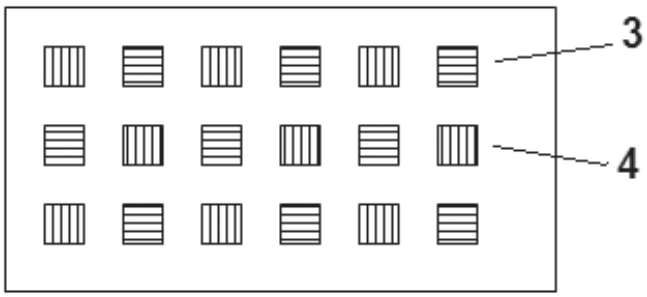

Figure 5

Figure 5 shows another embodiment, wherein said object is irradiated only at predetermined positions that are spaced apart. First areas 3 indicated with horizontal lines are irradiated in a first period; second areas 4 with vertical lines are irradiated in a second period. Such a spaced apart configuration is able to show deeper parts of the structure. By varying the spacing, lower and deeper parts of the object may be scanned.

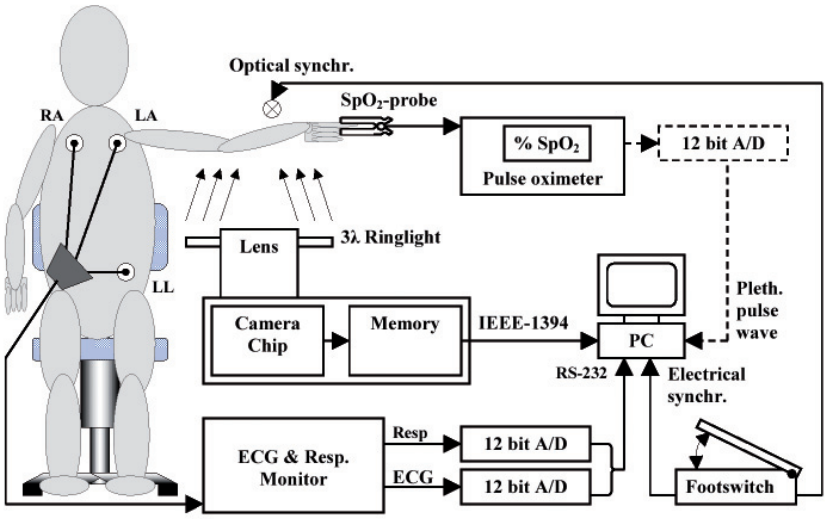

Figure 6

Figure 6 shows a testing arrangement, where an embodiment of the inventive method was tested using known markers such as an SpO_2 pulse oximeter, an ECG recording devise and a respiratory frequency monitor. The signals were recorded and sampled using the steps indicated in Figure 7.

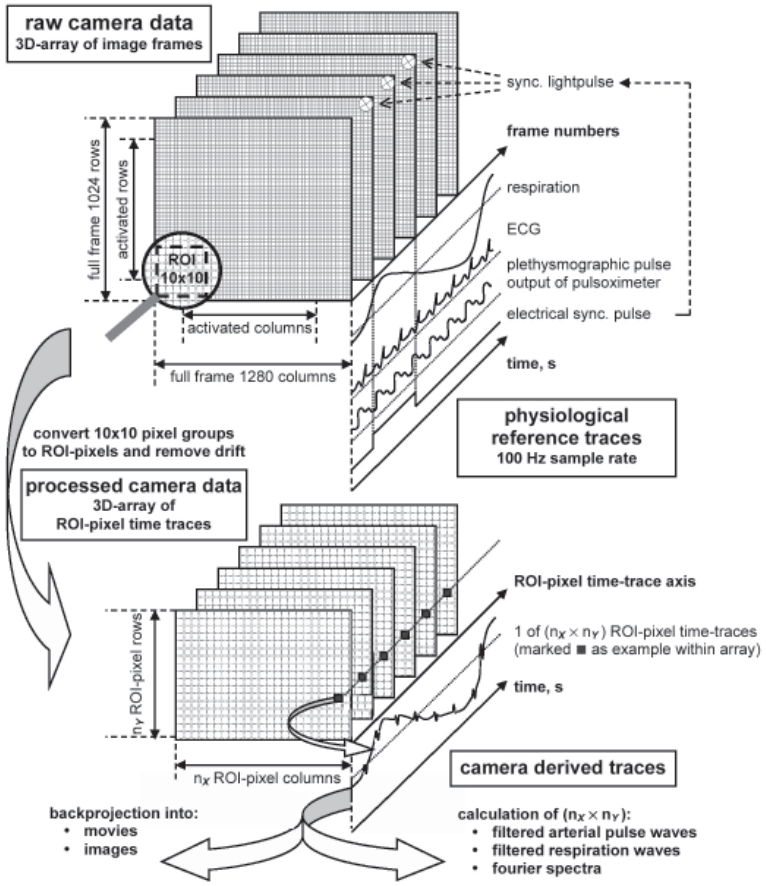

Figure 7

This leads to a pixel by pixel time-analysis of intensity variation. The frames were sampled at a 100Hz Sample rate and the recorded respiration, ECG and plethismographic pulse output were compared. The outcome is illustrated for a variety of wavelengths in Figure 8.

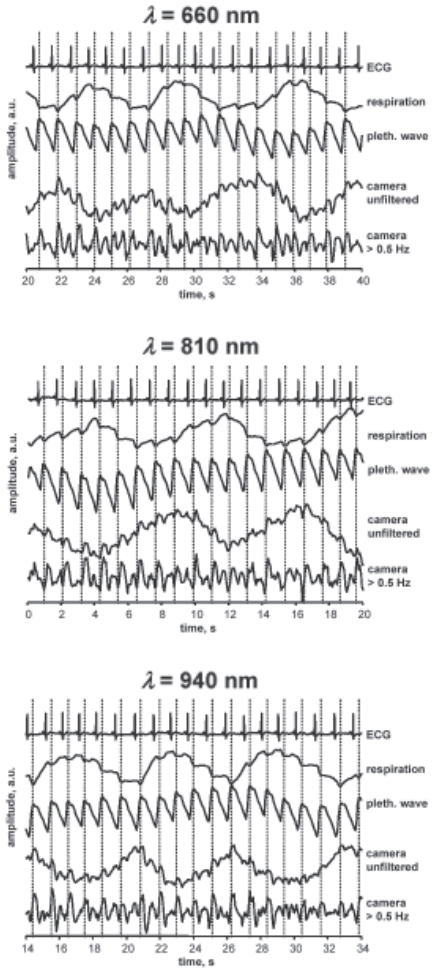

Figure 8

It is clearly shown how well the measured variation of the camera matches with the other pulse signals.

A special configuration with added value is based upon two cameras (e.g. CCD or CMOS monochromatic or multiband) positioned at a certain distance from each other (e.g. eye-to-eye distance) thus stereoscopically viewing the same object (e.g. biological tissue), a dual channel electronic image processing device and two display devices placed in front of both eyes.

Between each camera and the viewed object an additional optical system (maybe combining 2 channels) may be placed (e.g., a dual channel microscope, endoscope, colposcope, etc.).

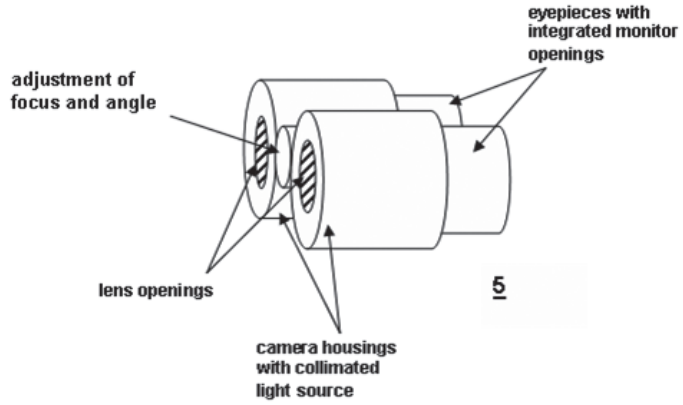

Figure 9

It is possible to incorporate a simple vizor-like construction 5 (see Figure 9) so that the device can be either put in front of the eye or be positioned out of the viewing angle to allow normal sight.

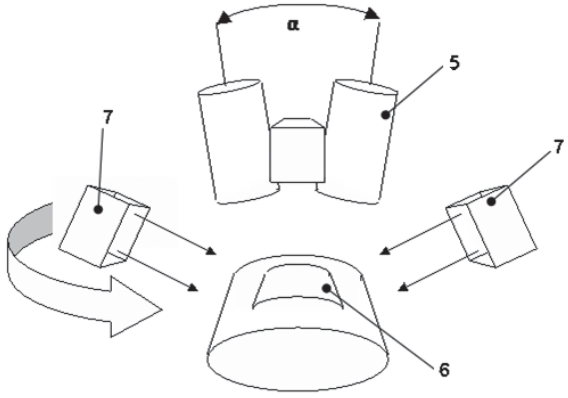

Figure 10

Figure 10 shows as an example the stereoscopic eyepiece 5 of Figure 9 in use. For the eyepiece, a color camera can be applied with a bayer color filter pattern of which all filter colors are highly transparent in the NIR-range. Also a multi-layered camera chip (Patent WO 02/27804 to Foveon Inc. or earlier patents like 4,238,760 to Carr) or the approach in our previous patent WO 01 15597 A1 can be applied. Preferably, the images in both spectral ranges match pixel to pixel.

The surface of the viewed biological tissue region 6 is irradiated at an oblique angle from two opposite sides by two light sources 7. These two sides need not to be aligned with the Left/Right axis of the eyepiece 5, but can be swiveled around in a plane perpendicular to the central axis of the joined cameras.

The light sources 7 can be controlled to independently send out broadband white light in the visible wavelength range (VIS; 400 - 780nm) or narrowband light in the near infrared range (NIR; e.g. 920 nm) as well as in both ranges (VIS & NIR). The light sources 7 are carefully constructed so that the geometrical beam profiles of VIS and NIR are aligned resulting in identical shadowing in the VIS and NIR images. As an alternative also a surgical stereo microscope or an endoscopic dual channel camera (as used in stereoscopic robot surgery) with two side fiber light guides can be used to collect the images.

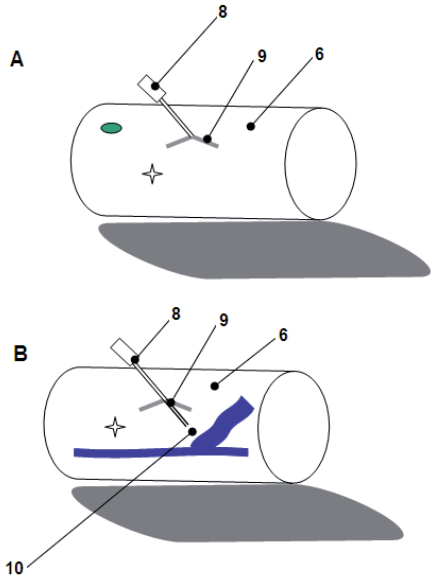

Figure 11

Figure 11 shows the result of the VIS (Figure 11 A) and NIR (Figure 11 B) images such as collected by the eyepiece 5 illustrated in Figure 10. Since NIR and VIS beams are matched, shadows produced by irregular shapes at the tissue surface (e.g. skin structure, skin folds, molds, etc.) will also match in both wavelength ranges. In the embodiment disclosed, the beams are oriented at a small angle with respect to the tissue region 6. As a result, skin folds etc. will produce sharp-edged shadows. Shiny areas that produce reflections and/or saturated pixels (marked as a star) will also match in both wavelength ranges. Due to the small angle, objects 8 that are brought towards the tissue surface 6 (e.g. needles, scalpels, probes, etc.) will produce two separate shadows. These shadows will meet and typically form a “V” pattern 9 when an object touches the surface. If e.g. a needle punctures the surface, then the needle tip 10 will quickly disappear from the VIS image (Figure 11 A). On the NIR image (Figure 11 B) however, the tip 10 will remain visible within the tissue 6.
On the VIS image (Figure 11 A), only very superficial blood vessels will be visible,

especially if the texture of the vessel deforms the skin. On the NIR image, however, blood vessels will be visible much better (even blood vessels at a depth of a few millimeters below the surface). Since skin pigment (melanin) has a very low absorbance within the NIR region this good NIR visibility will also be the case with dark skinned persons (also molds will lose their dark color).
After obtaining the NIR and VIS images in steps 11 and 12 respectively, a gradient edge enhancement step is applied for both spectral bands as will be illustrated with reference to Figure 12 (steps 13 and 14).

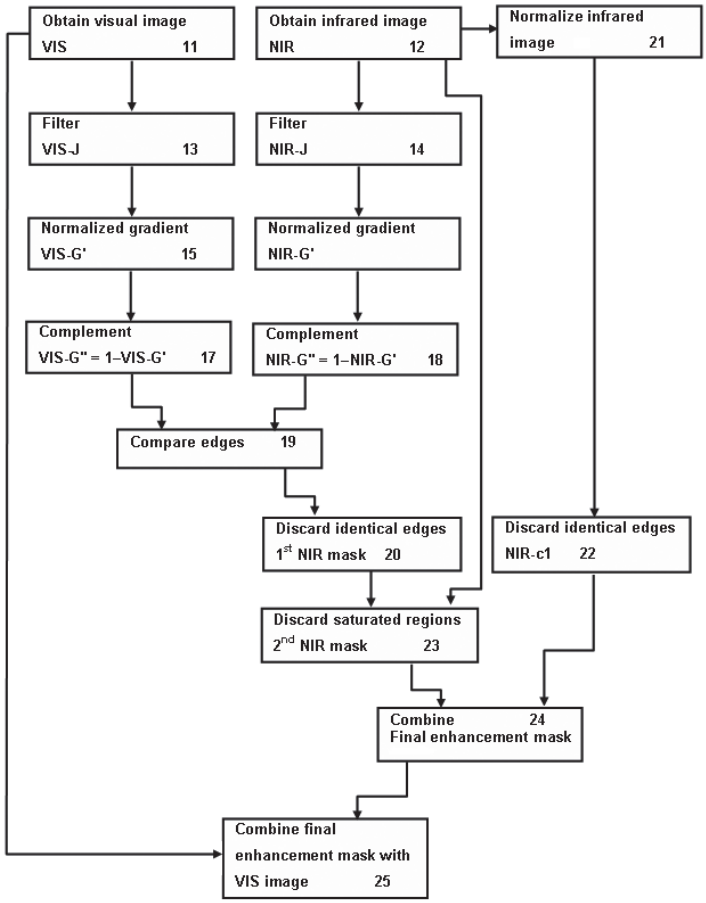

Figure 12

Image VIS-J and NIR-J are obtained by filtering with a smoothing filter to suppress noise from camera image NIR and VIS. In the current implementation this is an averaging filter. From each smoothed images VIS-J and NIR-J, two directional difference images Ix and Iy are calculated by means of a gradient filter. Currently this it performed with a Prewitt filter.

Next edge gradient images VIS-G and NIR-G are made. Then VIS-G and NIR-G are clipped and normalized to 1 to obtain VIS-G' and NIR-G' (Steps 15 and 16). Finally the images are complemented to 1-G' (Steps 17 and 18).
For a given tissue region a VIS image and a pixel to pixel matching NIR image are acquired.
The images from both spectral bands are subjected to an identical edge enhancement algorithm (see above), producing normalized NIR-edge and VIS-edge grayscale images so that edges are encoded black (0 = black and 1 = white; note that this is the negative of normal edge enhanced results).

Now corresponding edges in the NIR and VIS image are determined (Step 19) according to a pixel by pixel criterion:

NIR-edge-pixel < NIR_Treshold AND VIS-edge-pixel < VIS_Treshold
(Thresholds are both software configurable)

By combining information from both spectral regions, the pixel co-ordinates that match both requirements are identified as superficial artifacts and are discarded by setting the pixel value to 1 in the corrected NIR edge image (Step 20).
By doing the same in the raw NIR image after normalizing (Step 21) (no edge enhancement) a corrected normalized NIR image (Step 22) is defined by discarding saturated image areas.
To this end, the locations of all saturated pixels within the raw NIR image (e.g. 256 for an 8-bit image) are identified. For all pixels within the 1st NIR-mask that are saturated or direct neighbors of a saturated pixel, the edges are discarded by setting the pixel value to 1 (and thus completely ignoring edge information) is filled in, resulting in a second NIR-mask (step 23).
False edges resulting from saturated pixels are thus removed and the 2nd NIR-mask now contains the boundaries of subcutaneous blood vessels (and eventual other buried contrasting structures).
This approach can be varied by including second, third etc. neighboring pixels.
In a preferred mode, the raw IR image is used to provide "filled in" blood vessels; for example, by multiplying the 2nd NIR-mask with the 2nd corrected NIR image (step 24).
The amount of fill-in colorization can be varied with a user adjustable exponent N :

2^{nd} NIR-mask x $(1^{st}$ corrected NIR image$)^{N}$ = final enhancement mask

Finally, this final enhancement mask now is multiplied with the luminosity component of the raw VIS image (which preferably is a color image) in step 25. In this way only contrast information that truly originates from below the tissue surface is projected into the VIS image. If we look at the previous drawings with a needle inserted in tissue it is clear that these criteria will lead to superimposing only the buried needle tip

upon the VIS image. Shadows, wrinkles, reflections and the edges of molds will not be enhanced.

The detection of purely superficial artifacts thus can be further improved when instead of taking all colors of the visible region into account, only the Blue spectral range is used for the VIS edge enhancement input. This is done in order to suppress the visibility of blood vessels. This effect of blue light is because in the visible range, the reflectivity of vessels for blue light is the nearest to skin (the maximum visible vessel contrast lies outside the blue range). As another optional refinement the final enhancement mask may be selectively multiplied with e.g. only the Red and/or Green portion of the visible image (instead of the luminosity signal of the total visible color image).

When an interesting tissue portion is spotted, the user can switch to a mode that alters the image capturing sequence and allows the collection of an additional (second) NIR image within a selected region of interest (ROI). This ROI is virtually illuminated by photon injection just outside the ROI by means of EITHER a LED-array in contact with the tissue OR a pattern of laser dots or laser lines projected onto the tissue from a distance. During acquisition of this second NIR image the VIS and first NIR lighting are off.

In this way information obtained using two types of lighting geometries for the same wavelength range can be combined. This can be done with or without also using VIS and flashing needle tip lighting as will be illustrated with reference to Figure 13.

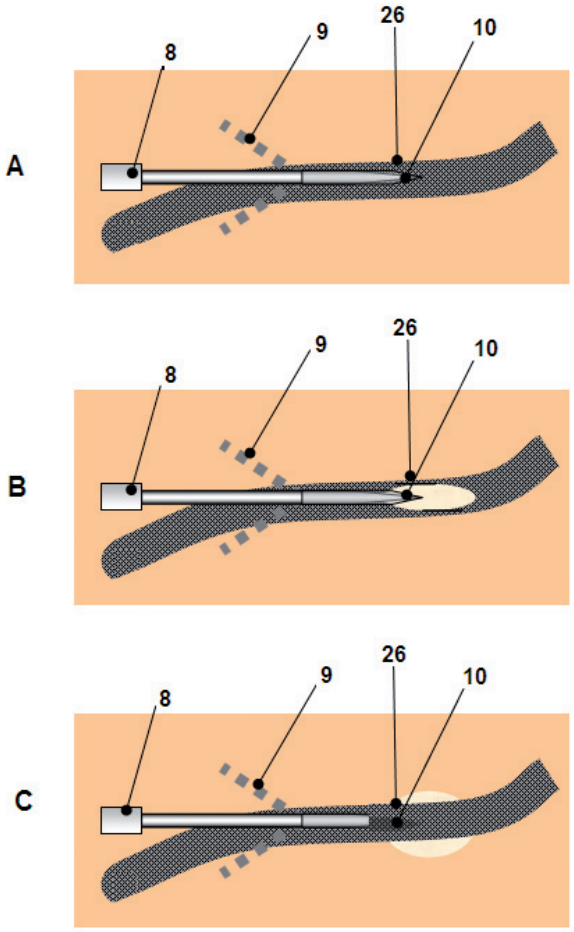

Figure 13

In Figure 13 a NIR-laser or NIR-LED is plugged onto a needle or catheter 8. Via a sterile window light is projected through or alongside the needle bore. In this way the needle tip 10 illuminates the vessel interior wall 26 when the needle is in the vessel (see fig 13B). If the needle punctures the distal vessel wall (see fig 13C) a drastic change in illumination is seen. The light source clipped to the needle may be synchronized with the cameras. A flashing tip illumination may be beneficial.

Although in the preceding the invention has been further illustrated with reference to the drawings and the description it will be clear that the invention is not limited thereto and that these embodiments are only disclosed for the purpose of illustration. Variations and modifications thereto are within the scope of the invention as defined in the annexed claims.

7.2.3 Claims

1. A method of obtaining an image of buried structures in an object, comprising:
   - providing a camera for imaging visual and infrared-images;
   - providing a bounded infrared light source;
   - partly irradiating said object by said bounded light source;
   - imaging a non-irradiated area of said object by said camera to image said buried structure; and
   - combining said buried structure image with a visual image of said object.

2. A method according to claim 1 wherein said irradiation is varied in time so as to provide a full image by subsequent combining of partial images.

3. A method according to claim 1 or 2, wherein said image is obtained by scanning a light beam over said object.

4. A method according to claim 1 or 2, wherein said image is obtained by subsequently irradiating said object by predetermined patterns.

5. A method according to claim 4, wherein said partial image is obtained by alternatingly irradiating said object by said predetermined complementary patterns.

6. A method according to claim 4 or 5, wherein said patterns are matrix-patterns, line patterns, dot patterns or concentric patterns.

7. A method according to any of claims 4-6, wherein said object is irradiated only at predetermined positions that are spaced apart.

8. A method according to any of claims 1-7, wherein said image is obtained by a CMOS-camera.

9. A method according to any of the preceding claims, further comprising:
   - aligning said infrared light source with a visual light source;
   - providing a first edge analysis of said infrared image;
   - providing a second edge analysis of said visual image;
   - comparing said first and second edge analysis; and
   - discarding edges in said infrared image that are also detected in said second image.

10. A method according to claim 9, further comprising:
    - correcting said first image to discard saturated image areas.

11. A method according to any of the preceding claims, wherein said images are provided stereoscopically.

12. A method according to any of the preceding claims 9- 10, wherein said first image is spectrally analysed, and wherein said spectral analysis is projected into said second image.

13. A method according to claim 12, wherein said spectral analysis comprises a pulsatility analysis and/or a hart beat frequency analysis and/or respiratory frequency analysis.

14. A method of enhancing imaging of buried structures in an object, comprising:
    - providing a first light source for providing first light of a wavelength that images said buried structure;
    - providing a second light of a wavelength that visually images said object, aligned with said first light source;
    - obtaining a first image by irradiating said object with said first light ;
    - providing an edge analysis of said first image in order to detect the edges of said buried structure;
    - obtaining a second image by irradiating said object with said second light;
    - providing an edge analysis of said second image;
    - comparing the edge analysis of said second image with the edge analysis of said first image;
    - discarding edges in said first image that are also detected in said second image; and
    - combining said first and second images for defining edges of said buried structure in said visual image.

15. A method according to claim 14, further comprising correcting said first image to discard saturated image areas.

16. System for obtaining an image of buried structures in an object, comprising:
    - a bounded light source for irradiating said object by light for providing a first image of said buried structure and for providing a second visual image of said object;
    - a camera device for obtaining said first and second images; and
    - a processing device arranged to:
    - providing a gradient analysis of said first image in order to detect the edges of said buried structure; and for providing a gradient analysis of said second image;
    - comparing the gradient analysis of said second image with the gradient analysis of said first image;
    - discarding edges in said first image that are also detected in said second image; and
    - combining said first and second images for defining edges of said buried structure in said visual image.

17. A system according to claim 16 further comprising:
    - a puncture tool for puncturing human tissue; and
    - an IR light source provided in said puncture tool.

18. A system according to claim 17, wherein said IR light is aligned along said puncture tool.

19. A system according to claim 17 or 18, wherein said IR light is provided in a tip of said puncture tool.

20. A system according to any of claims 17-19, wherein said puncture tool is provided with an IR radiating coating.

21. A system according to any of claims 17-20, wherein the IR light source and the bounded light source are alternatingly activated.

22. A puncture tool for puncturing human tissue; and an IR light source provided in said puncture tool.

7.3 References

[1] Wieringa FP, Bakker D, van der Steen AFW, Mastik F and van Melick RGM, *Imaging of buried structures*, EP1566142A1, 2005.

[2] Gostout CJ and Jacques SL, *Infrared video imaging of subsurface vessels: a feasibility study for the endoscopic management of gastrointestinal bleeding.* Gastrointestinal Endoscopy, 1995. 41(3): p. 218-224.

[3] Kono M, Ueki H and Umemura S, *Near-infrared finger vein patterns for personal identification.* Applied Optics, 2002. 41(35): p. 7429-7436.

[4] Ontikova NM, Iaroslavtsev DA and Lirman AV, *Increase in the information content of the image of the surface veins by using a television infrascope.* Meditsinskaia tekhnika, 1976(5): p. 20-22.

[5] Christ F, Bauer A and Brugger D, *Different optical methods for clinical monitoring of the microcirculation.* European Surgical Research, 2002. 34((1-2)): p. 145-151.

[6] Groner W, Winkelman JW, Harris AG, Ince C, Bouma GJ, Messmer K and Nadeau RG, *Orthogonal polarization spectral imaging: a new method for study of the microcirculation.* Nat Med, 1999. 5(10): p. 1209-12.

[7] ICNIRP, *Guidelines on limits of exposure to laser radiation of wavelengths between* 180 nm and 1000 μm. Health Physics, 1996. 71(5): p. 804-819.

[8] ICNIRP, *Guidelines on limits of exposure to broad-band incoherent optical radiation* (0.38 to 3 μm). Health Physics, 1997. 73(3): p. 539-554.

[9] ICNIRP, ICNIRP *statement on laser pointers*. Health Physics, 1999. 77(2): p. 218-220.

[10] ICNIRP, ICNIRP *statement on light-emitting diodes* (LEDs) *and laser diodes: Implications for hazard assessment.* Health Physics, 2000. 78(6): p. 744-752.

[11] ICNIRP, *Revision of guidelines on limits of exposure to laser radiation of wavelenghts between 400 nm and 1.4 μm.* Health Physics, 2000. 79(4): p. 431-440.

[12] ICNIRP, *General approach to protection against non-ionizing radiation.* Health Physics, 2002. 82(4): p. 540-548.

[13] ICNIRP, *Health issues of ultraviolet tanning appliances used for cosmetic purposes.* Health Physics, 2003. 84(1): p. 119-127.

[14] ICNIRP, *Guidelines on limits of exposure to ultraviolet radiation of wavelengths between 180 nm and 400 nm (incoherent optical radiation)*. Health Physics, 2004. 87(2): p. 171-186.

[15] ICNIRP/CIE, *Measurement of optical radiation hazards,* ed. R. Matthes and D. Sliney. 1998.

[16] IEC, IEC TR 60825-9 *Safety of laser products* - Part 9: *Compilation of maximum permissible exposure to incoherent optical radiation.* 1999.

Chapter 8

Remote non-invasive stereoscopic imaging of blood vessels: First in-vivo results of a new multispectral contrast enhancement technology

This chapter is based on the following publication:
"Remote non-invasive stereoscopic imaging of blood vessels: First in-vivo results of a new multispectral contrast enhancement technology"
by F.P. Wieringa, F. Mastik, F.J. ten Cate, H.A.M. Neumann and A.F.W. van der Steen published in Annals of Biomedical Engineering Vol. 34, No. 12, December 2006 pp. 1870-1878

8.1 Abstract

We describe a contactless optical technique selectively enhancing superficial blood vessels below variously pigmented intact human skin by combining images in different spectral bands.
Two CMOS-cameras, with apochromatic lenses and dual-band LED-arrays, simultaneously streamed Left (L) and Right (R) image data to a dual-processor PC. Both cameras captured color images within the visible range (VIS, 400–780nm) and grey-scale images within the near infrared range (NIR, 910–920nm) by sequentially switching between LED-array emission bands. Image-size-settings of 1280x1024 for VIS & 640x512 for NIR produced 12 cycles/s (1 cycle = 1 VIS L&R-pair + 1 NIR L&R-pair). Decreasing image-size-settings (640x512 for VIS & 320x256 for NIR) increased camera-speed to 25 cycles/s. Contrasts from below the tissue surface were algorithmically distinguished from surface shadows, reflections, etc. Thus blood vessels were selectively enhanced and back-projected into the stereoscopic VIS-color-image using either a 3D-display or conventional shutter glasses.
As a first usability reconnaissance we applied this custom-built mobile stereoscopic camera for several clinical settings:

- blood withdrawal;
- vein inspection in dark skin;
- vein detection through iodide;
- varicose vein and nevi pigmentosum inspection.

Our technique improves blood vessel visualization compared to the naked eye, and supports depth perception.

Keywords
Multispectral stereoscopy
Contactless enhanced viewing of superficial vasculature
Intuitive technology
Reconnaissance of feasibility for various clinical applications
3D-display

8.2 Introduction

Visually guided procedures provide instant feedback and meantime afford insights that would otherwise be difficult or even impossible to obtain [1]. This is a primary reason for mankind's continuous desire to extend vision beyond the boundaries of the human eye, which has resulted in many successful diagnostic imaging modalities like X-ray imaging, endoscopy, thermography, ultrasound scans and MRI that all found their way into the clinic.

While investigating the principal feasability of a camera for imaging blood oxygenation levels, we noticed that our multispectral images also contained information about subcutaneous vasculature, with improved contrast in the near infrared [2]. Near infrared imaging of superficial blood vessels in itself is not new; soon after infrared photography [3-5] early electronic cameras were used for experiments [6, 7]. Since then, numerous near infrared imaging methods have been developed using transillumination mode and/or reflection mode [8-12]. Our multispectral camera, however, provides the opportunity to obtain normal color images within the visible range (VIS) which are pixel-to-pixel matched with images obtained in the invisible near infrared range (NIR). By combining the image information content of both spectral bands with a processing algorithm, we developed a new technique that allows selective enhancement of superficial blood vessels with selectable pigment suppression within a normal color image [13].

The underlying principle does not necessarily require stereoscopic image acquisition to derive increased vessel contrasts from the tissue. When, however, developing a new medical imaging technique, deriving image information from patient tissue is not the only issue. Especially for visually guided procedures it is also crucial to put effort in an ergonomic human interface and avoid conflicts between the proprioceptional and visual perceptions of the user. The added value of stereoscopic image recordings already was recognized and successfully used to document medical cases more than a century ago [14]. We likewise reasoned that offering enhanced blood vessel contrast at the cost of depth perception would restrict the usefulness of our technique and therefore decided to realize a stereoscopic version of our vessel contrast enhancement device.

Visually guided procedures typically require a combination of well trained eyes and specific fine-motoric skills, since the coordination between eyes and hands is task dependent [15]. For eye-hand coordination, brain processes for perception and action interact so closely that they cannot be separated and the influence of visual illusions (like human depth perception) to motoric tasks becomes stronger when input takes places via lower levels in the brain [16]. The match between a human interface device and the visual and motoric brain processes strongly defines whether a technology can be applied intuitively or not. A new technology can be classified as intuitive if it speeds up the learning process for novices in a certain skill, without impairing the performance of persons already skilled in the existing art [17]. Thus a useful increase

in vascular contrast should neither imply a task-impairing decrease in depth perception (like in monoscopic techniques) nor distort spatial clues for human vision (like shadows) nor introduce false depth information (like projection parallax).

As a first reconnaissance of practical feasibility, we applied our new technique to several visual clinical procedures for which we expected that improved visualization of blood vessels would be of interest, being:

- blood withdrawal;
- vein inspection in dark skin;
- detection of veins through iodide;
- inspection of varicose veins and nevi pigmentosum.

8.3 Methods

8.3.1 Instrumental setup

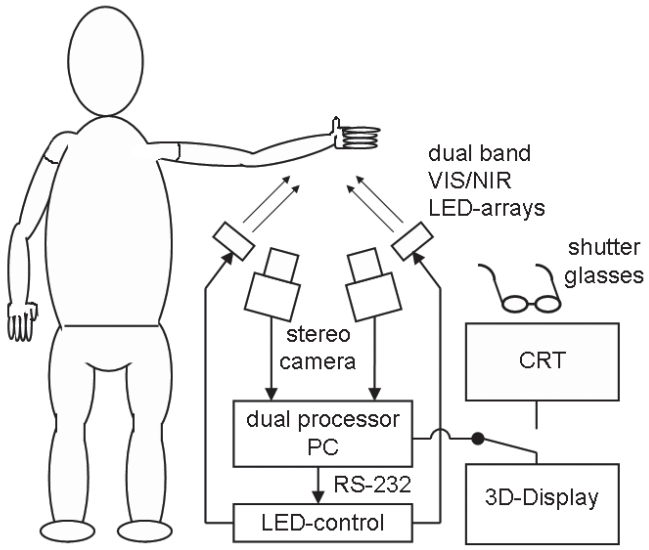

Figure 1: Experimental setup

Two CMOS-cameras, with apochromatic lenses and dual-band LED-arrays, simultaneously stream Left (L) and Right (R) image data to a dual processor PC. Both cameras captured color images within the visible range (VIS, 400–780nm) and grey-scale images within the near infrared range (NIR, 910–920nm) by sequentially switching between LED-array emission bands.

The instrumental hardware setup is schematically drawn in figure 1. Two synchronized identical single-chip CMOS-cameras (Vector Technologies Belgium, custom built) were equipped with apochromatic lenses and two identical custom-built dual-band LED-arrays (O_2-View, the Netherlands). These LED-arrays were current controlled and each had 2 individually programmable channels for the emission of in total ±1.2 Cd visible white light with adjustable color temperature (consisting of 40 broadband white LEDs with a yellow accent and 20 broadband white LEDs with a blue accent) as well as 1 programmable channel for the emission of near infrared radiation (20 LEDs, 920nm, max. 32mW per LED). The light sources were constructed so that the geometrical beam profiles of VIS and NIR matched very closely (and thus also any resulting shadows and/or reflections). Left (L) and Right (R) image data was simultaneously acquired and streamed to a dual processor PC equipped with a stereoscopic monitor (Sharp LL-151-3D). It was also possible to connect a conventional Cathode Ray Tube (CRT) monitor equipped with shutter glasses, for comparison of stereoscopic representation.

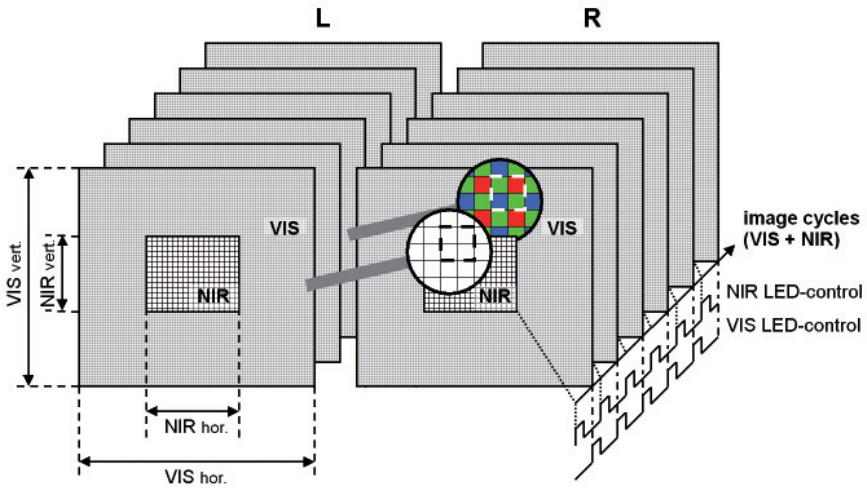

Figure 2: Schematic diagram of image aquisition.
The sequentially acquired alternating VIS and NIR raw image frames form 3D-matrices for the Left and Right channel. The NIR image size is smaller than the VIS image size to increase framerate while maintaining an overview of the imaged area. Enlarged details illustrate the NIR transparency of the Bayer pattern RGB-filters which are applied to obtain a VIS color image. The time domain axis is expressed in image cycles. Along this image cycle axis, the control signals for NIR and VIS LEDs (synchronized with respectively NIR and VIS camera exposures) are visualized.

A schematical representation of image aquisition and data structure is drawn in figure 2. The CMOS camera detector chips were equipped with a Bayer filter mosaic to obtain an RGB color image within the visible range (VIS). The camera pixels, however, were also sensitive to near infrared radiation because all three filter channels of

the Bayer mosaic (red, green and blue) were designed as highly transparant within the near infrared range (NIR). Thus 4 NIR-pixels were acquired for each VIS RGB color pixel group. By sequentially switching between emission bands of the LED-arrays, images within the Visual range (VIS, 400 - 780 nm) and Near Infrared range (NIR, 910 - 920 nm) were acquired in an alternating fashion. VIS and NIR image-size-settings could be varied independantly. For 8-bit encoding depth, at image-size-settings of 1280x1024 for VIS & 640x512 for NIR, 12 cycles/s were obtained (1 cycle = 1 VIS L&R-pair + 1 NIR L&R-pair). At the cost of decreasing image-size-settings downto 640x512 for VIS & 320x256 for NIR, camera speed could be increased up to 25 cycles/s. Encoding depths of 10-bit and 12-bit were also available, but only used for stills (due to the lower obtainable framerate).

8.3.2 Data aquisition

Multispectral stereoscopic movies were recorded in several typical clinical settings for which the technique was considered as possibly useful. LED currents and diaphragm settings were chosen so that for each movie saturated pixels were avoided. A preview mode allowed aiming, adjustment of converging angle α and focusing of the cameras. After software triggering the stereo-camera streamed a sequence of 8-bit digitally encoded image cycles to PC-memory (using auto-incremental numbering). All images were automatically saved on a fast SATA harddisk-array. Camera and light source settings were automatically stored in a text file and located in the same directory.
All patients and volunteers gave their informed consent for filming as well as for publishing the resulting image material. No diagnosis or therapy was based upon any of our results.

8.3.3 Data processing

General aspects

Processing was performed with custom developed software (programming language C^{++}) using the stored text file with camera and light source settings as additional input values. Figure 3 schematically represents this process.

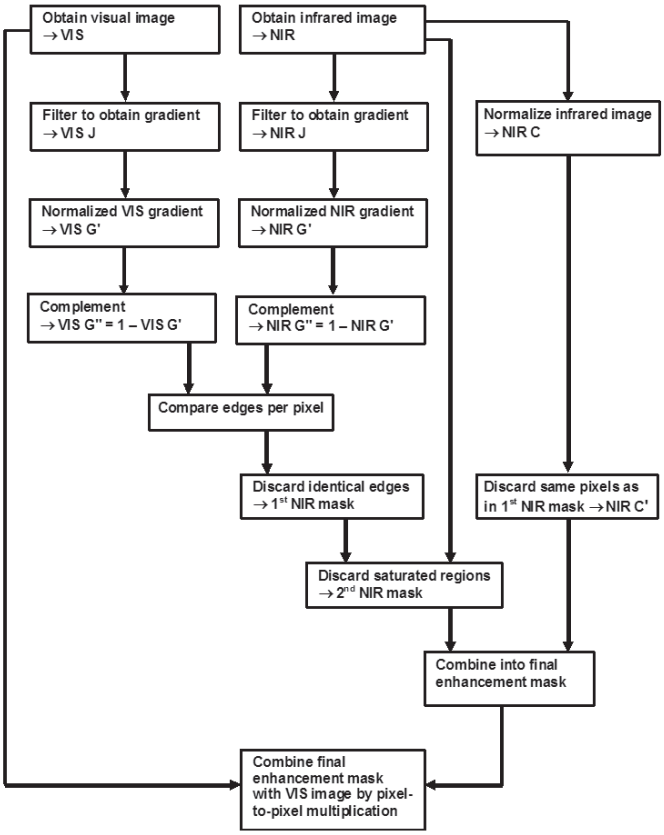

Figure 3: Schematic diagram of image processing.

The images captured within the visible range (VIS) and the images captured within the near infrared range (NIR) are combined, which reveals blood vessel patterns below the skin. The left and middle column focus on edge-enhancement and suppression of superficial artifacts, the right column serves to fill-in the blood vessel lumen. For raw VIS & NIR images as well as processed results see figures 6, 7, 8 and 9.

The processing method allowed discrimination between image information obtained from the tissue surface versus image information obtained from within the tissue. In order to achieve this, a distinction was made between shadows, reflections and absorption contrasts for both VIS and NIR.

Suppressing shadows on the surface

Since NIR and VIS beams were matched closely, shadows produced by irregular shapes at the tissue surface (e.g. skin structure, skin folds, nevi, hair, etc.) or by objects between the light sources and the tissue (fingers, needles, surgical tools, etc.) also matched well in both wavelength ranges. Our algorithm excluded such matching shadows from enhancement and left all useful aspects of shadows unaffected (e.g. depth clues).

Useful effects of shadows and lighting geometry

Due to the fact that the VIS and IR shadows matched very closely, the algorithm was able to selectively enhance contrast from below the surface while leaving shadows on the surface unaffected (thus not distorting these important depth clues).

Due to the shallow angle of the lightbeams, the skin texture was pronounced. Due to the lighting from two sides, objects that were brought towards the tissue surface (e.g. needles, scalpels, probes, etc.) when lighted from both sides, could produce two separate (not too heavy) shadows. These shadows met and typically formed a "V" pattern when an object touched the surface in the middle of the field of view, thus providing extra information for depth perception.

Enhancing absorption contrast of blood vessel walls

Edge detection by a Prewitt image filter was performed on each VIS and NIR image. Pixel positions containing edge information above a certain adjustable threshold in both spectral regions were classified as surface artefacts and excluded from enhancement. The boundary regions of absorption contrasts caused by structures below the tissue surface, produced edges that were mainly present in the NIR image. Enhancement was selectively performed only for pixel positions where the NIR image contained more edge information than the corresponding VIS image. These "valid" pixels identified the vessel boundaries. The positions of these valid pixels were stored in a 1st NIR mask.

Discarding reflections on the surface

Shiny areas that produced reflections and/or saturated pixels also matched in both wavelength ranges. This characteristic allowed to calculate a 2nd NIR mask in which superficial reflections were also excluded from enhancement. Neighbouring pixels of identified saturated pixels were excluded from enhancement. The radius of this exclusion region was programmable, but due to the favourable anti-blooming behaviour of the CMOS-camera chips, suppressing direct neighbour pixels appeared sufficient.

Enhancing absorption contrast of blood vessel lumen

The "content" of blood vessels was separately enhanced by raising pixel values of the normalized NIR image to the power of N (with N user adjustable between 0,5 and 2,5) while discriminating NIR pixels below a freely adjustable noise threshold

and excluding information from identified shadows. Multiplication with the 2nd NIR mask then produced a final enhancement mask for subsequential backprojection into the VIS image by pixel-to-pixel multiplication.

Suppressing contrasts originating from melanin pigment

Superficial contrasts within the visible range, originating from melanin pigment concentrations, could either be filtered out or left unchanged. Figure 4 illustrates the normalized distribution of the intensities for the aquired *separate* spectral bands (R, G, B and NIR) in relation to the intensity (I_{VIS}) of the *composed* visible RGB-image. Intensities were calculated using the Intel ippiRGBtoGray function [18]. Four clouds of data points can be discerned, being I_R / I_{VIS} (red channel), I_G / I_{VIS} (green channel), I_B / I_{VIS} (blue channel) and I_{NIR} / I_{VIS} (NIR channel).

By calculating the ratio of (I_R / I_{VIS}) / (I_{NIR} / I_{VIS}) and comparing the result for each pixel with an adjustable threshold, it can be decided whether or not to apply backprojection to a pixel. This concerns the pixels located within the overlapping region of I_R / I_{VIS} and I_{NIR} / I_{VIS} within figure 4. The resulting difference is clear when comparing between figure 9c and figure 9d with regard to the visualization of nevi pigmentosum and hair.

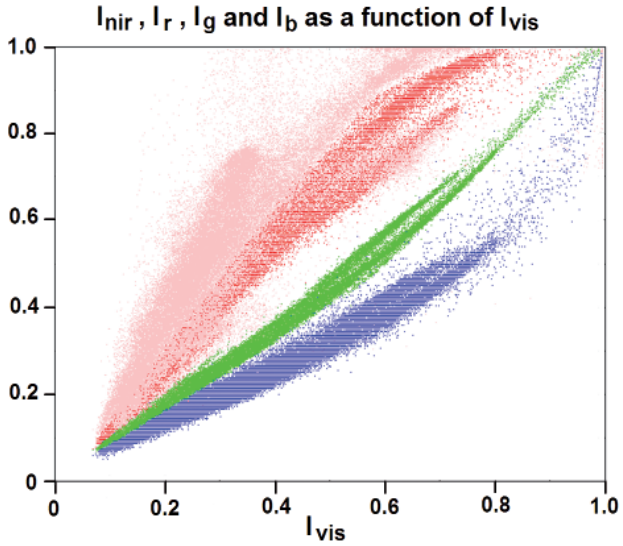

Figure 4: Relative intensity distribution of the different spectral bands

Dimensionless normalized distribution of the intensities for the 4 aquired red (I_R), Green (I_G), Blue (I_B) and near infrared (I_{NIR}) individual spectral bands expressed in ratio to the normalized intensity (I_{VIS}) of the composed RGB-image. The four data clouds (R, G and B labeled by their natural colors and NIR labeled as pink) show a generally marked separation, but especially for a number of pixels within the red and infrared the data clouds partly overlap. This indicates regions where the VIS contrast potentially is superior to the NIR contrast. By comparing an adjustable threshold with the calculated ratio of (I_R / I_{VIS}) / (I_{NIR} / I_{VIS}) it can be decided which spectral band provides superior contrast for the pertaining pixel and thus whether or not it is used for enhanced backprojection.

8.3.4 Data presentation

The images could either be displayed on an auto-stereoscopic Liquid Crystal Display (LCD) monitor or on a conventional Cathode Ray Tube (CRT) monitor equipped with shutter glasses.

The auto-stereoscopic LCD-monitor (Sharp LL-151-3D) was equipped with software controllable switching between stereoscopic (or 3D) and normal (monoscopic or 2D) mode. Monitor resolution was 1280 x 768 in monoscopic mode (XGA). In stereoscopic mode the available pixels were split-up in two separate images (L & R) by activation of a vertical LCD parallax barrier. The principle behind this technology is illustrated in figure 5.

The CRT-monitor (iiyama vision master 21) was used at a resolution setting of 1280 x 1024 in combination with wireless shutter glasses (e-Dimensional) and thus provided stereoscopic information without sacrificing resolution.

The enhancement algorithm occurs on a pixel-to-pixel basis and does not affect resolution.

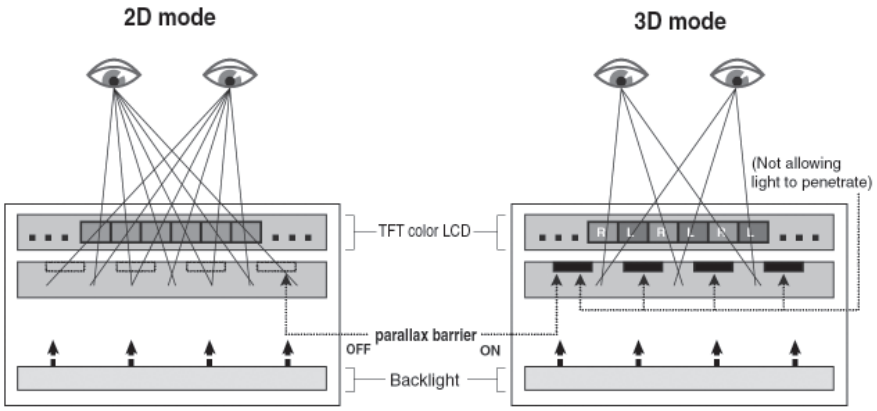

Figure 5: Principle of applied autostereoscopic LCD-monitor (reprinted with permission from Sharp)

In 2D mode, only one camera-channel is displayed (either from the L or R camera) and the parallax barrier is not actuated. Both eyes of an observer therefore receive the same image and a conventional flat image with full resolution is seen.

In 3D mode, both camera channels are displayed (L & R) and the parallax barrier is actuated. The left eye and right eye of an observer now receive different images, and a stereoscopic (in-depth image) with halve resolution is seen.

Our device offered several imaging modes for data presentation:

- Monocopic raw VIS preview (normal full color vision)
- Monoscopic raw NIR preview (greyscale)
- Off-line stereoscopic looped VIS view with and without enhanced blood vessel back-projection (with freely adjustable enhancement settings).

- Off-line stereoscopic looped raw NIR view or enhanced NIR view (with freely adjustable enhancement settings)
- Stereoscopic stills in all modes
- Monoscopic stills in all modes (freely switchable between Left and Right)

All modes offered the possibility for pause and scrolling forward or reverse frame-by-frame. By means of virtual slider controls and virtual pushbuttons the user interface allowed freely adjustable settings for shadow suppression, pigment suppression, noise threshold and vessel lumen fill-in contrast.

8.4 Results

8.4.1 Results for blood withdrawal

During routine blood withdrawal the inserted needle tip remained only slightly visible on the VIS image due to skin surface deformation (see figure 6a). On the raw NIR image, however, the inserted needle remained visible within the tissue for a few mm with some metallic reflection. Subcutaneous bleeding during needle removal could be detected in the raw NIR image while the needle tip was still in the tissue (see figure 6b). This was clearly highlighted by backprojection in the VIS image (see figure 6c). The processing settings used to obtain this backprojection mainly laid the accent upon enhancing the absorption contrast of blood vessel lumen, whereas edge enhancement was set to minimum. Reflections on the thumb nail did not lead to image distortion and the blood volume in the nail bed showed more contrast.

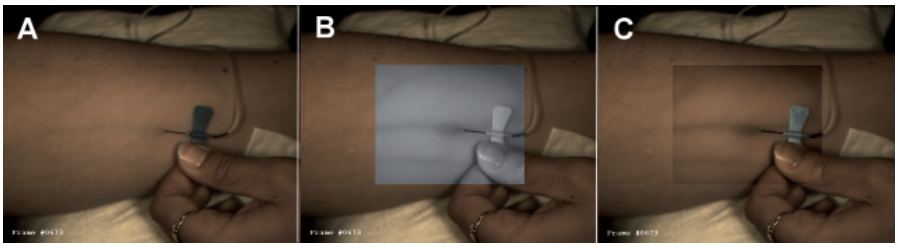

Figure 6: Routine blood withdrawal

Image pairs showing unprocessed images for VIS (fig. 6a) and NIR (fig. 6b) as well as the result after application of the new image processing method (fig. 6c). Note the forked shadow (which is not effected by the enhancement algorithm), the clearly visualized subcutaneous bleeding and the improved visibility of the needle tip.

8.4.2 Results for dark skin

Hardly any vascular contrast is present within the VIS image (see figure 7a). The NIR image, however, is not affected by skin pigmentation and reveals a subcutaneous vascular pattern (see figure 7b). The combined information results in an enhanced image (see figure 7c).

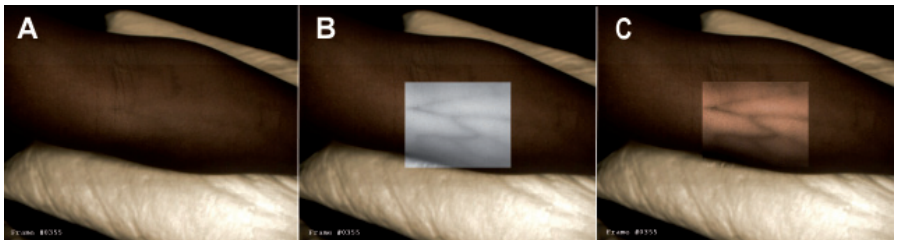

Figure 7: Influence of skin pigmentation

A dark skin color (7a) has no significance for the applied NIR wavelength of 920 nm. Blood vessels provide good contrasts (7b) and the resulting enhanced image (7c) offers an improved visualization of the vasculature.

8.4.3 Results for vein detection through iodide

Iodizing skin portions before surgery is a common clinical procedure which darkens the skin and lowers the visibility of blood vessels. Our method offers imaging right through iodide. To demonstrate this, we filmed a glass Petri dish, placed horizontally upon a volunteers arm while filling it up to a 3mm thick layer of iodide solution. From the VIS image no vessels could be detected through the iodide solution (see figure 8b) and hardly any through the empty Petri dish (see figure 8a). The raw NIR image, however, clearly showed superficial blood vessels even through the Petri dish (see figure 8c).

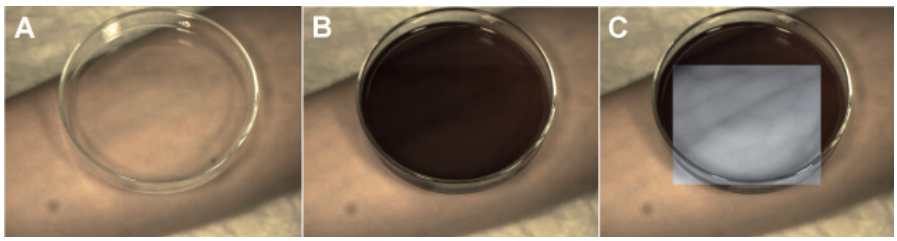

Figure 8: Vein detection through iodide

Within the visible range, the superficial vasculature is only vaguely discernable (fig 8a). After filling the Petri-dish with a 3 mm thick layer of iodide solution, this fully blocks out the tissue view within the visual range (fig 8b), whereas a clear view of the vasculature remains possible at the applied NIR wavelength of 920 nm (fig 8c).

8.4.4 Results for varicose vein and nevi pigmentosum inspection

The device was used to film varicosis patients during dermatological outpatient clinic. The visualization of varicose veins could be drastically improved. Even in cases where the blood vessels were covered by subcutaneous fat, they could be detected quite well (see figure 9). By either de-activating or activating the first NIR mask in the processing algorithm (see figure 3) it was also possible to choose whether pigment contrasts in the visual range were left intact or filtered out. The difference is clear when comparing between figure 9c and figure 9d with regard to the visualization of nevi pigmentosum and hair. By clicking a software screen button, this suppression of pigment contrast could be freely switched on and off during viewing.

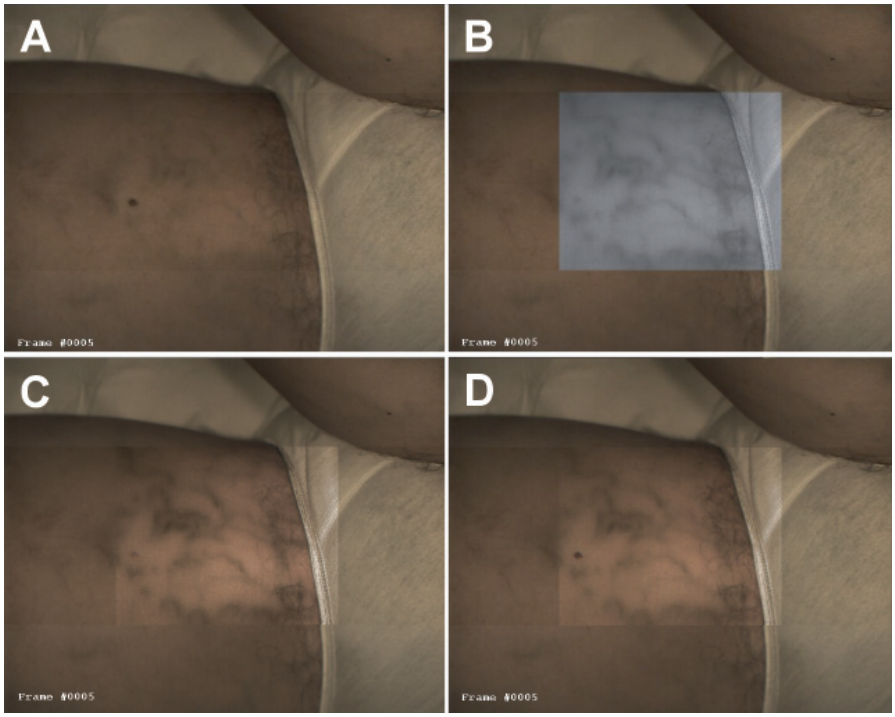

Figure 9:
The VIS image does not contain much information about the underlying vascular pattern (see figure 9a). The NIR image, however, clearly shows what's hiding beneath the surface (see figure 9b). Note that, when building the enhanced image, the nevus which is present in the VIS image can freely either be suppressed as a surface contrast (see figure 9c) or be kept visible (see figure 9d)

8.5 Discussion

From the figures presented in this article, it is clear that all experiments resulted in improved visualization of superficial blood vessels. Based upon the absorption coefficients of Hb versus HbO_2 , arteries provide superior contrasts at 920 nm. The presented images, however, show enhanced venous contrasts, because the larger arteries are buried deeper underneath the skin. Stereoscopic movies provide a more lifely impression of the underlying, but presentation of stereoscopic movies is not possible in a printed journal. We therefore offer the possibility to download viewer software and movies via the internet **http://www.erasmusmc.nl/ThoraxcenterBME/html/research/additional/bloodvesselcamera.htm**

For both the autostereoscopic LCD and the CRT display plus shutter glasses, we found that the perception of depth was less for *stills* than for *movies*. This qualitative observation matches research findings on stereoscopic display techniques in X-ray technology [19] and is also consistent with the differences between static and dynamic stereoacuity described by Mathias and Rudolf Sachsenweger [20]. Stereoscopic movies also showed an increase in apparent image sharpness compared to stereoscopic stills, which may be explained by Shipley's description of stereoscopic contour integration over blur [21]. Compared to the autostereoscopic LCD-display, the increase in perceived sharpness was much stronger when using a CRT with shutter glasses. For monoscopic stills, however, the LCD-display (switched to monoscopic mode) was superior to the CRT. These observations are in agreement with the technology overview by Szold [22] and can be explained by the sacrifice of resolution when using the LCD display in autostereoscopic mode, which prize has not to be paid when using the CRT with shutter glasses.

The beneficial effect of separately adjustable enhancement paths for blood vessel contours and blood vessel lumen, which we experienced during the development of our processing algorithm, is consistent with the findings of Yin et al. that surface-features and edge processes make different contributions in determining an object's unity and shape [23]. The perceived usefulness of stereoscopic information, however, also supports the concept formulated by Tse that ''mergeable'' volumes, rather than relatable contours, are the critical elements in completion [24].

With our technique we have aimed to avoid parallax errors and loss of vessel contrast by shadows which are inherent to other blood vessel contrast enhancement techniques projecting the vascular pattern via a projector onto the skin [25]. We exclude parallax errors because the user truly looks beneath the tissue surface trough two camera's. Absence of vessel contrast in shadows is avoided by lighting from two sides and by discrimination of superficial artifacts versus contrasts originating from below the surface.

This ability to selectively enhance contrasts from beneath the surface, while preserving the natural depth clues of shadows on the surface, supports both static and dynamic transmittance anchoring of the visual system which is crucial for depth perception [26].

Preservation of natural shadows is furthermore important for the correct interpretation of depth clues by occlusion (e.g. from a hand or an instrument positioned between observer and tissue) thus precluding errors in depth perception [27].
Since only carefully balanced white light is projected on the skin, there is no impairment of color perception. It is up to the user to freely switch between normal full color vision, color vision plus superimposed blood vessel backprojection and stereoscopic near infrared greyscale vision (with or without enhancement features).

The embodiment described in this article still has some drawbacks:

- Due to the fact that the pertaining configuration aquires VIS and NIR images sequentially, motion artifacts can lead to a backprojection shift.
- The deeper the vessels lie under the surface, the less we can visualize them. In the pertaining configuration, the depth range is limited to about 1 mm. Based upon the absorption coefficients of Hb and HbO_2, arteries provide superior contrasts at 920 nm. The presented images, however, show enhanced venous contrasts, because the larger arteries are buried deeper underneath the skin.

The above mentioned drawbacks require further development. Fortunately, many technological improvents still can be added. Allthough the device worked quite well under normal ambient lighting conditions (100 – 200 Lux), the use of a switchable filter might further improve spectral separation. Furthermore, known techniques like application of crossed polarizers, in combination with more powerful light sources, can offer a considerably larger penetration depth [28].

8.6 Conclusions

Compared to inspection with the naked eye under normal lighting conditions, the tested stereoscopic blood vessel contrast enhancer offered improved visualization in all investigated settings, providing the best stereoscopic image quality when using the Cathode Ray Tube (CRT) monitor with shutter glasses and the best monoscopic image quality when using the Liquid Crystal Display (LCD) set to monoscopic mode.
Our technique supports perception of depth, 3-dimensional motion and discrimination between tissue surface and underlying structures. It also has potential as an educational tool by offering the possibility to look and record trough the eyes of an experienced specialist. Further improvements on penetration depth, frame-rate and focus depth-of-field form targets for momentary ongoing further research.

8.7 Acknowledgements

This study was sponsored by TNO Quality of Life and by O_2view B.V. (both based in Leiden, the Netherlands).
Custom mechanical constructions were made by Mr. L. Bekkering and support on electronics was given by Mr. J. Honkoop (both from Biomedical Engineering, Thorax Centre).
We greatly appreciate the possibilities to record data in clinical settings and the assistance of the blood withdrawal team of the cardiology outpatient clinic as well as the staff of the dermatology outpatient clinic (all within Erasmus MC Rotterdam, the Netherlands).

8.8 References

[1] Woods DD, Patterson ES and Roth EM, *Can we ever escape from data overload? A cognitive systems diagnosis*. Cognition Technology & Work, 2002(4): p. 22-36.

[2] Wieringa FP, Mastik F and Van der Steen AFW, *Contactless multiple wavelength photoplethysmographic imaging: A first step towards "SpO2 camera" technology.* Annals of biomedical engineering, 2005. 33(8): p. 1034-1041.

[3] Haustein UF, *Infrared photodocumentation of the superficial venous system of the leg*. Ästhetische Medizin, 1967. 16(5): p. 155-160.

[4] Wissmanns HF, *Prophylaxis and treatment of venous diseases in general practice. Objective evaluation by means of infrared photography*. die Medizinische Welt, 1968. 20(3): p. 191-196.

[5] Dallow RL and McMeel JW, *Penetration of retinal and vitreous opacities in diabetic retinopathy. Use of infrared fundus photography.* Archives of ophthalmology, 1974. 92(6): p. 531-4.

[6] Jones CH and Newbery SP, *Visualization of superficial vasculature using a Vidicon camera tube with silicon target.* British Journal of Radiology, 1977. 50(591): p. 209-210.

[7] Ontikova NM, Iaroslavtsev DA and Lirman AV, *Increase in the information content of the image of the surface veins by using a television infrascope.* Meditsinskaia tekhnika, 1976(5): p. 20-22.

[8] Kono M, Ueki H and Umemura S, *Near-infrared finger vein patterns for personal identification.* Applied Optics, 2002. 41(35): p. 7429-7436.

[9] Webb S, *Imaging by diaphanography, in The physics of medical imaging,* S. Webb, Editor. 1995, Institute of physics publishing: Bristol.

[10] Elsner AE, Burns SA, Weiter JJ and Delori FC, *Infrared imaging of subretinal structures in the human ocular fundus.* Vision Research, 1996. 36(1): p. 191-205.

[11] Gostout CJ and Jacques SL, *Infrared video imaging of subsurface vessels: a feasibility study for the endoscopic management of gastrointestinal bleeding.* Gastrointestinal Endoscopy, 1995. 41(3): p. 218-224.

[12] Hayashi N, et al., *Identification and diameter assessment of gastric submucosal vessels using infrared electronic endoscopy.* Endoscopy, 1994. 26(8):686-9(8): p. 686-689.

[13] Wieringa FP, Bakker D, van der Steen AFW, Mastik F and van Melick RGM, *Imaging of buried structures,* EP1566142A1, 2005.

[14] Elschnig. *Elschnig demonstrirt ferner stereoskopische Photographieen. in Achtundzwansigte Versammlung der Opthalmologischen Gesellschaft.* 1900. Heidelberg: Bergmann.

[15] Rotman G, *Localization during pursuit eye movement, in Neurosciences*. 2005, Erasmus: Rotterdam. p. 102.
[16] de Grave DD, *The use of illusory visual information in perception and action, in Neurosciences*. 2005, Erasmus: Rotterdam. p. 112.
[17] Taffinder N, Smith SGT, Huber J, Russel RCG and Darzi A, *The effect of a second-generation 3D endoscope on the laparoscopic precision of novices and experienced surgeons.* Surgical Endoscopy, 1999. 13: p. 1087-1092.
[18] Intel, *Intel integrated performance primitives for Intel architecture* - Reference manual A70805-017US. 2006.
[19] Hardy J, Dodds S and Roberts A, *An Objective Evaluation of the Effectiveness of Different Methods of Displaying Three-Dimensional Information with Medical X-Ray Images.* Investigative Radiology, 1996. 31(7): p. 433-445.
[20] Sachsenweger M and Sachsenweger U, *Stereoscopic acuity in ocular pursuit of moving objects. Dynamic stereoscopy and movement parallax: relevance to road safety and occupational medicine.* Documenta Opthalmologica, 1991. 78: p. 1-133.
[21] Shipley TF, *Field processes in stereovision. A description of stereopsis appropriate to opthalmology and visual perception.* Documenta Opthalmologica, 1987. 66: p. 95-170.
[22] Szold A, *Seeing is believing - Visualization systems in endoscopic surgery (video, HDTV, stereoscopy, and beyond).* Surgical Endoscopy, 2005. 19: p. 730-733.
[23] Yin C, Kellman PJ and Shipley TF, *Surface integration influences depth discrimination.* Vision Research, 2000. 40: p. 1969-1978.
[24] Tse PU, *Volume Completion*. Cognitive Psychology, 1999. 39: p. 37–68.
[25] Zeman HD, Lovhoiden G and Vrancken C. *Prototype vein contrast enhancer. in Photonics West 2004: Biomedical Optics (BiOS).* 2004: SPIE.
[26] Anderson BL, Singh M and Meng J, *The perceived transmittance of inhomogenous surfaces and media.* Vision Research, 2006. 46: p. 1982-1995.
[27] Johnson LG, Edwards P and Hawkes D, *Surface transparency makes stereo overlays unpredictable: The implications for augmented reality.* Stud Health Technol Inform, 2002. 94: p. 131-136.
[28] Groner W, Winkelman JW, Harris AG, Ince C, Bouma GJ, Messmer K and Nadeau RG, *Orthogonal polarization spectral imaging: a new method for study of the microcirculation.* Nat Med, 1999. 5(10): p. 1209-12.

Chapter 9

Contrast enhancement of coronary arteries in cardiac surgery: A new multispectral stereoscopic camera technique

This chapter is based on the following publication:
"Contrast enhancement of coronary arteries in cardiac surgery: A new multispectral stereoscopic camera technique"
by F.P. Wieringa, F. Mastik, D.J.G.M. Duncker, A.J.J.C. Bogers and A.F.W. van der Steen published in Euro Intervention Vol. 2, pp. 389-394

9.1 Abstract

Objective: During open heart surgery, the myocardium usually provides sufficient visual contrast with both epicardial veins and arteries. However, visibility of coronary arteries may occasionally be impaired due to e.g. intramyocardial course of coronary arteries, increased epicardial fat, epicardial post-surgical adhesions, or pericarditis. Within the near infrared, coronary arteries show higher contrasts against the myocardium than coronary veins. Hence, we developed a non contact stereo-optical camera to selectively enhance coronary arteries by combining visible and near infrared images. In this paper we present our first results on porcine and human hearts.

Materials and methods: Two CMOS-cameras, with apochromatic lenses and dual-band LED-arrays, captured visible color (VIS, 400–780nm) and near infrared grey-scale (NIR, 910–920nm) images by sequentially switching between LED-array emission bands. Data was recorded by computer and processed off-line. Arterial NIR contrasts were algorithmically distinguished from shadows and specular reflections. Detected arteries were selectively enhanced and back-projected into the stereoscopic VIS-color-image using either a 3D-display or conventional shutter glasses.

Results: Our technique visualized coronary vasculature and allowed to identify concealed parts of coronary arteries using off-line processing. Raw VIS & NIR images were real-time, processing took < 15s after filming.

Conclusion: The applied principle works, but needs further development.

Keywords
Multispectral stereoscopy of the heart
Non contact enhanced viewing of coronary arteries
Intuitive technology
Cardiac surgery

9.2 Introduction

For visually guided procedures like cardiac surgery, it is obvious that a good view upon a well lighted operating field is crucial. A well lighted myocardium usually forms a sufficiently contrasting background for the dark coronary veins and for the lighter coronary arteries. In this regard most of the coronary arteries can be readily identified. In some instances - like intramyocardial course of coronary arteries, increased epicardial fat, epicardial adhesions after previous surgery, or pericarditis - visibility of the coronary arteries may be impaired. When, however, extending vision beyond the boundaries of the human eye into the near infrared, this situation is changed: visual penetration depth is increased and coronary arteries show an improved contrast against the myocardium which even dominates compared with the coronary veins. This is caused by the different optical properties of hemoglobin and oxyhemoglobin as illustrated in figure 1 [1-4].

We previously described a new non contact optical technique that allows selective enhancement of superficial blood vessels beneath the skin by combining images obtained in the visible range (VIS) with images obtained in the invisible near infrared range (NIR) [5]. We added a "surgical mode" to the image processing software of this device to utilize differences in blood oxygenation levels to enhance the visualization of coronary arteries. By filming pigs' hearts, the method was fine-tuned up to a level that could be handled in a clinical environment. This article describes our first recordings during human cardiac surgery.

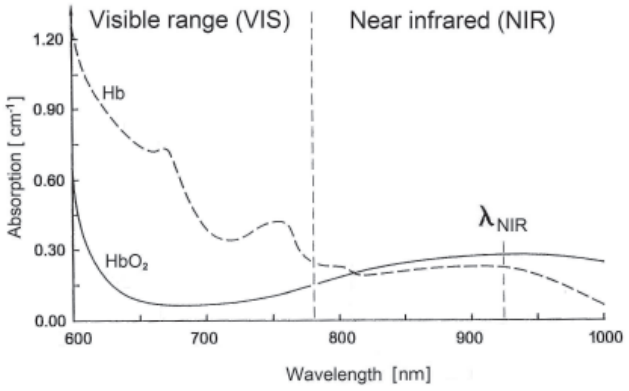

Figure 1: Spectral absorption for hemoglobin (Hb) and oxyhemoglobin (HbO_2)

The wavelength axis shows the spectral range from 600 nm (visible reddish orange) to 1000 nm (invisible infrared). The boundary between the visible range (VIS) and near infrared (NIR) lies at 780 nm. The vertical scale indicates the degree of light absorption. Within the visible range, highly oxygenated blood absorbs less red light than poorly oxygenated blood, which explains the bright red appearance of arterial blood.

Within the near infrared, absorption is significantly lower and thus the light can penetrate deeper. For the applied wavelength λ_{NIR} of 920 nm, highly oxygenated blood absorbs stronger than poorly oxygenated blood.

9.3 Methods

9.3.1 Instrumental setup

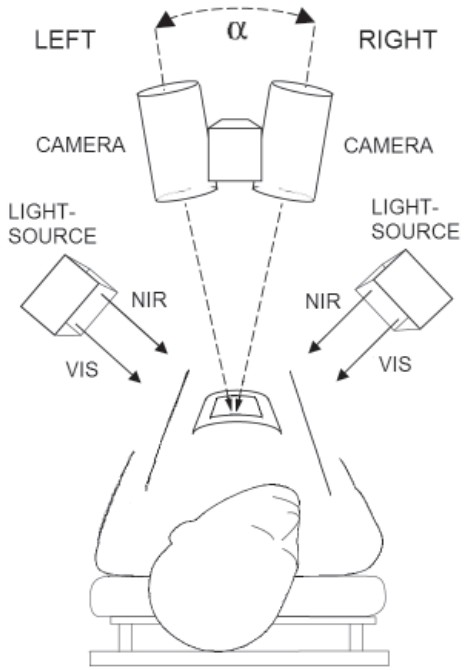

Figure 2: Device principle

Two identical cameras, set apart at normal eye distance (7 cm), are aligned at an angle α (similar to the human eye) and focused on the heart. Both cameras capture color images within the visible range (VIS, 400–780nm) but also grey-scale images within the near infrared range (NIR, 910–920nm). This is achieved by sequentially switching between the VIS and NIR LED-array emission bands. The information contained in both image-types is then selectively combined by software.

The instrumental hardware front-end setup is schematically drawn in figure 2. Two custom built synchronized identical single-chip CMOS-cameras (Vector Technologies Belgium,) were equipped with apochromatic lenses and specially constructed dual-band LED-arrays. These LED-arrays were current controlled and had individually programmable channels for the emission of visible white light (with an adjustable color temperature) as well as for the emission of near infrared radiation. The lightsources were carefully constructed so that the geometrical beam profiles of VIS and NIR matched very closely. Any resulting shadows and/or reflections thus also matched for both spectral ranges, which allowed adequate discrimination between contrasts originating from the tissue surface versus contrasts originating from within the tissue [6]. Cameras and lightsources were placed on a custom made balanced mechanical support with six adjustable joints. The cameras were capable to obtain normal color

images within the visible range but additionally were sensitive to near infrared radiation, which was achieved by a special NIR-transparent RGB filter mosaic on the camera-chip. By sequentially switching between emission bands of the LED-arrays, pixel-to-pixel aligned images within the Visual range (VIS, 400 - 780 nm) and Near Infrared range (NIR, 910 - 920 nm) were acquired. Left (L) and Right (R) image data was simultaneously acquired by 2 dedicated image acquisition boards and streamed to a dual 3.06 GHz Xeon-processor PC equipped with a high-speed SATA-disk array and 2Gb of RAM. The images were processed by custom software and either presented on an auto-stereoscopic Liquid Crystal Display (LCD) monitor or on a normal Cathode Ray Tube (CRT) monitor equipped with LCD-shutter glasses.

9.3.2 Data aquisition

Multispectral stereoscopic movies were recorded during cardiac surgery with the sterile packed stereo camera located at a distance of approximately 45 cm from the heart (see figure 3). Real-time raw VIS and NIR images were available from a preview mode which allowed aiming, adjustment of converging angle α and focus of the cameras. After software triggering the cameras streamed all raw image data via the image acquisition boards to the PC that automatically saved all raw image data in 8 bit encoding depth on a fast SATA harddisk-array, together with the applied camera and lightsource settings.

Figure 3: The device in practice

A cart with the device was placed near the head-side of the patient support, the stereo-camera was positioned on an adjustable balanced arm, thus avoiding interference with the surgical procedure. Normal disposable transparent sterile covers were applied. Average recording distance was 45 cm.

9.3.3 Data processing

The stored raw image data was subjected to post-processing using custom developed software (programming language C++) which facilitated viewing the contrast information contained in visible and infrared light in a combined image [6]. The processing method allowed discrimination between image information obtained from the tissue surface versus image information obtained from shallow depth within the tissue. Additionally, the difference in spectral absorption (see figure 1) between hemoglobin (Hb) and oxyhemoglobin (HbO_2) was exploited to selectively enhance the coronary arteries, using the ratio between the intensity of the visible red and invisible infrared pixel values as a decision criterium whether or not to enhance a pixel.

9.3.4 Data presentation

The images could either be displayed on an auto-stereoscopic LCD-monitor (Sharp LL-151-3D) or on a CRT-monitor (iiyama vision master 21) equipped with shutter glasses (e-Dimensional). The post-processing software offered the possibility for pause and scrolling forward or reverse frame-by-frame. The user could freely switch between stereoscopic (3D) or monoscopic (flat) display of normal color view (VIS), greyscale near infrared view (NIR) or a combined virtual reality view (VR). By means of virtual slider controls and virtual pushbuttons, settings for shadow suppression, noise threshold and blood vessel contrast could be adjusted.

9.4 Results

9.4.1 Results obtained with pigs' hearts

The method was developed using movies aquired during cardiac surgery on pigs, in conformance with the "Guide for Care and Use of Laboratory Animals" published by the US National Institutes of Health (NIH publication No. 85-23, revised 1996) and under the regulations of Erasmus MC Rotterdam. Figure 4a shows the normal VIS image of a pigs' heart. The myocardium forms a visually well contrasting background for the dark coronary veins and a somewhat less contrasting background for the lighter colored coronary arteries. Figure 4b shows that beyond the boundaries of the human eye, in the near infrared, this situation is changed: the coronary arteries show a higher contrast against the myocardium than the coronary veins. In figure 4c this information has been incorporated in the visible image, which drastically improves arterial contrasts but decreases venous contrasts. Figure 4d finally contains the "best of both worlds" by combining the VIS venous contrast and the NIR arterial contrast in one virtual reality (VR) image. Some motion artifacts are present in figure 4d. These are caused by the time interval between the VIS and NIR acquisition. This can be solved by increasing the frame rate and/or by using parallel acquisition of both wavelength ranges instead of the here applied sequential image aquisition.

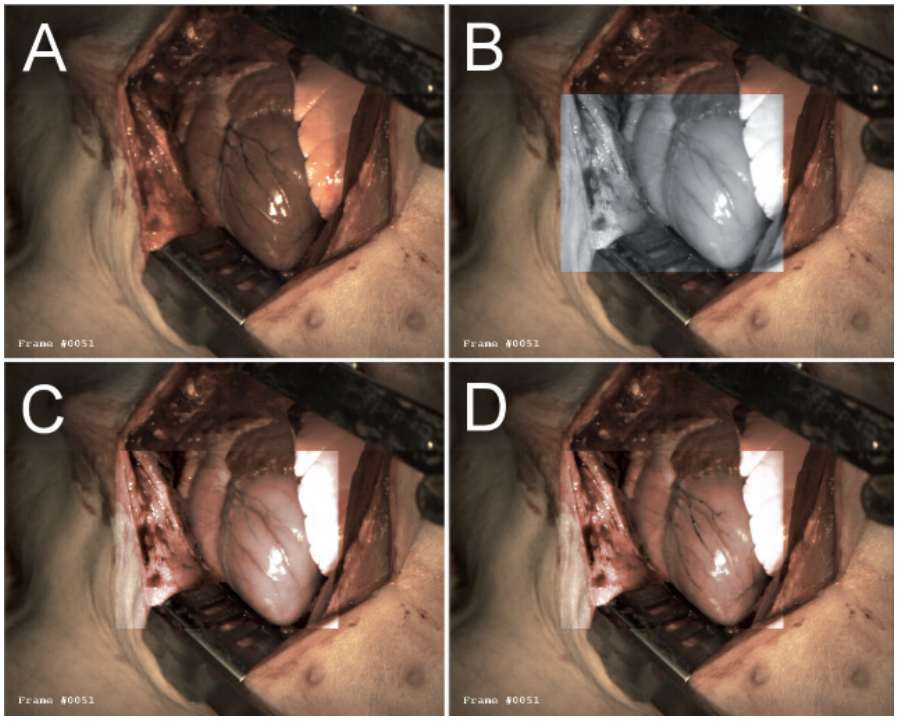

Figure 4: Example of results for pigs' hearts

Normal visual (VIS) image of a pigs' heart (fig. 4a) compared to a near infrared (NIR, 920 nm) image within a centered region of interest reveals an improved contrast for the epicardial arteries (fig. 4b).

Selective combination of VIS and NIR vascular contrasts results in an improved visualization of the epicardial arterial diagonal branches (fig. 4c). Adjusting the software parameters so that venous contrasts from the VIS image are also preserved combines the best vascular contrasts of both spectral ranges (fig. 4d). The veins in fig. 4d look thinner than those in fig. 4b. Also the diagonal branches of the epicardial arteries do not completely overlap when comparing the VIS (fig. 4b) and NIR (fig. 4c) images. These effects are caused by heart motion during the interval between VIS and NIR exposure (due to the relatively low frame-rate).

9.4.2 Results for human hearts

Figure 5 shows results obtained during our first recordings of a human heart. Within the visual range, the fat layer around the heart decreases the visibility of coronary vasculature (see figure 5a for overview and fig. 5d for zoomed ROI). The NIR image, however, reveals more of the vascular pattern (see figure 5b for NIR-mode ROI in VIS-overview frame and figure 5e for zoomed NIR-mode ROI). The combined information results in an enhanced image (see figure 5c for enhanced ROI in VIS-overview frame and figure 5f for zoomed enhanced ROI).

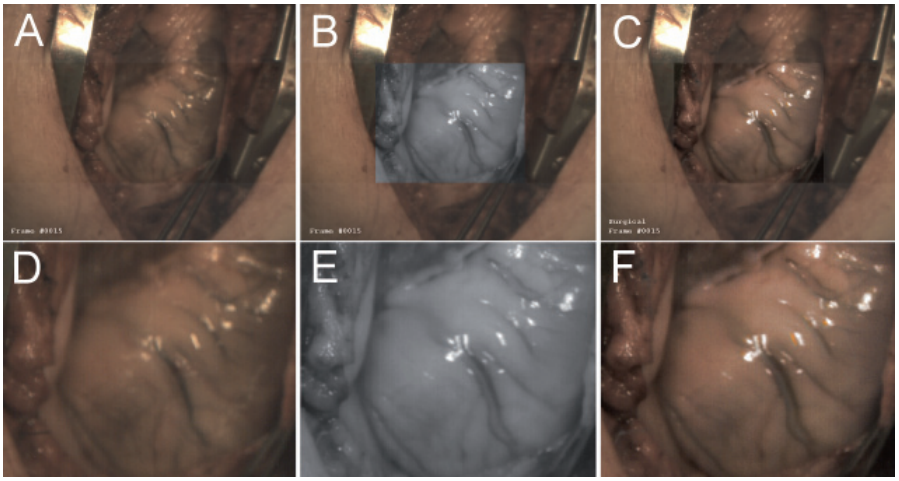

Figure 5: Results of our first recordings of a human heart

Figure 5a presents a full overview captured in the visible range (VIS). In figure 5b (NIR) and 5c (enhanced) the centered region of interest are displayed framed within a larger overview captured in the visible range. Figure 5d zooms in on the centered ROI in VIS-mode, whereas figure 5e shows the zoomed ROI in NIR-mode and figure 5f displays the zoomed ROI in enhanced mode. Although these first recordings were not optimally focused, it is clear that the VIS image (fig. 5a & 5d) contains less vascular contrast than the NIR image (fig. 5b & 5e). The resulting combined image (fig. 5c & 5f) clearly shows two vessels (whereas fig. 5a & 5d only show one).

Figure 6 shows results from another patient, after implementation of a few small mechanical camera modifications, consisting of a wider height adjustment range and an additional rotation axis.

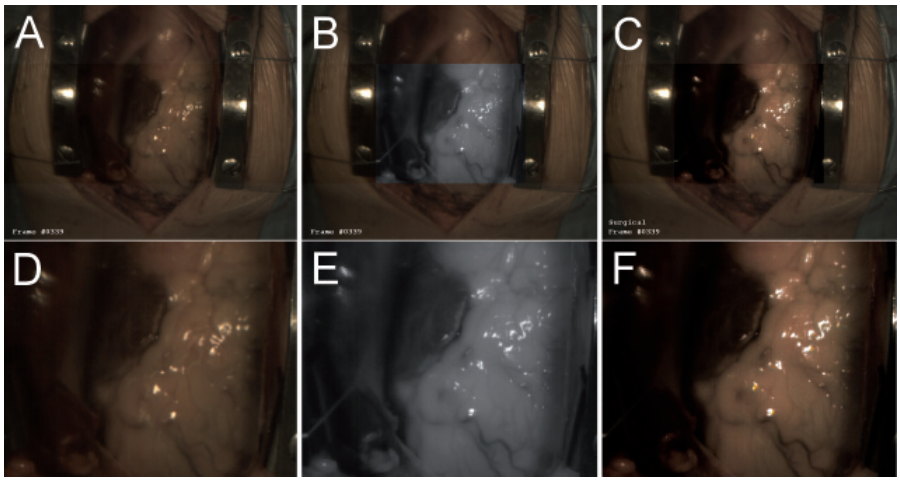

Figure 6: Typical results viewing epicardial fat on a human heart
The upper row of figures shows the centered region of interest, 6a (VIS), 6b (NIR) and 6c (enhanced), framed within a larger overview captured in the visible range. Within the lower row of figures, only the corresponding centered regions of interest are shown 6d (VIS), 6e (NIR) and 6f (enhanced). Two blood vessels already contrasting fairly well within the VIS image (fig. 6a & 6d) appear more pronounced in the NIR image recorded at a wavelength of 920 nm (fig. 6b & 6e). Also here, processing clearly enhances vascular visualization (fig. 6c & 6f).

9.5 Discussion

These first results are encouraging and proof that the technology works in principle. As can be seen in figure 4, the contrast of coronary arteries can be increased on a "clean" heart with almost no epicardial fat. Using the ratio between the intensity of the red and infrared signal values as a criterium whether or not to replace the original VIS-pixel by an enhanced version, can be seen as a crude qualitative blood oxygenation related discriminator [7]. Arterial contrasts thus can be selectively enhanced without effecting already good venous contrasts in the visual range.
The figures 5 and 6 demonstrate that coronary vessels buried by epicardial fat can significantly be enhanced. This technique also holds potential for improved visualization in cases of intramyocardial course of coronary arteries, epicardial adhesions after previous surgery and pericarditis. Exploration of these topics will be our next step after implementation of modifications which address the limitations of the present device:

- sub-optimal image sharpness caused by motion, due to a limited frame-rate;
- limited focus depth range due to limited light source power;
- limited penetration depth within the tissue due to relatively simple optics for these first experiments.

Hardware and software solution strategies for these points already have been identified, and the implementation of these technological improvements is now in progress.

9.6 Conclusions

Our experiments resulted in improved visualization of coronary vessels. Raw preview VIS & NIR image were real-time available, processed results were available within < 15 seconds. The method looks promising, but needs further development before it can be used as a real-time vision-enhancement device during cardiac surgery. Our planned improvements are designed to be obtained without sacrificing stereoscopic viewing, since it is clear that depth perception is crucial for surgical procedures [8-12].

9.7 Acknowledgements

This study was sponsored by TNO Quality of Life and by O_2view B.V. (both based in Leiden, the Netherlands).
Custom mechanical constructions were made by Mr. L. Bekkering and support on electronics was given by Mr. J. Honkoop (Biomedical Engineering Thorax Centre, Erasmus MC Rotterdam, the Netherlands). We greatly appreciate the possibilities to film during cardiac surgery.
We therefore thank the involved surgeons Dr. A.B.M. Maat and Dr. J. Kluin as well as the OR-staff that supported the work (especially Dr. A. van der Woerd for photography) and the Department of Experimental Cardiology that facilitated filming in the animal lab OR (all within Erasmus MC Rotterdam, the Netherlands).

9.8 References

[1] Neumann A, Hardeman JH and Wieringa FP, *Device for determining oxygen saturation of blood,* EP0793942, 1997.

[2] Zijlstra WG, Buursma A and Meeuwsen-van der Roest WP, *Absorption Spectra of Human Fetal and Adult Oxyhemoglobin, De-Oxyhemoglobin, Carboxyhemoglobin and Methemoglobin.* Clinical Chemistry, 1991. 37(9): p. 1633-1638.

[3] Farmer J, *Blood oxygen measurement, in Design of pulse oximeters,* J.B. Webster, Editor. 1997, Institute of Physics Publishing, Dirac House, Temple Back, Bristol BS1 6BE, UK: Bristol. p. 21-39.

[4] Wieringa FP and Van der Steen AFW, *Pulsoxymetrie, een techniek met toekomst maar ook randvoorwaarden.* Klinische Fysica, 2001(4): p. 4-8.

[5] Wieringa FP, Mastik F, ten Cate FJ, Neumann HA and van der Steen AFW, *Remote non-invasive stereoscopic imaging of blood vessels: First in-vivo results of a new multispectral contrast enhancement technology.* Annals of biomedical engineering, 2006. 34(12): p. 1870-1878.

[6] Wieringa FP, Bakker D, van der Steen AFW, Mastik F and van Melick RGM, *Imaging of buried structures*, EP1566142A1, 2005.

[7] Wieringa FP, Mastik F and Van der Steen AFW, *Contactless multiple wavelength photoplethysmographic imaging: A first step towards "SpO2 camera" technology.* Annals of biomedical engineering, 2005. 33(8): p. 1034-1041.

[8] Dallow RL and McMeel JW, *Penetration of retinal and vitreous opacities in diabetic retinopathy. Use of infrared fundus photography.* Archives of ophthalmology, 1974. 92(6): p. 531-4.

[9] Hardy J, Dodds S and Roberts A, *An Objective Evaluation of the Effectiveness of Different Methods of Displaying Three-Dimensional Information with Medical X-Ray Images.* Investigative Radiology, 1996. 31(7): p. 433-445.

[10] Sachsenweger M and Sachsenweger U, *Stereoscopic acuity in ocular pursuit of moving objects. Dynamic stereoscopy and movement parallax: relevance to road safety and occupational medicine.* Documenta Opthalmologica, 1991. 78: p. 1-133.

[11] Taffinder N, Smith SGT, Huber J, Russel RCG and Darzi A, *The effect of a second-generation 3D endoscope on the laparoscopic precision of novices and experienced surgeons.* Surgical Endoscopy, 1999. 13: p. 1087-1092.

[12] Yin C, Kellman PJ and Shipley TF, *Surface integration influences depth discrimination.* Vision Research, 2000. 40: p. 1969-1978.

Chapter 10

General discussion and summary

10.1 Pulse oxigraphy

The aim of this thesis was to investigate the feasability of contactless imaging pulse oximetry (proposed term: *pulse oxigraphy*). The patent disclosed in chapter 2 claims that such pulse oxigraphy can be achieved with camera-derived photoplethysmographic pulse waves at three wavelengths, preferably being 660, 810 and 940nm.
From the absorption curves of hemoglobin and oxyhemoglobin it can be easily derived that two of these wavelengths (660 and 940nm) contain oxygenation-related information, and they have proven to be useful for conventional pulse oximetry (in transmission-mode as well as in reflectance-mode). The additional third wavelength (810nm) lies at a so-called isobestic point where the absorption curves of hemoglobin and oxyhemoglobin intersect. Thus, images and/or plethysmographic pulse waves recorded at 810nm do not contain oxygenation-related information, which is useful for reference purposes when dealing with shadows, reflections, movement artifacts and variations in geometry. With regard to pulse oxigraphy the following results were obtained:
In chapter 3 we proved that it is possible to derive photoplethysmographic pulse waves containing the heart rythm of a living person at all three required wavelengths from camera recordings collected at a distance of 72 cm.
To investigate and validate the capabilities for pulse oxigraphy with this set up, direct measurements on volunteers were sub optimal, because of: Signal-to-noise issues, sequentially recorded heartbeats for oxygen saturation calculations, and lack of a method to induce prolonged stable and adjustable oxygen saturation levels.
In chapter 4 we disclose an idea for an in-vitro phantom with exactly beat-to-beat reproducible “pulse waves” at an improved signal-to-noise ratio, being capable to provide prolonged hypoxic conditions. We developed this idea, because such a phantom would allow us to bypass the limitations encountered in chapter 3. Additionally, a stable phantom can serve to solve calibration issues in “normal” pulse oximetry [1, 2].
In chapter 5 we describe a first prototype phantom (based upon the patent application described in chapter 4), applying it for in-vitro experiment to verify the feasibility of our camera-concept. Using this phantom, we could derive monotone and reproduceable relations between pulse oximeter readings and camera-derived ratio-of-ratios as well as between pulse oximeter readings and laboratory values.
In chapter 6 we finally apply the camera for a first exploration of the imaging aspect, by filming a modified phantom having two discrete regions with different oxygen saturation (achieved by injecting arterial and venous freshly withdrawn blood sample pairs.

10.2 Vascular enhancement

During the research for this thesis we developed a relatively simple method for the non-invasive enhanced visualization of subcutaneous blood vessels. The patent, disclosed in chapter 7, claims that it is possible to achieve this by combining images obtained in the visual range with pixel-to-pixel matching images obtained in the near infrared range. The method allows to discern between contrasting blood vessels from within the tissue versus shadows and reflections originating from the tissue surface, so that the latter can be excluded from enhancement (but remain present as depth clues within the resulting combined image).
With regard to vascular enhancement the following results were obtained:
In chapter 8 we proved that the visualization of subcutaneous vascular patterns can be significantly improved and that our method offers benefits for blood withdrawal, vein inspection in dark skin, varicose vein inspection and nevi pigmentosum inspection. The demonstrated vascular enhancement through iodide forms a clear illustration of the power of multispectral imaging.
In chapter 9 we proved that visualization of coronary vasculature can be enhanced. We demonstrated a slightly improved penetration into epicardial fat, but the most interesting result was the ability to selectively and separately enhance arterial and venous contrasts.

10.3 Conclusions

Since it is clear that engineering issues like signal-to-noise-ratio, framerate and simultaneous spectrally resolved image acquistition are solvable, and that both laboratory analysis and reflectance mode pulse oximetry are clinically well accepted, the combined chapters 3, 4, 5 and 6 indicate that: Non contact imaging pulse oximetry (pulse oxigraphy) is feasible.
The above mentioned engineering issues certainly are not trivial and it will require extensive labour to develop a clinically useful SpO_2-camera. This thesis, however, provides the justification to undertake such efforts.
As for the enhanced visualization of buried structures, the combined chapters 7, 8 and 9 indicate that: Remote non-invasive stereoscopic imaging of subcutaneous vasculature is possible; and Improving the anatomical view of coronary vasculature covered by epicardial fat, and the physiological view of the arterial/venous contrast ratio both offer benefits for heart surgery.

The engineering needed to produce a clinical device falls within reach of modern biophotonics industry.

10.4 Future perspectives

The described methods for pulse oxigraphy and vascular enhancement can be regarded as complementary modalities that, once technologically matured, can relatively easy be integrated within one device. Basically, the hardware needed for pulse oxigraphy also offers the possibility to collect the data needed for vascular enhancement. The main difference lies in the processing.

A first embodiment of an SpO_2-camera therefore might use our vascular enhancement technique to identify bloodvessels, and then apply pulse oxigraphy processing only to ROIs that match with these identified blood vessels. Within chapter 9, the figures 4C and 4D illustrate the results of a simple qualitative oxygenation dependent enhancement that only utilizes oxygen dependent absorption differences without using a pulsatile component.

In chapter 3 a relatively strong respiration-correlated component of the recorded in-vivo photoplethysmographic pulse waves was demonstrated, which may be useful to perform venous oxigraphy. In 2000, Nitzan *et al*. demonstrated photoplethysmographic registrations of respiration-induced blood volume oscillations in the hand [3]. In 2002 Francescini *et al*. demonstrated the feasability of contact-mode venous oximetry by using this respiratory-correlated pulsation and suggested the term spiroximetry for it [4].

In addition to blood withdrawal, vein inspection in dark skin, varicose vein inspection and nevi pigmentosum inspection, numerous other clinical applications can be imagined, like:

- Studying the physiology of oxygen gradients in the microcirculation [5];
- Verification of tissue oxygenation during reconstructive surgery [6, 7];
- Evaluation of burn wounds [8];
- Monitoring of vascular conditions in diabetic patients (e.g. feet) [9, 10];
- Guided puncturing of shunts in dialysis patients;
- Identification of vasculature buried in fat during laparoscopy .

Some of these applications only require the vascular enhancement modality, others additionally require pulse oxigraphy and thus more engineering effort.

For both modalities our next research focus is the simultaneous collection of the required different spectral bands, thus directly improving framerate.

As for issues like dynamic range, signal-to-noise ratio and economical aspects: Time is on our side, since camera technology is still evolving rapidly.

10.5 References

[1] ISO/TC121/SC3-IECSC62D/JWG4, IEC/CD 60601-2-54 *Medical electrical equipment - Part 2-54: Particular requirements for the basic safety and essential performance of pulse oximeters for medical use.* 2002, ISO/IEC.

[2] ISO/TC121/SC3, ISO/DIS 9919 *Medical electrical equipment - Particular requirements for the basic safety and essential performance of pulse oximeters for medical use.* 2003, ISO.

[3] Nitzan M, Babchenko A, Khanokh B and Taitelbaum H, *Measurement of oxygen saturation in venous blood by dynamic near infrared spectroscopy.* Journal of Biomedical Optics, 2000. 5(2): p. 155-162.

[4] Franceschini MA, et al., *Near-infrared spiroximetry: noninvasive measurements of venous saturation in piglets and human subjects.* Journal of Applied Physiology, 2002. 92(January 2002): p. 372-384.

[5] Tsai AG, Johnson PC and Intaglietta M, *Oxygen gradients in the microcirculation.* Physiological Reviews, 2003. 83: p. 933-963.

[6] Thorniley MS, Sinclair JS, Barnett NJ, Shurey CB and Green CJ, *The use of near-infrared spectroscopy for assessing flap viability during reconstructive surgery.* Br J Plast Surg, 1998. 51(3): p. 218-226.

[7] Holzle F, Rau A, Swaid S, Loeffelbein DJ, Nolte D and Wolff KD, *Simultaneous noninvasive monitoring for radial forearm and fibula flaps using laser Doppler flowmetry and tissue spectrophotometry.* Mund Kiefer Gesichtschir, 2005. 9(5): p. 290-299.

[8] Sowa MG, Leonardi L, Payette JR, Fish JS and Mantsch HH, *Near infrared spectroscopic assessment of hemodynamic changes in the early postburn period.* Burns, 2001. 27(3): p. 241-249.

[9] Rajbhandari SM, Harris ND, Tesfaye S and Ward JD, *Early identification of diabetic foot ulcers that may require intervention using the micro lightguide spectrophotometer*. Diabetes Care, 1999. 22(8): p. 1292-1295.

[10] Beckert S, Witte MB, Konigsrainer A and Coerper S, *The impact of the Micro-Lightguide O2C for the quantification of tissue ischemia in diabetic foot ulcers.* Diabetes Care, 2004. 27(12): p. 2863-2867.

Chapter 11

Algemene discussie en samenvatting

11.1 Pulsoxygrafie

De doelstelling van dit promotie onderzoek was om de haalbaarheid na te gaan van het contactloos verkrijgen van pulsoxymetrie-beelden (voorgestelde NL-term: *pulsoxygrafie*). Het in hoofdstuk 2 beschreven patent betoogt dat pulsoxygrafie kan worden gerealiseerd met behulp van uit camerabeelden afgeleide fotoplethysmografische registraties van de polsgolf bij drie golflengtes, en wel bij voorkeur 660, 810 and 940nm.
Vanuit de absorbtiecurves van hemoglobine en oxyhemoglobine kan direct worden afgelezen dat twee van deze golflengten (660 en 940nm) zuurstof-gerelateerde informatie bevatten, en de bruikbaarheid van deze golflengtes voor conventionele pulsoxymetrie is algemeen bekend (zowel in transmissie- als in reflectie-mode).
De aanvullende derde golflengte (810nm) ligt op een zogenoemd isobest punt waarbij de absorbtiecurves van hemoglobine en oxyhemoglobine elkaar snijden. Daarom bevatten beelden en/of fotoplethysmografische registraties die bij een golflengte van 810nm worden verkregen géén zuurstof-gerelateerde informatie, hetgeen nuttig is als referentie bij het corrigeren voor schaduwen, reflecties, bewegingsartefacten en variaties in optische geometrie.

Met betrekking tot pulsoxygrafie werden de volgende resultaten bereikt:
In hoofdstuk 3 is aangetoond dat het mogelijk is om bij een vrijwilliger vanaf 72cm afstand bij alle drie genoemde golflengten hartslag-gerelateerde fotoplethysmografische registraties af te leiden uit camerabeelden.
Om de mogelijkheden van pulsoxygrafie verder te onderzoeken met de gerealiseerde opstelling, leken verdere metingen op vrijwilligers sub-optimaal vanwege: Signaal/ruis problemen, de sequentiële opname van de drie voor berekening van zuurstofsaturatie benodigde golflengten en vooral het ontberen van een methode om variabele en langdurig stabiele zuurstofsaturaties te realiseren.
Hoofdstuk 4 beschrijft vervolgens een idee voor een in-vitro fantoom dat een nauwkeurige “slag-voor-slag” reproduceerbare fotoplethysmografische “polsgolf” produceert bij een verbeterde signaal/ruis verhouding en dat tevens in staat is om gedurende langere periodes te voorzien in hypoxie. Dit idee werd door ons ontwikkeld omdat een dergelijk fantoom ons in staat zou stellen om de in hoofdstuk 3 geïdentificeerde beperkingen te omzeilen. Tevens kan een stabiel fantoom mogelijk toepasbaar zijn bij de calibratie van “normale” pulsoxymeters [1, 2].
Hoofdstuk 5 beschrijft een eerste prototype van het fantoom (gebaseerd op de patent-

tekst in hoofdstuk 4), toegepast bij een in-vitro experiment ter verificatie van de haalbaarheid van ons camera-concept. Met behulp van dit fantoom konden monotone en reproduceerbare relaties worden aangetoond tussen pulsoxymeterwaardes en camera-bepaalde ratio-van-ratio waardes, en ook tussen pulsoxymeterwaardes en laboratoriumwaardes.
Hoofdstuk 6 beschrijft een eerste verkenning van de zuurstofsaturatie-afbeeldende eigenschappen van de gerealiseerde camera. Hiertoe werd het fantoom aangepast door het aanbrengen van twee gescheiden gebieden met verschillende zuurstofsaturaties (gerealiseerd door het gelijktijdig injecteren van vers afgenomen arteriële en veneuze bloedmonster-paren).

11.2 Verbeterde visualisatie van bloedvaten

Gedurende dit promotie-onderzoek werd een relatief simpele non-invasieve methode ontwikkeld voor de verbeterde visualisatie van onderhuidse bloedvaten. Hoofdstuk 7 beschrijft een naar aanleiding hiervan ingediende patenttekst. Hierin wordt aangegeven dat het mogelijk is om de zichtbaarheid van bloedvaten te verbeteren door beelden uit het zichtbare spectraalgebied te combineren met pixel-voor-pixel in positie overeenkomende beelden vanuit het nabij-infrarood. De methode is in staat om onderscheid te maken tussen contrasten veroorzaakt door bloedvaten in het weefsel enerzijds, versus schaduwen en reflecties vanaf het weefseloppervlak anderzijds. Hierdoor is het mogelijk om de contrasten veroorzaakt door schaduwen en reflecties ongemoeid te laten (en daarmee ook hun nuttige bijdrage aan dieptezicht) terwijl het contrast van de bloedvaten selectief kan worden versterkt.

Met betrekking tot verbeterde visualisatie van bloedvaten werden de volgende resultaten bereikt:
In hoofdstuk 8 wordt aangetoond dat inderdaad een significant verbeterde visualisatie van onderhuidse bloedvaten mogelijk is en dat de methode mogelijkheden biedt bij bloedafname, de inspectie van bloedvaten onder een donkere huid, spatader-onderzoek en visueel onderzoek van moedervlekken (nevi pigmentosum). De tevens gedemonstreerde visualisatie van bloedvaten door een jodium-oplossing vormt een duidelijke illustratie van de krachtige mogelijkheden van deze multispectrale techniek.
In hoofdstuk 9 wordt aangetoond dat een verbeterde visualisatie van coronairvaten mogelijk is. We demonstreren een licht verbeterde penetratie in epicardiaal vet, maar het meest interessante resultaat is de mogelijkheid om arteriële en veneuze contrasten naar keuze apart te versterken.

11.3 Conclusies

Aangezien het duidelijk is dat ontwerptechnische vraagstukken zoals signaal/ruis verhouding, beeldfrequentie en het simultaan registreren van spectraal gescheiden beelden in principe oplosbaar zijn, en dat zowel laboratorium-bloedgasbepalingen als reflectie-mode pulsoxymetrie klinisch geaccepteerde methoden zijn, volgt uit combinatie van de hoofdstukken 3, 4, 5 en 6 dat contactloze beeldvormende pulsoxymetrie (pulsoxygrafie) mogelijk is.
De bovengenoemde ontwerptechnische vraagstukken zijn zeker niet triviaal en het zal intensieve inspanningen vergen om een klinisch toepasbare SpO_2-camera te ontwikkelen. Dit proefschrift levert echter de onderbouwing dat dergelijke inspanningen gerechtvaardigd zijn.

Aangaande de verbeterde visualisatie van in weefsel verborgen bloedvaten, volgt uit combinatie van de hoofdstukken 7, 8 en 9 dat: Het enerzijds mogelijk is om een stereoscopische verbeterde visualisatie van onderhuidse bloedvaten te realiseren middels een op enige afstand opgestelde camera; en dat anderzijds bij open-hart chirurgie zowel een verbeterde visualisatie van door epicardiaal vet bedekte coronairvaten alsook een fysiologische afbeelding van de arterieel/veneuze contrastverhouding, voordelen kunnen bieden.
De technische uitdagingen die nog overwonnen moeten worden om tot een klinisch toepasbaar apparaat te komen, liggen binnen de mogelijkheden van de moderne biofotonica-industrie.

11.4 Toekomstperspectieven

De beschreven methoden voor pulsoxygrafie (SpO_2-camera) en de visualisatie van bloedvaten (de “vaatkijker”) kunnen beschouwd worden als complementaire modaliteiten die, indien zij eenmaal technologisch volwaardig zijn, relatief eenvoudig in één apparaat kunnen worden geïntegreerd. De hardware die nodig is voor pulsoxygrafie biedt in principe tevens de mogelijkheid voor registratie van de informatie die nodig is voor de “vaatkijker”. Het belangrijkste verschil zit in de bewerkingsprocessen.
Als eerste uitvoering van een SpO_2-camera kan daarom gedacht worden aan een apparaat dat eerst de ligging van de bloedvaten vaststelt en daarna de bewerkingen voor pulsoxygrafie selectief toepast op de ROI-pixels die samenvallen met de geïdentificeerde bloedvaten. De figuren 4C en 4D uit hoofdstuk 9 illustreren de resultaten van een simpele kwalitatieve oxygenatie-afhankelijke beeldbewerking die alleen de zuurstof-afhankelijke absorbtieverschillen benut, zonder gebruik te maken van de pulsatiele component.
In hoofdstuk 3 werd een relatief sterke respiratie-gecorreleerde component gevonden in de geregistreerde in-vivo fotoplethysmogrammen. Deze kan mogelijk bruikbaar

zijn voor veneuze oxygrafie. In 2000, werden door Nitzan *et al*. door respiratie veroorzaakte bloedvolume oscillaties in de hand aangetoond middels fotoplethysmografische registraties [3]. In 2002 werd door Francescini *et al*. aangetoond dat veneuze oxymetrie mogelijk is met behulp van multispectrale registratie van respiratie-gecorreleerde fotoplethysmogrammen verkregen middels een contact-mode sensor. Hiervoor werd als term spiroximetry voorgesteld [4].

Naast toepassingen bij bloedafname, vaatinspecties door donkere huid, spataderonderzoek en visuele inspectie van moedervlekken, zijn talloze andere klinische toepassingen denkbaar zoals:

- Bestudering van de fysiologie van zuurstofgradiënten in de microcirculatie [5];
- Verificatie van weefseloxygenatie gedurende reconstructieve chirurgie [6, 7];
- Beoordeling van brandwonden [8];
- Het volgen van de vasculaire conditie van diabetes patiënten (b.v. voeten) [9, 10];
- Het onder geleide aanprikken van shunts bij dialyse patiënten;
- Identificatie van in de vetschort verborgen bloedvaten bij laparoscopie .

Sommige van deze toepassingen hebben genoeg aan de verbeterde visualisatie van bloedvaten, andere vereisen daarnaast pulsoxygrafie (en dus meer technische inspanning).

Voor beide modaliteiten zullen onze verdere onderzoeksinspanningen eerst gericht worden op het simultaan registreren van de verschillende vereiste spectrale banden, waardoor de beeldfrequentie rechtstreeks wordt verbeterd.

Aangaande zaken als signaal/ruis verhouding, dynamisch bereik en economische aspecten werkt de tijd in ons voordeel omdat de cameratechnologie zich nog steeds snel ontwikkelt.

11.5 Referenties

[1] ISO/TC121/SC3-IECSC62D/JWG4, IEC/CD 60601-2-54 *Medical electrical equipment - Part 2-54: Particular requirements for the basic safety and essential performance of pulse oximeters for medical use.* 2002, ISO/IEC.

[2] ISO/TC121/SC3, ISO/DIS 9919 *Medical electrical equipment - Particular requirements for the basic safety and essential performance of pulse oximeters for medical use.* 2003, ISO.

[3] Nitzan M, Babchenko A, Khanokh B and Taitelbaum H, *Measurement of oxygen saturation in venous blood by dynamic near infrared spectroscopy.* Journal of Biomedical Optics, 2000. 5(2): p. 155-162.

[4] Franceschini MA, et al., *Near-infrared spiroximetry: noninvasive measurements of venous saturation in piglets and human subjects.* Journal of Applied Physiology, 2002. 92(January 2002): p. 372-384.

[5] Tsai AG, Johnson PC and Intaglietta M, *Oxygen gradients in the microcirculation.* Physiological Reviews, 2003. 83: p. 933-963.

[6] Thorniley MS, Sinclair JS, Barnett NJ, Shurey CB and Green CJ, *The use of near-infrared spectroscopy for assessing flap viability during reconstructive surgery.* Br J Plast Surg, 1998. 51(3): p. 218-226.

[7] Holzle F, Rau A, Swaid S, Loeffelbein DJ, Nolte D and Wolff KD, *Simultaneous noninvasive monitoring for radial forearm and fibula flaps using laser Doppler flowmetry and tissue spectrophotometry.* Mund Kiefer Gesichtschir, 2005. 9(5): p. 290-299.

[8] Sowa MG, Leonardi L, Payette JR, Fish JS and Mantsch HH, *Near infrared spectroscopic assessment of hemodynamic changes in the early postburn period.* Burns, 2001. 27(3): p. 241-249.

[9] Rajbhandari SM, Harris ND, Tesfaye S and Ward JD, *Early identification of diabetic foot ulcers that may require intervention using the micro lightguide spectrophotometer*. Diabetes Care, 1999. 22(8): p. 1292-1295.

[10] Beckert S, Witte MB, Konigsrainer A and Coerper S, *The impact of the Micro-Lightguide O2C for the quantification of tissue ischemia in diabetic foot ulcers.* Diabetes Care, 2004. 27(12): p. 2863-2867.

Dankwoord

Een proefschrift komt niet vanzelf tot stand, door de jaren heen zijn er vele mensen die mij hebben bemoedigd en verder geholpen. Ik kan ze niet allemaal noemen, want het zijn er heel veel. Mijn grote dank aan:

Mijn vader en moeder voor alle goede zorgen (en er zullen vast veel zorgen zijn geweest). Mijn broer Tholejan voor het beschermde gevoel dat ik altijd een grote broer had waarop ik kon terugvallen. Mijn zus Catharina voor de momenten van slappe lach die we samen hebben gehad (Háh, ie kinnen oans toch nait…). Ik zie de verwantschap terug in mijn dochters. Mijn zwager Marc voor het op handen dragen van mijn zus (het Vlaamse woord "schoonbroer" doet je meer recht dan het Nederlandse "zwager").

De familie Akkermans, die voor mij een synoniem is voor Friese degelijkheid, betrouwbaarheid en gastvrijheid: Klaas, voor je vriendschap en de vele jaren waarin we samen muziek maakten. Jij maakte er je beroep van, ik was (helaas) met minder talent gezegend. Roelof voor je stevige handdruk en onverwoestbare enthousiasme. Doretta voor de gezelligheid tijdens genoeglijke zondagmiddagen. Mevrouw Akkermans voor de catering tijdens alle muziekopnames. Meneer Akkermans voor zijn (zo mogelijk) nóg steviger handdruk en het mogen gebruiken van alle gereedschappen die ik zelf (toen nog) niet had.

De familie ter Beest, waar ik letterlijk kind aan huis mocht zijn: Martin, voor je vriendschap en de talloze chemische experimenten die we samen, onder vanuit ARBO-technisch oogpunt uiterst discutabele omstandigheden, uitvoerden. Je zussen waren niet altijd even goed te spreken over de merkwaardige geurtjes die dit soms opleverde. Mevrouw ter Beest† voor de gastvrije gezelligheid en de humor. Mijnheer ter Beest† voor de uiterst rake samenvattingen van zijn kijk op de wereld.

Mijn eerste werkgever Geert van der Bijl† voor het vertrouwen dat hij had in 2 broers van 8 en 11 jaar.

Alle docenten van het Lauwerscollege die het twijfelachtige voorrecht hadden om mij les te geven, maar in het bijzonder de heer C. Bok voor zijn geschiedenislessen (die blijkbaar toch nog enigszins overgekomen zijn) en voor de humorvolle commentaren op de schelmenstreken van Martin en mij. Wij werden door hem gewoonlijk aangeduid als ingenieur Fokkinga en Doctor het Beest en in dit verband geldt inderdaad *"en de leraar die mij altijd placht te dreigen: Jongen jij komt nog op het verkeerde pad, kan tevreden zijn en hoeft niets meer te krijgen; dat wil zeggen hij heeft toch gelijk gehad"*.

Mijnheer Broersma, omdat hij mijn interesse wekte voor optiek, fotografie en filmen. Bedankt voor alle kennis daaromtrent (en voor de lessen over hoe je iets verkoopt) alsmede voor het uitlenen van de microfoons t.b.v. de eerste opnames die ik ooit met een bandje maakte. Mevrouw Broersma vanwege haar optimistische natuur en oprechte belangstelling voor haar medemensen. Voor jullie in het bijzonder hoop ik dat de zegswijze "wie goed doet, goed ontmoet" uitkomt.

"Hubo" Reitsma uit Buitenpost, voor het gebruik van de machines bij het bouwen van mijn eerste gitaren.

Aan mijn HTS-periode heb ik warme herinneringen en goede vrienden overgehouden. Schelte Heeringa (mister analog devices en een uitstekend muzikant), Peter Mous (onze diplomaat), Koster_komma_G_punt_A_punt (mister software) en Wim Schoo (the Fonz, maar wel op tijd olie peilen…). Dank aan al mijn leraren uit die tijd, maar vooral aan de heren van Dijk en de Graaf. Pappa India 5 Lima Tango Victor uit.

Alle collega's van de afdeling Klinische Fysica uit Rijnstate (John, Ruud, Pieter, Harry, Gerda, Wilma, Jan, Maarten, Gerrit1, Gerrit2, Cor, Sandra, André en Egbert) en natuurlijk ook de afdeling Radiodiagnostiek (goed voorbeeld doet goed volgen Tjeerd) de afdeling Nucleaire Geneeskunde (Ton, je hebt heel wat teweeg gebracht toen je me aanzette tot mijn eerste poster en voorstelde aan Judocus) het Klinisch Laboratorium (met name Henk en Gudi) en de Apotheek (vooral Herman en natuurlijk Adriaan - je voorspelling is nu uitgekomen !).

Judocus Borm voor de hulp bij het maken van mijn eerste poster.

Herr Rexhausen† en Dr. Braun van Biotronik die (op voorspraak van Gert van Alst) na het aanhoren van John Hardeman's en mijn ideeën over pacemakers en pulsoxymetrie besloten tot octrooi-aanvraag.

De familie Mons voor alle raad en daad waarmee zij ons terzijde hebben gestaan. Dat krijg je er nou van wanneer je door Gert mee naar huis wordt gesleept vanuit een jeugdavond (Gert vroeg of laat krijg je die compressor wel spits).

Mijn schoonouders Toon en Martha Gerritsen voor alle steun gedurende de afgelopen 18 jaren. Ik hoop dat jullie samen nog een hoop mooie plekjes op deze aardbol mogen verkennen. Anja en Marcel ook bedankt voor de steun.

Familie van Schuylenburg: Jan en Jeanette (jullie voelen voor Hetty en mij aan als broer en zus), Eline (voor alle hulp in huis), Jeroen (een gouden hart, twee gouden handen en een goed verstand kunnen het samen ver brengen met wat discipline) en Nada (isn't she cute).

Aad en Jaqueline Nijmeijer (die ook als een broer en zus voelen voor Hetty en mij), Wilbert† (je hebt dit niet meer meegemaakt, maar ik weet dat je het prachtig had gevonden) en Jorrit (je bent een edelmoedige kerel).

Ad Voerman, voor de vele avondlijke gesprekken, zijn heldere analyses en de aanleg van het "Voermanplein" tussen woonhuis en tuinhuis te Duiven.

Alle "medisch-technische" TNO-collega's (ik kan niet iedereen apart noemen, maar een paar namen moet ik echt naar voren halen).
Arthur Leefmans voor zijn wijze raad en leermeesterschap in elektrische veiligheid, elektrostatische verschijnselen en elektromagnetische compatibiliteit. Roel Bakker voor zijn goudeerlijke omgang met mensen (altijd door en door betrouwbaar). Ina Kloosterboer voor haar doortastende manier van organiseren en het altijd weer in de bres springen voor "haar" mannen. Robert Bezemer voor alle steun (leuk om samen een octrooi in depot te hebben). Carool Teirlinck die me terzijde stond bij het zwaarste incidenten-onderzoek dat ik ooit meemaakte (Piet van Beek ook jij bedankt). Mark van Abkoude voor zijn onontbeerlijke hulp bij het oplossen van problemen in de kliniek (soms tot na middernacht). Cock Pastoor voor zijn kalme en hulpvaardige natuur. Reinout Hensbroek voor zijn introductie in de analyse van systemen. Cees Zeelenberg voor het feit dat hij mij introduceerde bij de Erasmus Universiteit. Adrie Dumay voor de wijze waarop hij de fakkel van Cees hierin later overnam.

Collin Driscoll, for his good advise and remarkable statement: *"In photobiology there are no teachers, only students"*. Frank de Gruijl voor het reviewen van mijn eerste boekje over UV-straling.
All members of CEN TC 169 / WG 8 "Photobiology" for the splendid meetings and discussions that we had. When I once saw a photograph made during the Solvay conferences, it showed a remarkable resemblance with our evening discussions. Thank you Harald, Jean Pierre, Serge, Andy, Terje, Peter and Bruno.

Klaas Bom en Ton van der Steen voor het (onvergetelijke) gesprek waarin zij binnen 15 minuten het geschetste principe van pulsoxygrafie begrepen en er ook toepassingen voor zagen. Ad Bogers die mij bij de perfusionisten introduceerde (bedankt Ricardo en Annemarie) en steeds met nagenoeg de snelheid van het licht mijn vragen om commentaar beantwoordde. Dirk Duncker die mij op het spoor zette van de selectieve visualisatie van coronaire arteriën. Rob van den Bremer, wiens regeltalent en geduld bijgedragen hebben aan enkele cruciale experimenten. Alle OK-medewerkers voor hun ondersteuning.

Mr. J. van Melle die keer op keer en met veel geduld de essentie van mijn ideeën uit mij wist te peuteren om deze vervolgens helder te formuleren in een octrooi-aanvrage (zie de hoofdstukken 2, 4 en 7). De heer B. Plat (voor zijn onuitputtelijke optimisme en vermakelijke verhalen over zijn kleurrijke loopbaan) en de heer E. Land (voor zijn zakelijke adviezen).

Mary van Veen en Willem Flantua voor jullie goede raad en (samen met alle medewerkers van het Colombine huis) voor de fantastische dagen die we bij jullie te gast waren. Ik kan nu dat jasje met al die horloges erop eindelijk uit doen.

René van Melick en Dirkjan Bakker die vanaf het begin in het idee geloofd hebben en dit door de oprichting van O_2view B.V. in daden hebben omgezet.

Alle vrijwilligers die geduldig stil gezeten hebben in het donker voor het maken van de opnames voor hoofdstuk 3 (met name Jerome Borsboom voor zijn sublieme vasculatuur en zeer stabiele hartslag).
De Sanquin bloedbank te Rotterdam en alle donoren die hebben gebloed voor dit onderzoek.

Alle “nerds” uit Delft die in de loop van de jaren met me meeleefden (ik bedoel echt allemaal, maar kan niet iedereen noemen, al wil ik ook hier een paar namen echt naar voren halen). Allereerst Norbert Koster (mister vacuümtechniek en naar ik denk de slimste persoon die ik ken), Bas Mertens (dou ze de boks op daar in Braboland), Roland van Vliet (die de betekenis van “to manage” écht in de praktijk weet te brengen) en Patrick de Jager (waarmee ik menig technisch-filosofisch gesprek heb gevoerd). Aan jullie klankbord is mij veel gelegen.
Rik Janssen (de meest relaxte en coole collega die ik ooit heb gehad), Jan van Elp (met het hart op de goede plaats) en Ellen Staak (onze “moeder-overste” in de oudbouw).
Uiteraard ook Annemieke van de Runstraat (veel succes), Jacques van der Donck (a gentleman in sports and science), Ton Bastein (die me het eerst “ontdekte” vanuit Delft) en Anton Duisterwinkel (may the Van der Waals force be with you). Gezamenlijk hebben jullie mij de diepere betekenis van het woord “schoon” bijgebracht. Henri Werij en Bart van Mierlo, voor het grote in mij gestelde vertrouwen.

Alle collega’s van de afdeling Biomedical Engineering, met name Jan Honkoop en Wim van Alphen voor de “elektriek” alsmede Leo Bekkering (vakmanschap is meesterschap) en Geert Springeling voor de “fijne mechanica”. Verder Radj Baldewsing voor de talloze discussies en culinaire introducties tot de exotische keuken (een beroepskeuze-advies: wordt géén automonteur) alsmede Doctor-Doctor Johannes Schaar (the guitar man) voor zijn humorvolle en rake analyses aangaande cultuur en wetenschap.

Ook aan alle medewerkers en ex-medewerkers van het secretariaat ben ik veel dank verschuldigd. Met name aan Corry en Riekje (bedankt voor de gezelligheid, het regelen van vele zaken en ettelijke tientallen kilo's zure beren) Mieke (go for it), Marianne (in Rotjeknor regelen we het gewoon) en Annet (voor de hulp bij de laatste loodjes).

Johan Sweep, Ab Klippel en Naomi Nathan voor de ondersteuning vanuit de medische techniek. De priksters van de polikliniek cardiologie voor hun medewerking aan de opnames tijdens bloedafname. Martino Neumann voor het meedraaien op het spataderspreekuur. Jos Lenoble voor de kans om mee te mogen helpen bij het lopende onderzoek naar sepsis-diagnostiek. De medewerkers van het klinisch laboratorium van het Thorax centrum voor alle bloedgas-analyses.

Dan kom ik uit bij Frits Mastik. Frits, ik weet dat je niet graag in de schijnwerpers staat, maar zonder jou zou dit proefschrift simpelweg niet tot stand gekomen zijn. Dankzij jouw programmeerwerk werd uit gigabytes aan camerabeelden de juiste informatie gedistilleerd en werden artikelen en afbeeldingen altijd net even beter dan wanneer ik ze alleen had gemaakt. Officieel had ik geen co-promotor, maar voor mij heb je die rol zeker vervuld. Mijn oprechte dank voor de honderden donderdag-avonden en de lange dagen achter de hart-long machine die je samen met mij hebt gespendeerd tijdens dit onderzoek. Het is een eer en een voorrecht om je te kennen.

Tenslotte, maar zeker niet in het minst, wil ik alle leden van mijn gezin bedanken:
Mijn vrouw Hetty voor het oneindige geduld waarmee zij mij de afgelopen jaren heeft vergeven wanneer ik weer eens een afspraak of plechtig beloofd uit te voeren karweitje was vergeten. Hetty, tevens bedankt voor de manier waarop je me altijd weer in de realiteit terug wist te brengen als ik zat te dromen, een vaardigheid die zich overigens reeds vroeg in onze verkering openbaarde ("hij is rood mijnheer Wieringa" bij nadering van een verkeerslicht).

Mijn dochter Jolinka voor haar bereidwillige hulp en inzicht bij alle technische karweitjes in en om het huis en voor haar cynische commentaren en rake opmerkingen ("stresskip") aangaande mijn gedrag bij vakanties en overige uitjes in gezinsverband.

Mijn dochter Maranke, voor haar bemiddeling bij de contacten met mijn adviseurs, de heren B. Plat en E. Land, alsmede voor het mogen raadplegen van haar historische pharmaceutische bibliotheek en voor haar terloopse bijdrage aan de ruimtevaart.

Mijn zoon Wimjan voor het voorrecht steeds weer deelgenoot te worden gemaakt van zijn schier onuitputtelijke voorraad wilde ideeën, zijn wereldomvattende complottheorieën (waarin ene Jaques von Hamsterville herhaaldelijk figureert) en het zich telkenmale bereidwillig ontfermen over mijn pantoffels gedurende de tijd dat ik niet thuis ben. Eindelijk is nu het moment gekomen dat ik je zitzak kan ophangen.

Curriculum Vitae

Fokko Pieter Wieringa was born in Haarlem on the 20st April 1965. When he was 4 weeks old, his family moved to Kollum, where he went to primary school (Prins Bernhardschool) from 1971 to 1977. Repeatedly the remark "Fokko is a dreamer" was made in school reports.

From 1977 to 1983 he attended the VWO (Lauwerscollege, Buitenpost) and passed his exams for Dutch, English, German, Math I, Math II, Chemistry and Physics.

His next step in education was HTS-Electronics, specializing in medical technology (Noordelijke Hogeschool, Leeuwarden) from 1983 to 1987. During this time he served for two apprentice projects at the Nuclear Physics Accellerator Institute in Groningen and at the St. Elisabeth Hospital in Arnhem respectively. In the St. Elisabeth Hospital he produced the Report: *"Pressure measurements in orthopaedics – a clinical study of the possibilities for pressure measurements within muscles and bone marrow"* in co-operation with Dr. Prakke†, an innovative orthopaedic surgeon.

After having finished his studies he became employed as a medical instrumentation engineer by the St. Elisabeth Hospital, that meantime had merged with the County Hospital into De Malberg and later again merged with the Diacony Hospital into Rijnstate Hospital.

He married Henriette Gerritsen in 1989 and soon they bought their first house in Duiven (within emergency response reach of the hospital).

During his hospital years he did several courses, being:

- Systematic Analog Design, Haagse Hogeschool (1989-1990)
- Systematic Digital Design, Haagse Hogeschool (1990-1991)
- Ionizing Radiation expert level 3, Interfacultary Reactor Institute, Delft University (1991-1992)
- Design of pneumatic control systems, Festo Didactic Tilburg (1992)

Aside of his daytime job at the hospital, he did some projects as a freelance advisor and designer of custom hard- & software for various industry (merely for the fun of it).

Together with his boss John Hardeman he wrote his first two patents on opto-electronic sensor technology (oxygen saturation measurement) that were filed by Biotronik in Berlin.

Meantime they were blessed with three children: daughter Maranke in 1992, daughter Jolinka in 1993 and son Wimjan in 1995.

In 1999 his wife Henriette miraculously survived an accident when a truck rammed her stationwagon. The truck driver was reading a newspaper while driving. Henriettes resulting whiplash still remains.

In 1997 Fokko was invited to come to work with Arthur Leefmans and Roel Bakker at TNO Prevention and Health in Leiden, where he started in October 1997. Again he did some courses:

- Lead Assessor ISO 9001 (1998)
- Post Academic Training EMC, Technical University Eindhoven (1999)

Apart from this, Arthur and Roel learned him essential skills in electrical safety measurements on hospital installations and medical devices. Also the subjects electrostatics (ESD) and electromagnetic compatibility (EMC) were practiced and for the latter subject his colleague Reinout Hensbroek was an efficient teacher. The associated necessary reporting skills were developed as well.
Fokko started to take a growing interest in standardization and helped Arthur with the work for IEC on electrical safety in hospitals.
In 1999 his superiors Rene van Melick and Cees Zeelenberg offered him the opportunity to broaden his horizon within TNO by entering the world of optical radiation interaction with tissue (in particular ultraviolet radiation). He was encouraged by Collin Driscoll, and Frank de Gruijl, whom both introduced him to many others within the photobiological community, and he finally became a member of several workgroups in the field.

In response to an idea that led to another patent application (see chapter 2), TNO was willing to let him work on a research project for one day per week in order to prove the concept. Cees Zeelenberg introduced Fokko to prof. N. Bom and prof. A.F.W. van der Steen and in December 2001 he started his research within the Thorax Centre of Erasmus University in Rotterdam. This book contains the resulting thesis.

Meanwhile, in addition to medical technology, Fokko got involved in a large research framework on Extreme UV Lithography (EUVL, the intended next generation of wafer stepper technology for semiconductor manufacturing, operating at a wavelength of 13 nm). This project was carried out by TNO in Delft. ASML, Carl Zeiss and Philips were the funding partners. Hired via TNO in Leiden (renamed to Quality of Life) Fokko spent part of the week in Delft for this project over several years and co-authored several patent applications. He enjoyed the fun of developing frontier technology in an excellent team. At home his family called it the “nano-nerd bunch”.

In May 2005 the Wieringa family moved from Duiven to Elst. Since daughter Jolinka had become progressively dependent on a wheelchair, their previous house had become too small. The new house turned out to be a good move, especially since recently also daughter Maranke progressively becomes wheelchair dependent.

Since January 2006, Fokko spent 50% of his work time as a consultant for TNO Certification (a Notified Body for CE-marking of medical devices) for knowledge transfer on electrical safety in medicine.

Starting in May 2007, he has been assigned to stimulate innovations in Life Science technology in addition to the EUVL and nano work that he already did at TNO Science & Industry in Delft.
His medical research in Erasmus MC will furthermore be continued in part-time.

Job history

Medical Instrumentation R&D engineer

Rijnstate hospital Arnhem, department of Clinical Physics
Main occupation from July 13th 1987 until September 30st 1997

Lecturer of medical technology for post higher education of nurses: Intensive Care, Cardio Care, Obstetry and Paediatrics (on demand)
Scholingsinstituut ENA Arnhem
Side occupation from 1988 until 1997

Freelance advise and design of custom hard- & software for various industry.
- Measurement & Control systems (electronic & electro-pneumatic)
- Analog electronics
- Opto electronics
- Sensordesign

Side occupation from january 1990 until august 1997.

Applied Physics Advisor

Division of Technology in Healthcare, TNO-Quality of Life Leiden
Main occupation from October 1st 1997 until May 1st 2007

Technology assessor (on demand)
Technology Rating Amsterdam
Side occupation from 1997 until 2001.

Optical & plasma cleaning researcher

TNO I&T Delft
Department of Semiconductor equipment
2001 until 2007 part-time; main occupation from May 1st 2007 until now

Lecturer of optical radiation safety (on demand)
Yearly post higher level education for industrial hygienists.
Hogeschool Brabant, Nova Medical
2002 until 2005

Biophotonics researcher (1 day/week via TNO)

Erasmus Medical Center Rotterdam
Department of Biomedical Engineering
2001 until now

Publications

A phantom for stomach emptying studies: Validation of a method to obtain time-location curves
F.P. Wieringa, J.J.J. Borm, A.J.M. Rijnders, E.J. Visser, W.J. Reinalda and E.A. van Royen
European journal of nuclear medicine, vol.19(8) 1992

Gentamicin containing Implantable devices; In vitro elution characteristics
A.A. van Sorge, J.P. Yska, M.A. Ullmann, R. Feith, F.P. Wieringa
Vancomycin implantation tablets; In vitro elution characteristics
A.A. van Sorge, A.W.G. Essink, Y.P. Yska, R. Feith, F.P. Wieringa
In 4th Internet World Congress on biomedical sciences 1997 in UOEH, Kitakyushu, Japan

Veilig medisch gebruik van ultraviolette straling: Recente ontwikkelingen
F.P. Wieringa, C.J.M.P. Teirlinck
Klinische Fysica October 2000

Ein automatisches PC-gesteuertes Messgerät zur geometrischen und spektroradiometrischen Charakterisierung von UV-Phototherapiegeräten
F.P. Wieringa, R.A. Bezemer
6th DAfP Symposium, Stuttgart 14-15 May 2001.

Pulsoxymetrie een techniek met toekomst, maar ook randvoorwaarden
F.P. Wieringa, A.F.W. van der Steen
Klinische Fysica 4/2002 (non-reviewed paper, Dutch language)

Arbeidsveiligheidsaspecten bij industrieel, medisch en cosmetisch gebruik van kunstmatige ultraviolette straling
F.P. Wieringa
NVS-Nieuws 2002/1 (non-reviewed paper, Dutch language)

Oriënterend onderzoek inzake de algemene veiligheid van medische technologie in Nederland
Public domain TNO-report on the condition of hospital installations and equipment
PG/TG/2002.277 October 2002 (Dutch language)

Measurement and assesment of radiation exposures by artificial UV-sources in the workplace -Announcing a new European standard
F.P. Wieringa, R.A. Bezemer
In 2nd Worldcongress of the International UV Association (IUVA)
Vienna; 9-11 July 2003

EN 14255-1 *"Incoherent optical radiation – Part 1: Measurement and assessment of radiation exposures by artificial UV-sources in the workplace"*
European standard; co-author as CEN member

Some information with regard to Sunbeds and Solaria in the Netherlands
F.P. Wieringa, R.A. Bezemer
Euroskin workshop on sunbeds, Stockholm 20th September 2003

EN 14255-2 *" Measurement and assessment of personal exposures to incoherent optical radiation — Part 2: Visible and infrared radiation emitted by artificial sources in the workplace"*
European standard; co-author as CEN member
Licht en Gezondheid voor werkenden
G.J. van den Beld, C. Beije, B. Gerritsen, P.J.M. IJsselmuiden, J.H.G.M. de Kort, H.J.J. Meutzner, G.H. van Rheenen, A. Rommers-Jong, G.W. Stoer, A.M.C. Schoutens, V. Vallenduuk, J. Veldhuis, F.P. Wieringa
Nederlandse Stichting voor Verlichtingskunde (NSVV)
ISBN 90-76549-19-2 1st edition November 2003

Jaarboek Arbeidshygiëne 2004
Chapter 23: Non ionizing radiation; Part II: Optical radiation
ISBN 9013007759 Kluwer 2004 (followed by revized and extended 2005 edition)

NEN-TNO Praktijkgids: *Elektrische veiligheid in medisch gebruikte ruimten*
(electrical safety in medically used rooms; Dutch language)
F.P. Wieringa, A. Leefmans, L.J. Dias, G.M.A. van Abkoude
ISBN 9052541051 NEN Delft 2004

Standardizing biological UV-radiometry, an introduction to EN 14255-1
F.P. Wieringa, R.A. Bezemer
196th PTB Workshop Traceability in UV-dosimetry (invited lecture)
Karlsruhe 22-24 Sept 2004
IUVA, DafP & DVGW European Conference on UV radiation

Electrical safety in the Endosuite concept
in The OR of the future and robotics; 2nd MCL Leeuwarden update in minimally invasive surgery
Leeuwarden 1-3 Nov 2004

An update on optical radiation safety in Europe
F.P. Wieringa, A.M.T.I. Vermeulen
IUVA News Vol.7(2) p.p. 27-31; 2005

Contactless multiple wavelength photoplethysmographic imaging: A first step towards "SpO2 camera" technology
F.P. Wieringa, F. Mastik, A.F.W. van der Steen
Annals of biomedical engineering, 2005 Vol.33(8) p.p. 1034-1041

NEN 1010-7/A3
Dutch national Electrotechnical standard for medically used rooms
Co-author as CEN 64 and CENELEC member (European standard)

Directive 2006/25/EC of the European Parliament and of the council of 5 April 2006 on the minimum health and safety requirements regarding the exposure of workers to risks arising from physical agents (artificial optical radiation)
Co-author of Annex II

Five Frequently Asked Questions About UV-Safety
F.P. Wieringa
IUVA News Vol.8(2); p.p. 28-32; 2006

Optische straling in arbeidssituaties - Praktische aspecten bij implementatie in Nederland van de EU-richtlijn betreffende de blootstelling aan bronnen van kunstmatige optische straling. 30 juni 2006
F.P. Wieringa, C.J.P.M. Teirlinck en J.W.A.M. Alferdinck
Review: prof. D. van Norren
TNO-Report number KZ/2005.190; 116 pages & 5 appendices (Dutch language)
Assignment and printing by: Dutch ministry of social affairs and employment (SZW)

Contrast enhancement of coronary arteries in cardiac surgery: A new multispectral stereoscopic camera technique
F.P. Wieringa, F. Mastik, D.J.G.M. Duncker, A.J.J.C. Bogers, A.F.W. van der Steen
Euro Intervention; Vol.2; p.p. 389-394; 2006

Remote Optical Stereoscopic Multispectral Imaging during Cardiac Surgery
F.P. Wieringa, F. Mastik, D.J.G.M. Duncker, A.J.J.C. Bogers, C. Zeelenberg, A.F.W. van der Steen
In *Computers in Cardiology* Vol.33; p.p. 693-696; ISSN 0276−6547; Valencia Spain 2006

Remote non-invasive stereoscopic imaging of blood vessels: First in-vivo results of a new multispectral contrast enhancement technology
Annals of biomedical engineering; Vol.34(12); p.p. 1870-1878

Remote optical stereoscopic multispectral imaging of buried vasculature
F.P. Wieringa, F. Mastik, A.F.W.van der Steen
In *1st Dutch congress on biomedical engineering*, January 18-19 2007
Egmond aan Zee

Pulse oxigraphy: A non contact imaging approach
F.P. Wieringa, F. Mastik, A. Dumay, A.F.W. van der Steen
In *Innovations and applications of monitoring oxygenation & ventilation*
March 15-17 2007
Duke University, Durham, North Carolina, USA

Stellingen

bij het proefschrift

PULSE OXIGRAPHY

And other new in-depth perspectives
through the near infrared window

Fokko Pieter Wieringa

1. Het is mogelijk om de verdeling van zuurstofsaturatie in weefsel te visualiseren met behulp van een op afstand opgestelde camera die simultaan beeldreeksen registreert op 3 verschillende golflengten. (dit proefschrift)

2. Fotoplethysmografische signalen afgeleid uit camerabeelden van de onderarm bevatten een duidelijke ademhalings-gerelateerde pulserende component met een daarop gesuperponeerde zwakkere hartslag-gerelateerde component. (dit proefschrift)

3. Een nieuwe meetmethode kan gecalibreerd worden ten opzichte van een gouden standaard via een onbekende (maar stabiele) referentie door toepassing van een additionele bewezen meetmethode op de betreffende referentie, gevolgd door triangulatie. (dit proefschrift)

4. Tijdens open hartchirurgie kunnen arteriële contrasten selectief worden versterkt zonder aantasting van veneuze contrasten. (dit proefschrift)

5. Wanneer we informatie visualiseren, groeien onze inzichten. (dit proefschrift)

6. De medische uitdrukking *"deze patiënt is door mij gezien"* benadrukt het belang van visuele onderzoekstechnieken.

7. Multispectrale stereoscopie komt neer op het in een ander licht beschouwen van de patiënt teneinde de zaken anders te zien zonder noodzakelijkerwijs van standpunt te hoeven veranderen, waarbij de dingen in het juiste perspectief moeten blijven.

8. Je kunt speerpunt-technologie niet succesvol lanceren zonder er eerst een behoorlijke schacht aan vast te maken.

9. *"Antwoorden hebben de juiste vragen nodig om nuttig te worden."* (A.F.W. van der Steen)

10. Alles pulseert.

11. *"De vrije verstrekking van zure beertjes stimuleert zowel de creativiteit als de tandartspraktijk."* (vrij naar R. Daane)

1. It is possible to visualize the distribution of blood oxygen saturation in tissue by using a remote camera that simultaneously acquires movies at 3 different wavelengths. (this thesis)

2. Camera-derived photoplethysmographic signals from the lower arm contain a distinct respiration-correlated pulsatile component with a superimposed weaker heartbeat-related component. (this thesis)

3. A new measurement method can be calibrated to a gold standard via an unknown (but stable) reference by applying an additional proven measurement method to that reference and then using triangulation. (this thesis)

4. On the exposed heart, coronary arterial contrasts can be selectively enhanced without affecting venous contrasts. (this thesis)

5. If we visualize information, our insights literally grow. (this thesis)

6. The expression *"to be seen by a doctor"* emphasizes the importance of visual examination techniques.

7. Stereoscopic multispectral imaging comes down to putting the patient in an another light in order to see things differently without necessarily having to change one's point of view, whilst keeping everything in the right perspective.

8. You cannot successfully launch spear point technology without first carefully attaching a proper shaft to it.

9. *"Answers need the right questions to become useful."* (A.F.W. van der Steen).

10. Everything pulsates.

11. *"Free administration of sour bears stimulates creativity and dental practice."* (after R. Daane)